REPORT NO. DOT-TSC-141-1

STUDY OF THE PERFORMANCE REQUIREMENTS OF A VORTEX MONITORING SYSTEM

ROGER W. GOFF
ADVANCED DEVELOPMENT LABORATORIES
EQUIPMENT DIVISION
RAYTHEON COMPANY
SUDBURY, MA. 01776

MARCH 1972
TECHNICAL REPORT

Prepared for:

DEPARTMENT OF TRANSPORTATION
TRANSPORTATION SYSTEMS CENTER
CAMBRIDGE, MA. 02142

1. Report No. DOT-TSC-141-1	2. Government Accession No.	3. Recipient's Catalog No.
4. Title and Subtitle STUDY OF THE PERFORMANCE REQUIREMENTS OF A VORTEX MONITORING SYSTEM - FINAL REPORT		5. Report Date March 1972 6. Performing Organization Code
7. Author(s) Roger W. Goff		8. Performing Organization Report No.
9. Performing Organization Name and Address Raytheon Company Advanced Development Laboratories, Equipment Div. Sudbury, MA 01776		10. Work Unit No. R2106 11. Contract or Grant No. DOT-TSC-141
12. Sponsoring Agency Name and Address Department of Transportation Transportation Systems Center Cambridge, MA 02142		13. Type of Report and Period Covered Technical Report March 1971- March 1972 14. Sponsoring Agency Code
15. Supplementary Notes		

16. Abstract

This study involved four basic task items. The first was a general review of the characteristics of trailing vortex wakes. The second task item involved the generation of envelopes showing the expected vortex drift for the Boeing 747 and 727 aircraft. The third task item was an investigation of the environmental factors with which a vortex monitoring system would interact. The final task item was the application of the vortex drift data and operational usage considerations to the investigation of the performance requirements for a vortex monitoring system.

17. Key Words	18. Distribution Statement
Vortex Meterology	Availability is Unlimited. Document may be Released To the National Technical Information Service, Springfield, Virginia 22151, for Sale to the Public.

19. Security Classif. (of this report)	20. Security Classif. (of this page)	21. No. of Pages	22. Price
Unclassified	Unclassified	133	

CONTENTS

CONTENTS (continued)

ILLUSTRATIONS

ILLUSTRATIONS (continued)

ILLUSTRATIONS (continued)

SECTION 1

INTRODUCTION AND SUMMARY

This report is the final report under Department of Transportation, Transportation Systems Center Contract DOT-TSC-141, to study the performance requirements for an aircraft trailing vortex monitoring system for the terminal area.

The work was performed under the cognizance of Mark Gorstein, manager of the Aircraft Wake Vortices Detection System Project Office at the Transportation Systems Center in Cambridge, Massachusetts. The report summarizes the work performed during a 12-month period ending March 15, 1972.

The study involved four basic task items. The first was a general review of the characteristics of trailing vortex wakes. This included a brief examination of the velocity distribution in the vortex wake behind several aircraft, an examination of vortex wake decay in which NAFEC tower flyby data was used to define the limits of vortex endurance, and an investigation of the transport characteristics of the wake in order to define the maximum and minimum expected drift rates. The work performed in this area is described in Section 2 (Vortex Wake Characteristics).

The second task item involved the generation of envelopes showing the expected vortex drift for the Boeing 747 and 727 aircraft, both in and out of ground effect under worst case environmental conditions. The results obtained are discussed in Section 3 (Vortex Drift Envelopes).

The third task item was an investigation of the environmental

factors with which a vortex monitoring system would interact. The environment was assumed to include the NAS ATC System and its hardware, runway geometry and airport operational usage, as well as meteorological conditions. These considerations are discussed in Section 4 (Interaction of a Vortex Monitoring System with NAS ATC Elements).

The final task item was the application of the vortex drift data and operational usage considerations to the investigation of the performance requirements for a vortex monitoring system. The study was performed for a particular runway combination used at Logan Airport in Boston, Massachusetts. In addition, a correlation analysis between theoretically derived vortex drift rates and drift rates measured at NAFEC during aircraft flyby tests was conducted. The results obtained are presented in Section 5 (Application of Data to Airport Monitoring Requirements).

The studies have shown that the analysis of vortex monitoring requirements are intimately connected to the geometry, runway selection, and operational procedures of a given airport. Once these are defined, procedures are available to locate vortex hazard regions about the airport surface and define the corresponding vortex monitoring regions. However, before the present and similar results can be applied with confidence in the development of systems to predict or monitor vortices in the terminal area, more detailed assessment should be made of (1) the accuracy of the theoretical models for vortex drift upon which the data is based and (2) the accuracy of vortex endurance assumptions.

SECTION 2

VORTEX WAKE CHARACTERISTICS

2.1 INTRODUCTION

The work presented in this section covers background information on the nature of the trailing vortex wakes behind jet transport aircraft. The information will be used during the latter phases of the study. The work performed covers the following items. First, the velocity distribution in the vortices immediately behind several large jet aircraft has been examined, using contemporary theory; second, the decay of trailing vortices generated near the ground was examined to define the limits of wake endurance; and third, the transport characteristics of the trailing vortex wake were examined in order to define the maximum and minimum expected drift rates.

2.2 VORTEX RADIAL VELOCITY DISTRIBUTION

Prior to the introduction of the Boeing 747, aerodynamicists investigating the tangential velocity distributions in the trailing vortices generated by aircraft usually assumed simple vortex flow where the streamlines are circles and the velocity varies inversely with the distance from the center of the vortex

$$V_\theta = \frac{\Gamma}{2\pi r} \tag{2-1}$$

where Γ is the circulation. For an elliptically loaded wing Γ can be shown to be equal to

$$\Gamma = \frac{4L}{\rho V \pi b} \tag{2-2}$$

where L is the lift being generated, ρ is the air density, V is

the aircraft velocity, and b is the aircraft span.

Since Equation (2-2) predicts an infinite tangential velocity as the center of the vortex is approached, a cut-off distance was assumed within which the flow was assumed to rotate as a solid body. Sprieter and Sacks in Reference 12 gives a radius of 0.0775b for this distance.

The experimental testing of the trailing vortex wakes conducted early in 1970 proved that these simple equations did not provide a very realistic representation of the actual vortex velocity distribution. The vortices generated behind a clean wing were found to possess much higher rotational velocities with small well defined core regions. In the case of the T-tail jets (B-727 and DC-9) tangential velocities of the order of 200 ft/sec were measured.

Two contemporary formulations have been developed which hopefully describe the velocity distribution more exactly.

In Reference 10, McCormick presents the following equations for determining the tangential velocity distribution in the vortex.

The radius of the solidly rotating core (a) is given by

$$a = 0.02\ cc_{\ell} \tag{2-3}$$

where cc_{ℓ} is the span loading at the wing root (c is the chord length and c_{ℓ} the sectional lift coefficient of the wing).

The tangential velocity for radii greater than a is given by

$$V_{\theta_m} = 0.68\ C_L \left(\frac{1 + \ell n \frac{r}{a}}{\frac{r}{a}} \right) \tag{2-4}$$

In Reference 4, Donaldson presents the following equations for the tangential velocity distribution. For $r/b \leq 1/3$

$$V_{\theta_D} = \frac{\Gamma}{2\pi r} \left[6 \frac{r}{b} - 9 \left(\frac{r}{b} \right)^2 \right]^{1/2} ; \qquad (2\text{-}5)$$

for $r/b > 1/3$

$$V_{\theta_D} = \frac{\Gamma}{2\pi r} \qquad (2\text{-}6)$$

As shown by the latter equation, the tangential velocity in this method is equal to that of a potential vortex (Equation (2-1)) for all radii greater than b/3.

In the references both techniques are compared with experimental data taken at NAFEC and for the cases examined show reasonable agreement. However, neither method predicts the variations in core size and peak velocities which occur in the experimental data when the wing flap configuration is varied.

Both methods were used to compute the velocity distribution behind a B-747 and a B-707 aircraft. The results are compared with each other and with the velocity distribution predicted by a potential vortex in Figures 2-1 and 2-2. As shown, the McCormick formulation predicts higher tangential velocities than that of the Donaldson method. In the range of 10 to 50 feet radius, the potential vortex equation lies between the two.

The data points shown on Figure 2-2 were determined from measurements taken at NAFEC for the Boeing 727 aircraft in the landing configuration as reported in Reference 9. As shown, the data matches quite closely the Donaldson curve that was computed for the B-707 aircraft.

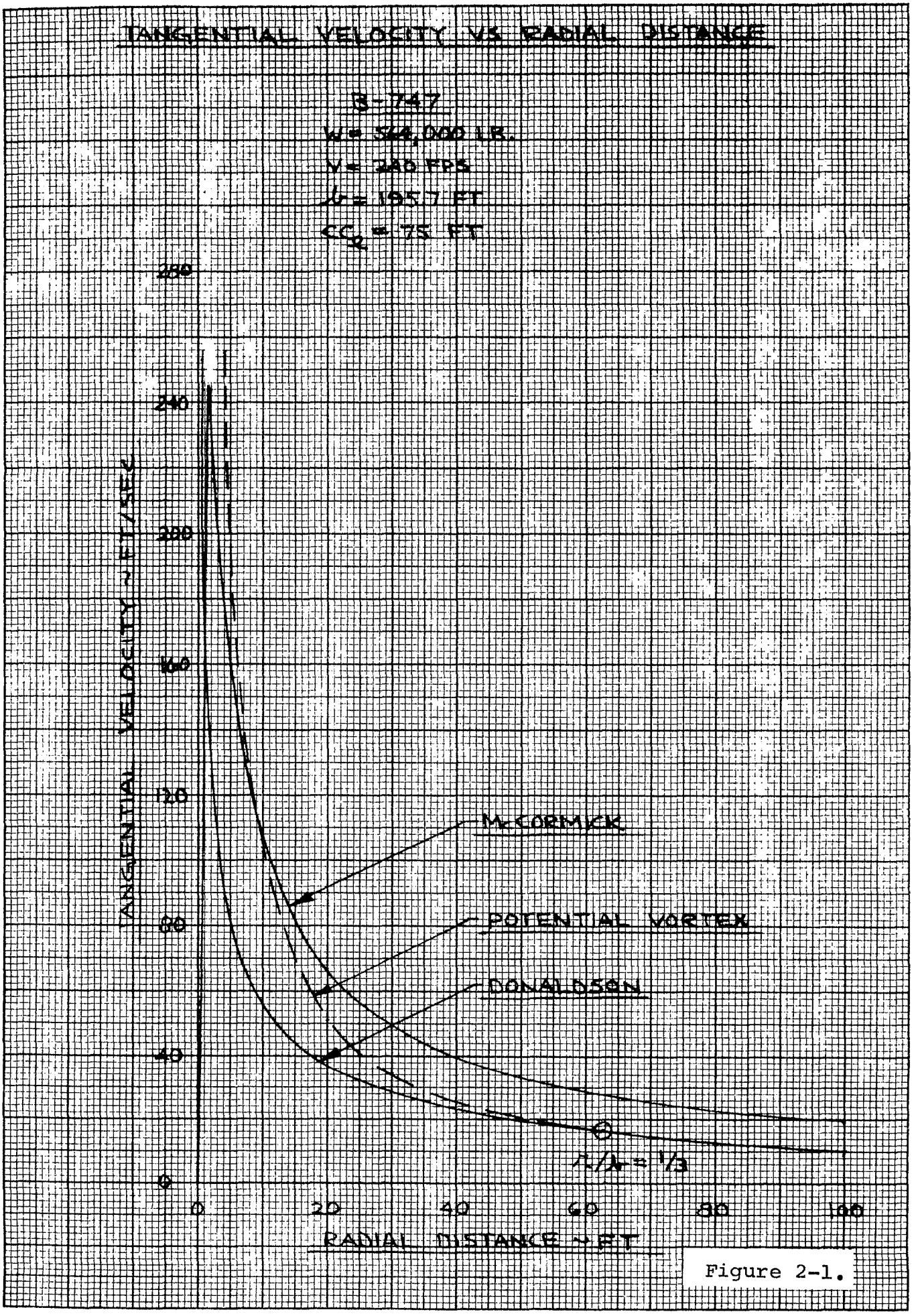
TANGENTIAL VELOCITY VS RADIAL DISTANCE
B-747
W = 564,000 LB.
V = 240 FPS
r_t = 195.7 FT
CC_R = 75 FT
TANGENTIAL VELOCITY - FPS
280
240
200
160
120
80
40
0
McCORMICK
POTENTIAL VORTEX
DONALDSON
$r_c/r_t = 1/3$
0
20
40
60
80
100
RADIAL DISTANCE - FT

Figure 2-1.

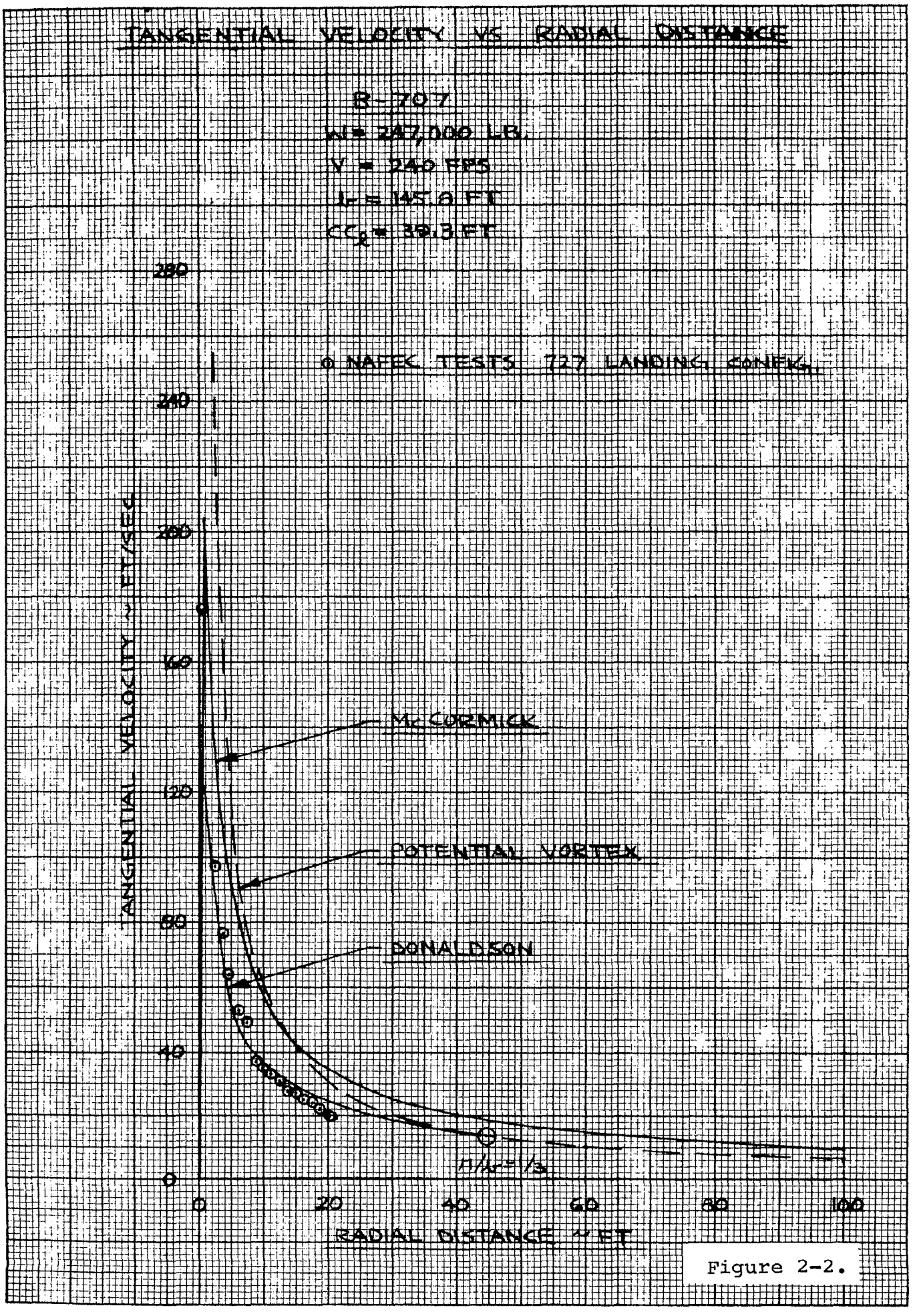
TANGENTIAL VELOCITY VS RADIAL DISTANCE
R = 707
W = 247,000 LB.
V = 240 FPS
l_r = 145.6 FT
CC_g = 39.3 FT
NAFEC TESTS 727 LANDING CONFIG.
TANGENTIAL VELOCITY, FT/SEC
RADIAL DISTANCE - FT
MC CORMICK
POTENTIAL VORTEX
DONALDSON
$\Gamma/k = 1/3$
0
20
40
60
80
100
120
140
160
180
200
220
240
260
280

Figure 2-2.

It should be noted that in generating the McCormick curve the Equations (2-4, 2-5) were used exactly as they appear. In McCormick's equations the circulation does not appear explicitly and therefore some of the variation between the Donaldson and McCormick curves can be attributed to the fact that the curves correspond to different levels of total circulation.

2.3 VORTEX DECAY AND BREAKUP

Experimental data taken during Special Tasks Numbers Two and Three of the Wake Turbulence Test Program conducted by the FAA have been utilized to obtain an estimate of the endurance of the vortex wakes of large jet aircraft when operating near the ground with flaps extended in either the landing or takeoff configuration.

Special Task Two (Reference 5) involved the investigation of jet aircraft vortex systems descending into ground effect and those generated within ground effect. The tests were conducted at NAFEC and the aircraft involved were the B-727-100, B-707-300, DC-9-10 and the CV-880. All aircraft in these tests were flown at altitudes of less than 120 feet.

Special Task Three (Reference 6) involved the investigation of the relatively long time history vortex characteristics of the CV-880 jet aircraft in terminal area type operations. Tests were conducted at NAFEC and all flights were at altitudes of less than 140 feet.

In both Tasks 2 and 3, a 100-foot high tower instrumented with hot-film anemometers was used to measure the aircraft vortex induced velocities at each 10-foot level.

For Task 2 a total of 153 aircraft fly-bys were flown. These consisted of 43 flights for the B-727, 12 for the DC-9, 11 for the B-707 and 87 for the CV-880.

For Task 3 a total of 122 CV-880 tower fly-bys were conducted.

For purposes of the present contract it was desired to define for large jet aircraft the limits of vortex wake endurance with critical circulation velocities. The data taken at NAFEC was not comprehensive enough to obtain precise descriptions of the significance of atmospheric and aircraft parameters on the complex vortex decay and breakup phenomena. However, the data was useful in estimating the probable maximum vortex durations for the variety of aircraft, aircraft flap configurations and environmental conditions existing during the tests.

The data considered in the analysis described herein was restricted to the CV-880 aircraft and to the flaps-down condition corresponding to either the landing or takeoff configuration for this aircraft. This eliminates data variations between aircraft and also eliminates the possibility of overestimating vortex duration near the ground by including data for aircraft in the clean configuration. This configuration is not commonly used when flying in the terminal area.

In the dirty configuration the vortices generated do not normally exhibit the characteristics of a narrow core tubular structure, but are of the diffuse large core type. The exceptions to this are the T-tail jets, DC-9, B-727, which as reported in Reference 5 still exhibit the small core under flap-down conditions. Except for these jets and the Delta-winged SST's, it is assumed that the decay of the peak tangential velocity of the vortex wake of all large jet aircraft will behave similar to the CV-880 aircraft provided the flap settings and environmental conditions are similar.

Neglecting vortex breakup due to bursting or sinusoidal instabilities, the vortex tangential velocities decay due to viscous diffusion. Under these conditions the level of atmospheric tur-

bulence directly affects the decay rate. Since the mean wind speed is a good index to the atmospheric turbulence level near the ground (Reference 1), the time required for the tangential velocities within a vortex to decay to a particular level should vary approximately inversely with the wind speed. This correlation has been noted by McGowan and he has presented vortex lifetime data in this format (Reference 11).

In Task 3 the ambient wind level was recorded in addition to the regular test data. This enabled the measured data of vortex speed as a function of vortex age to be correlated with wind speed provided a satisfactory method was found to extrapolate the data to a common tangential speed level. The latter being the minimum speed causing an undesirable upset to an encountering aircraft.

Unfortunately, due to the finite 10-foot spacing of the sensors, the data measured at NAFEC does not correspond to the core or peak velocity in each instance. However, the data for the CV-880 included in the present analysis was with flaps down. With the increased core diameter that results with this configuration, the likelihood of so-called core-intercepts is increased. All of the tangential speed versus vortex age data points for the CV-880 with flaps down from Tasks 2 and 3 are shown in Figure 2-3. The square symbols correspond to Task 2 data and the circular symbols to Task 3.

The two data points marked with the question marks were considered questionable and were not included in the data sample because (1) they were considerably higher in speed than the other data points taken at a comparable vortex age and (2) they were the only instances recorded where both wing-tip vortices passed through the tower in which the speed measured for the second vortex (at a greater age) exceeded that of the first vortex.

Ignoring the two questionable data points and the curves

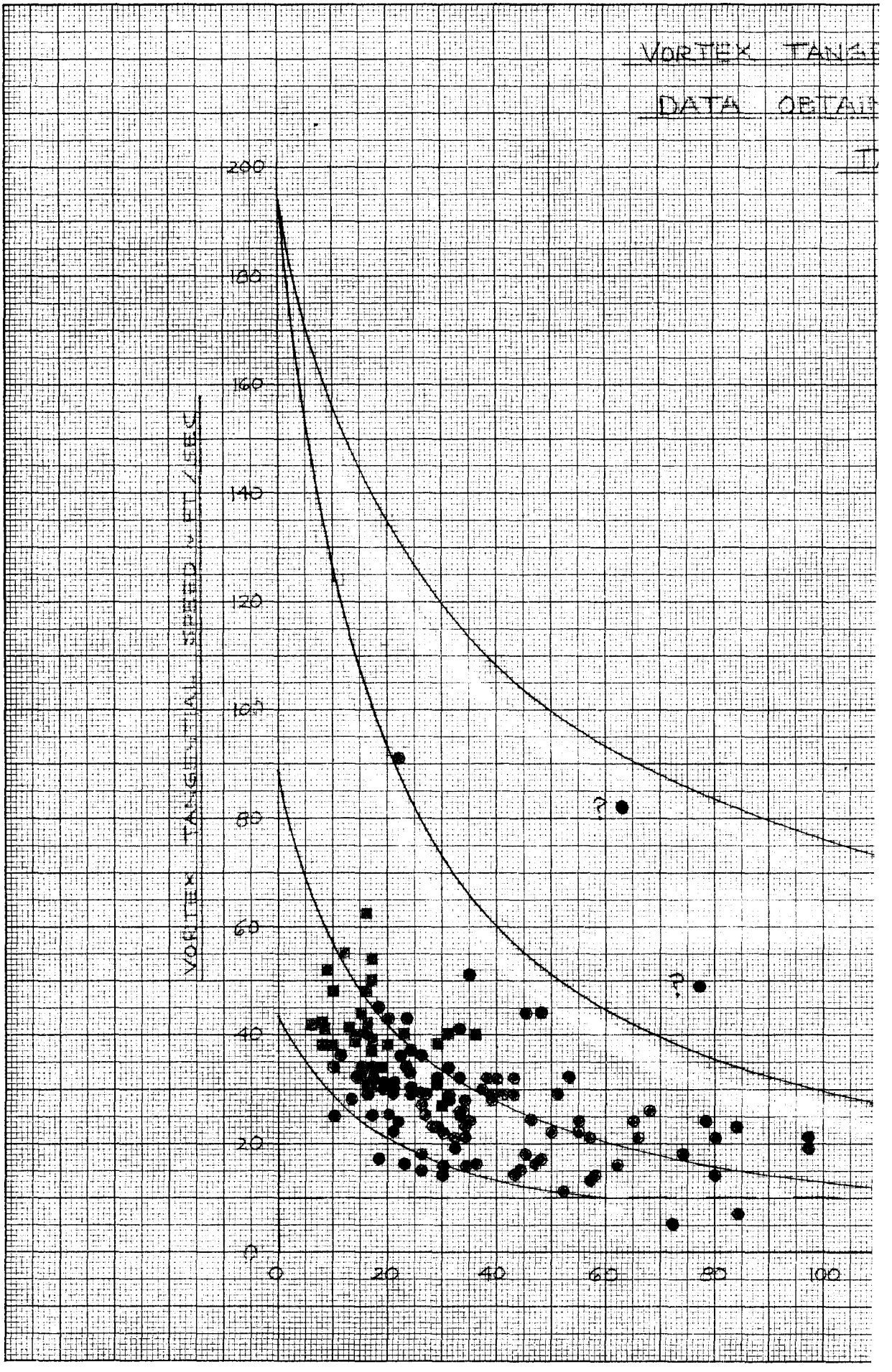
VORTEX TAN
DATA OBTAI
T
VORTEX TANGENTIAL SPEED, FT/SEC
200
180
160
140
120
100
80
60
40
20
0
0
20
40
60
80
100
?
?

AL APPLIED TO AGE FOR CV-880 AIRCRAFT

EROM SPECIAL TASKS 2 & 3 (NEAR GROUND)

OFF OR LANDING CONFIGURATION ONLY

● TASK 3
■ TASK 2

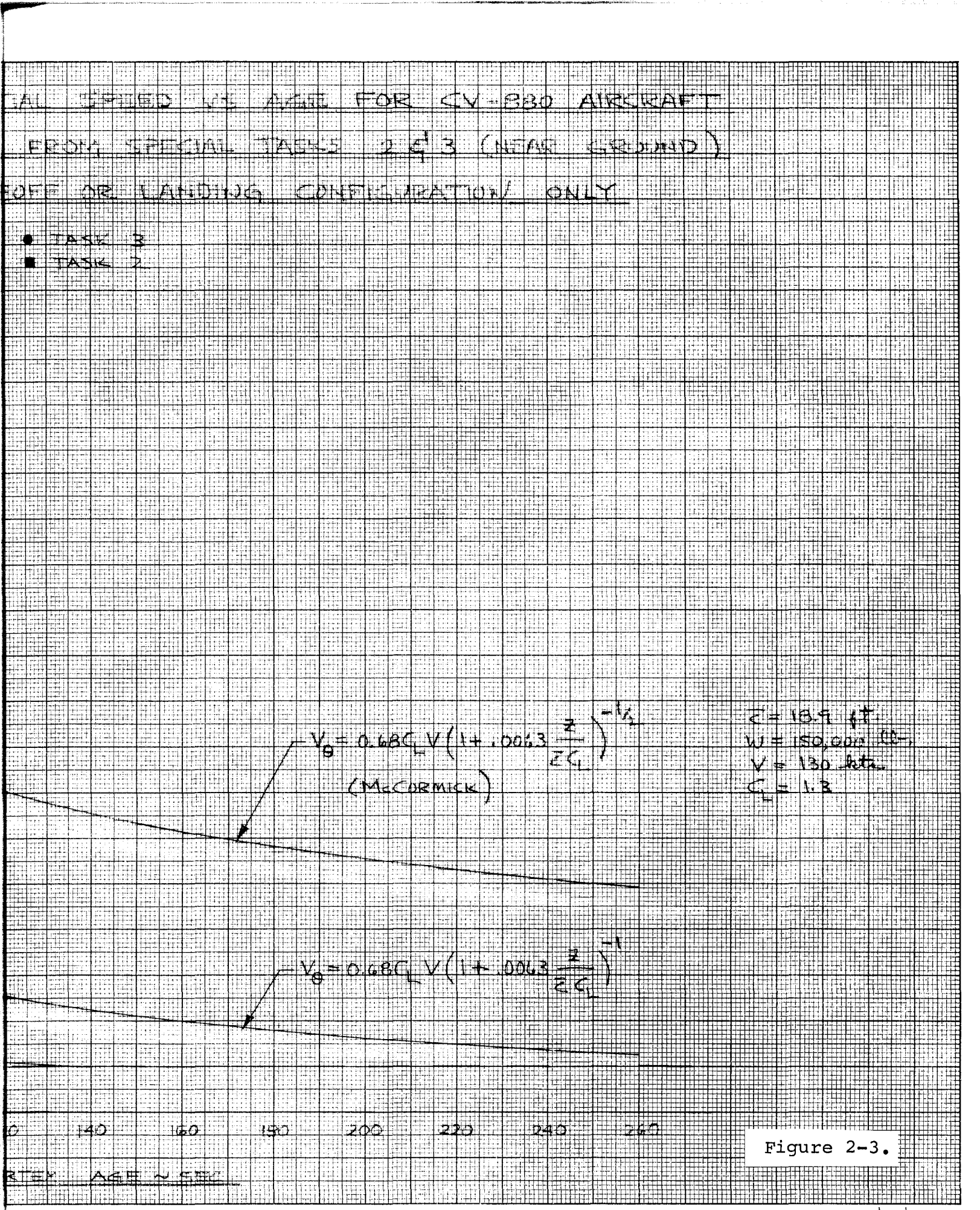

Figure 2-3.

4/16/71
RWG

drawn on the figure, it is seen that an envelope drawn to enclose the data points falls off in speed as vortex age increases. It was assumed that this envelope would be representative of the maximum vortex endurance for a large jet aircraft.

The next step was to obtain an analytic expression for a curve fitting this envelope. This equation could then be applied to the data points for which the ambient wind speed was recorded to normalize them to a common vortex tangential speed level.

McCormick (References 9, 10, and11) has obtained semi-empirical expressions for the variation of vortex tangential speed with vortex age. These equations were examined to see how closely they matched the envelope of the data points. In each instance these equations overestimated the vortex tangential speed as a function of age.

In Reference 10, McCormick gives the following expression for the decay of the maximum tangential velocity of a vortex with downstream distance

$$V_\theta = 0.611\ C_L V \left(1 + 0.0065\ \frac{z}{\bar{c}}\right)^{-1/2}, \qquad (2\text{-}7)$$

where: V = the aircraft velocity
$\bar{c}$ = the mean aerodynamic chord
z = the downstream distance (Vt)
C_L = the aircraft lift coefficient

and, $C_L = \frac{W}{qS}$
S = the aircraft wing area
W = the aircraft weight
q = the dynamic pressure

After review of the NAFEC test results, the following equation for predicting the peak tangential velocity distribution with distance was presented by McCormick in Reference 11.

$$V_\theta = 0.68\ C_L V \left(1 + 0.00063 \frac{z}{\bar{c}\ C_L}\right)^{-1/2}. \qquad (2\text{-}8)$$

Since the value of the lift coefficient is generally of the order of 1 or 2, Equations (2-7) and (2-8) can be compared directly. It can be seen that Equation (2-8) predicts a more gradual decay of the peak vortex velocity with distance.

In order to fit a curve to the data envelope, Equation (2-8) was used. Because of previous experience with Equation (2-7), it was felt that a typing error had caused the coefficient in the equation to be reduced by an order of magnitude. The correct equation was assumed to have a coefficient of .0063. This modified equation was examined assuming the following values for the CV-880 aircraft, $\bar{c}$ = 18.9, W = 150,000 lbs., V = 130 knots, C_L = 1.3. The resulting curve is shown at the top of Figure 2-3. It is seen that even with the error in the coefficient the equation predicts too gradual a decrease in tangential speed with vortex age to describe the envelope.

Since the McCormick equations are basically empirical, modifications to obtain a better fit were examined by varying the exponent in the equation. An exponent of -1, when used in the equation, was found to provide a reasonable approximation to the envelope of the data points as shown on Figure 2-3 by the curve appropriately labeled.

If the equation relating two points on this curve, namely,

$$\frac{V_{\theta(1)}}{V_{\theta(2)}} = \frac{\left(1 + .0063 \frac{z_1}{\bar{c}\ C_L}\right)^{-1}}{\left(1 + .0063 \frac{z_2}{\bar{c}\ C_L}\right)^{-1}}, \qquad (2\text{-}9)$$

is rearranged and the substitution Vt = z made, the following equation can be obtained describing the vortex age (t_2) when a data point (V_{θ_1}, t_1) will decay to a specified velocity (V_{θ_2}).

$$t_2 = \frac{159\ \bar{c}\ C_L}{V}\left(\frac{V_{\theta_1}}{V_{\theta_2}} - 1\right) + \frac{V_{\theta_1}}{V_{\theta_2}}\ t_1. \qquad (2\text{-}10)$$

The other two curves shown on the figure represent the decay predicted by the above equation for other values of the data.

This equation was used to normalize each of the data points for which the wind was recorded to a common decay velocity of 15 ft/second. This latter velocity was assumed to be a level critical to encountering aircraft.

The extrapolated data was then replotted as the vortex age at a velocity of 15 ft/second versus the ambient wind speed as shown in Figure 2-4. Superimposed on this figure is the original decay curve suggested by McGowan in Reference 11. The curve has been truncated at a maximum time of 240 seconds and a maximum wind speed of 35 MPH. As shown, no significant departure from the McGowan curve can be discerned from the data extrapolated in this manner. Therefore, it was assumed that the McGowan curve,

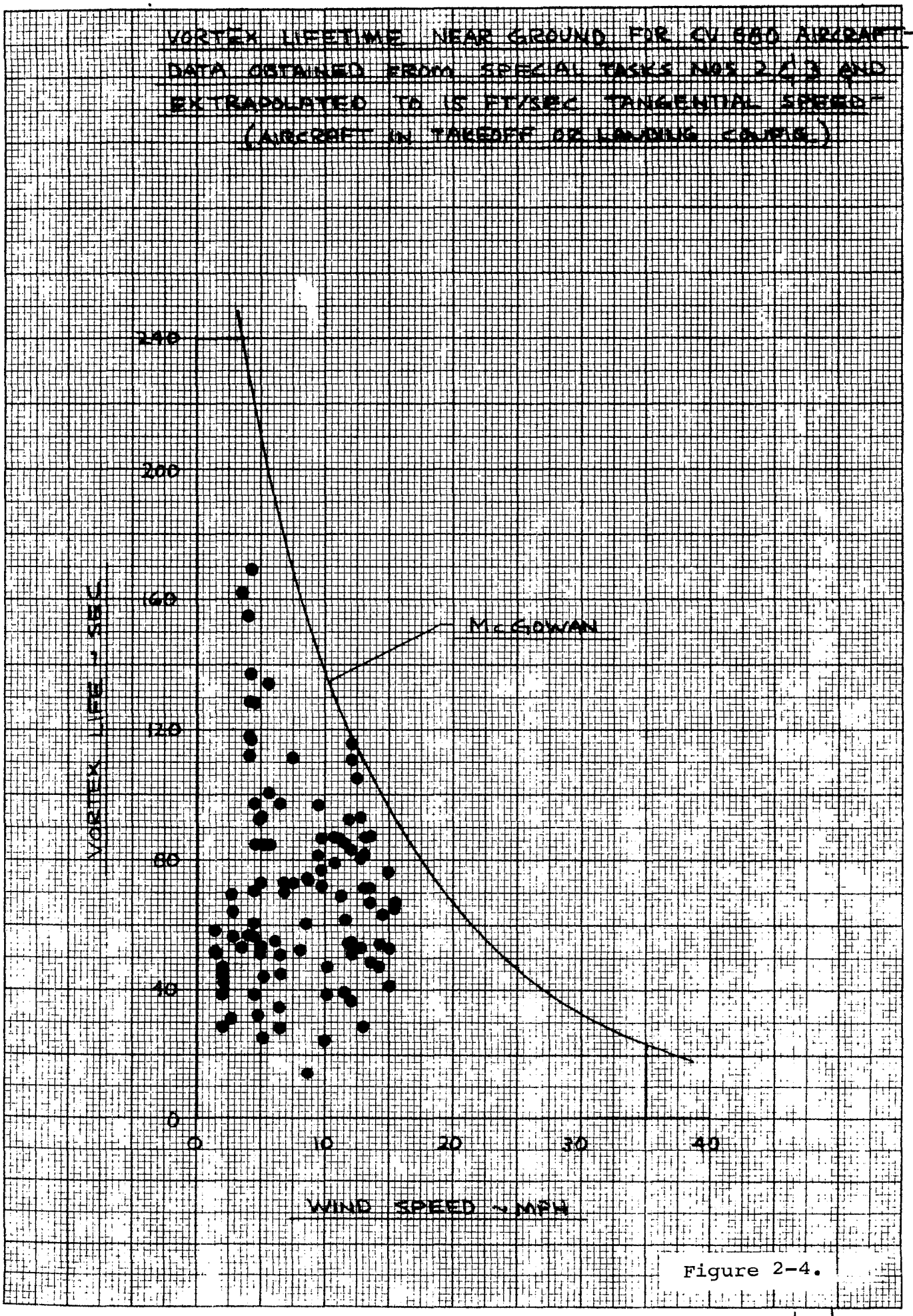

Figure 2-4.

4/29/71

truncated as shown, would be utilized in studies of vortex transport. It is apparent that data at higher wind speeds and greater vortex age for the CV-880 and other aircraft is necessary to substantiate any departures from the McGowan curve.

Extrapolating the data by assuming an exponential decay does not consider the possibility of rapid vortex collapse due to vortex instabilities. Confirmation of the exact vortex decay pattern and endurance near the ground will require more elaborate test instrumentation and a wider range of test conditions. When this data becomes available, it may well show that the maximum vortex durations for aircraft operating near the ground with flaps extended may be considerably less than the maximum of 4 minutes assumed herein.

The curve shown in Figure 2-4 was used to examine the size of the vortex drift envelope for the Boeing 747 aircraft. The results were used in a preliminary analysis of the significance of runway and aircraft operational procedures on vortex monitoring requirements at Logan Airport in Boston as discussed in Reference 7.

2.4 VORTEX TRANSPORT CHARACTERISTICS

Motion of the trailing vortex wake generated by an aircraft is caused by a combination of vortex pair mutual induction, induction due to the underground vortex images and wind drift. If the motion caused by these three factors is combined with knowledge of the decay of the vortex wake, envelopes can be generated which indicate the extent to which the vortex wake can drift and constitute a hazard to other aircraft.

A computer program has been generated which enables the computation of the motion of an incremental element of a vortex filament. Motion of this element is computed as a function of time up to a maximum time corresponding to the vortex endurance.

The program is based on the Biot-Savart equation:

$$V = \int_{-\infty}^{+\infty} \frac{\Gamma}{4\pi} \frac{\cos \beta \, ds}{r^2}, \tag{2-11}$$

which specifies the velocity (V) induced at a point (p) by a vortex filament of strength (Γ). Figure 2-5 defines the geometry.

If the vortex filament is linear the integration gives:

$$V = \frac{\Gamma}{2\pi h} \tag{2-12}$$

where h is the perpendicular distance between the filament and the point.

Using this result the horizontal and vertical velocity components induced on an element of a vortex filament by its companion filament and the underground image filaments can be determined from the following equations. (The geometry is defined in Figure 2-5.)

$$\dot{y} = \frac{\Gamma}{4\pi} \left(\frac{1}{z} - \frac{z}{y^2 + z^2} \right), \tag{2-13}$$

$$\dot{z} = - \frac{\Gamma}{4\pi} \left(\frac{1}{y} - \frac{y}{y^2 + z^2} \right). \tag{2-14}$$

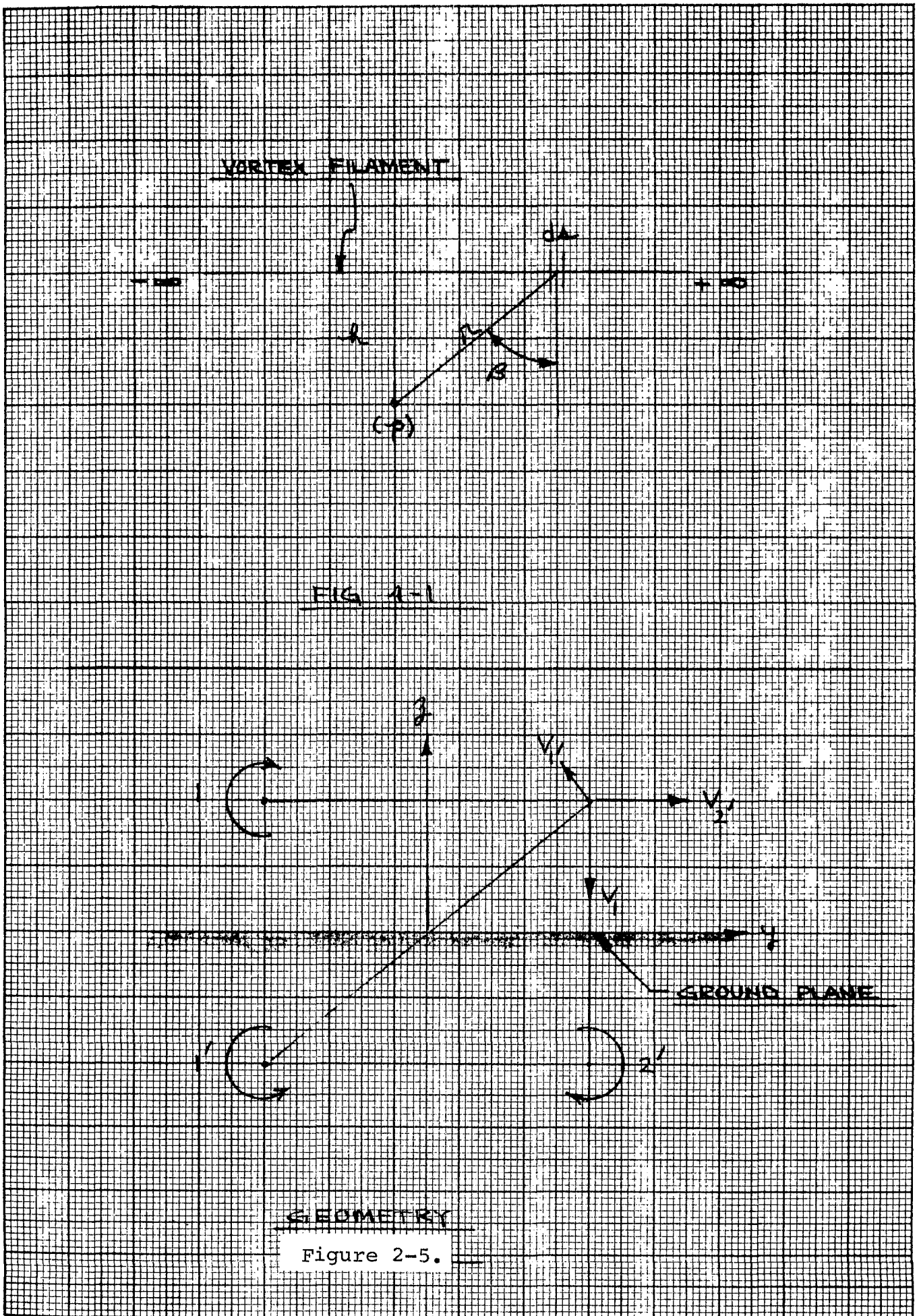

Figure 2-5.

6/15/71

If these expressions are rearranged and integrated (see Reference 3), closed form expressions for the vertical and horizontal displacements of the vortex element can be obtained as a function of time.

The computer program combines vectorially the displacements given by these expressions with the wind induced displacement to obtain the net movement of the vortex element.

The program has been used to investigate the maximum and minimum lateral drift velocities that can be attained by the vortices due to ground effect and due to a combination of ground effect and wind. The program was used to compute the lateral drift of the vortex due to ground effect at each 30-second interval up to the maximum vortex endurance of 240 seconds (Figure 2-4). This distance divided by the endurance gives the average ground induced lateral transport velocity. If this velocity is combined with the maximum wind speed for each endurance time, the maximum average lateral drift velocity is obtained. This velocity times the endurance increased by the semi-span distance initially separating the two vortex filaments gives the maximum lateral drift distance with respect to the flight path.

The minimum average lateral drift velocity of the vortex is the lateral distance traversed divided by 240 seconds, the assumed maximum vortex endurance.

These quantities are shown plotted in Figure 2-6 for the Boeing 747 assuming an aircraft weight of 564,000 pounds and a velocity of 240 ft/sec. The figure shows that a significant increase in maximum lateral distance occurs as the altitude of vortex generation is reduced. It has been reported (References 5 and 6) that vortices generated in ground effect are weaker, less well defined and do not persist as long as those generated at greater heights. Therefore the curves shown for vortices generated at 50 feet and 100 feet may be optimistic. Neglecting this,

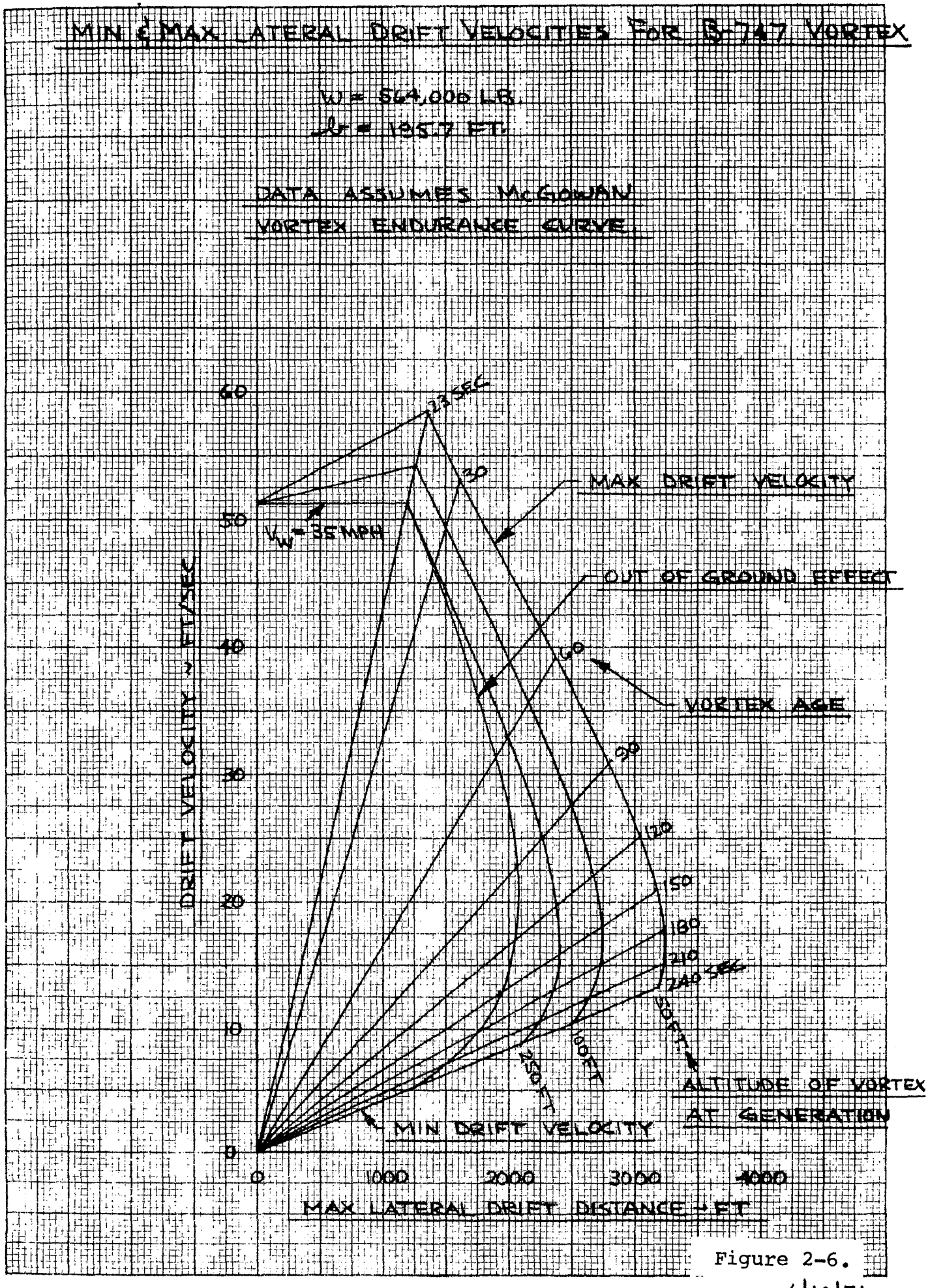

Figure 2-6.

6/14/71

it can be seen that for a lateral distance of 2000 feet the minimum drift velocity is 8.3 ft/second allowing 240 seconds for the vortex to cover this distance and the maximum drift velocity is 45.5 ft/second allowing approximately 45 seconds for the vortex to cover this distance.

The theoretical steady-state ground induced velocity of separation of one vortex from the plane of symmetry is given by:

$$v_i = \frac{8}{\rho V \pi^3} \left(\frac{W}{b^2}\right), \qquad (2\text{-}15)$$

where W/b^2 is the aircraft parameter affecting the steady-state lateral drift speed. This parameter has been evaluated for several aircraft in addition to the 747 as listed in Table 2-I. The value R is the W/b^2 parameter of each aircraft divided by the corresponding value for the 747. This number gives the ratio by which the vortex induced transport speed and distance would be increased over that given in Figure 2-6 for the 747.

The most striking departure is obtained with the Concorde SST. Because of the relatively short span of this aircraft the rolled-up vortices are spaced more closely, resulting in large induced velocities. In actual fact, this factor may result in the very rapid diffusion or breakup of these vortices. The answer will require the experimental examination of the wakes behind these aircraft.

The next largest aircraft in magnitude of the W/b^2 parameter is the DC-10. For this aircraft the vortex induced transport speed can be expected to be 50% greater than the peak induced transport speed for the 747. Thus, the maximum lateral vortex drift speed of 58.5 ft/sec for the 747 would be increased to approximately 62 ft/sec for the DC-10.

The lateral transport velocity assuming ground induced motion

Table 2-I.

A/C	WT (lb)	b (ft)	W/b^2 (lb/ft^2)	R
747	564,000	195.7	14.7	1.0
CV-880	150,000	120.0	10.4	0.71
C5A	728,000	223.0	14.6	0.99
Concorde	385,000	84.0	54.6	3.71
L1011	409,000	155.0	17.0	1.16
707-320C	332,000	146.0	15.6	1.06
727	160,000	108.0	13.7	0.93
737-200	93,500	89.0	11.8	0.80
DC10,20	530,000	155.0	22.1	1.50

of the vortex is shown as a function of vortex age for the B-747 in Figure 2-7. The data was generated as discussed previously and curves are presented for initial vortex altitudes of 50, 100, and 250 feet.

The figure shows that in ground effect the initial height of the aircraft has a strong effect on the vortex transport speed. As the vortex filament height is reduced, the theoretical lateral speed induced by the underground image increases. Because of this fact and the uncertainty in the magnitude of the wind influencing the vortex, correlations of vortex drift test data with theoretical calculations can be disappointing.

The variation of the ground induced vortex transport speed for the CV-880 aircraft has been estimated from the 747 data by using the ratio listed in Table 2-I. This data is shown in Figure 2-8. Superimposed on this data is the data published in Reference 5 for the transport speed determined from measurements made

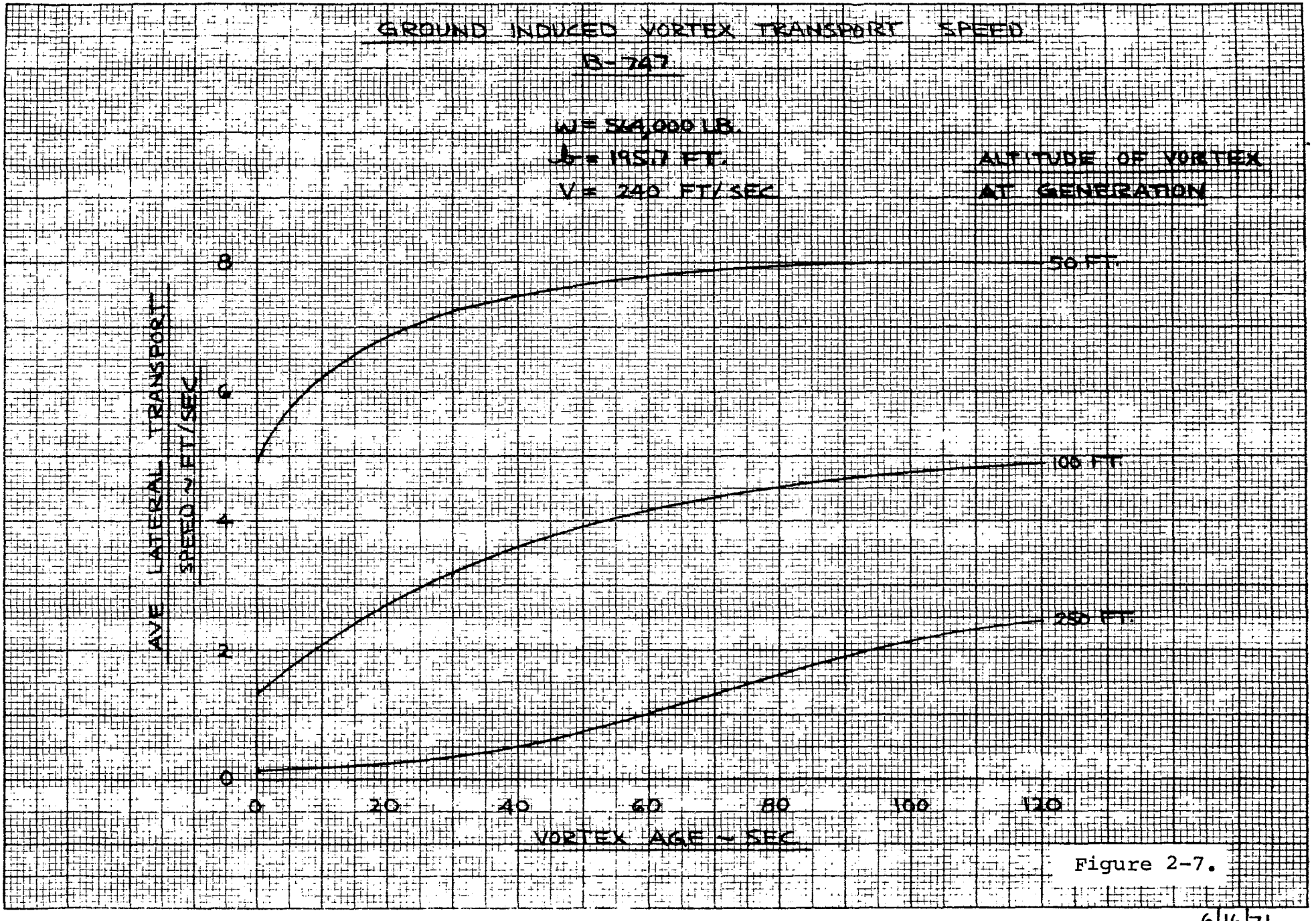

Figure 2-7.

6/16/71

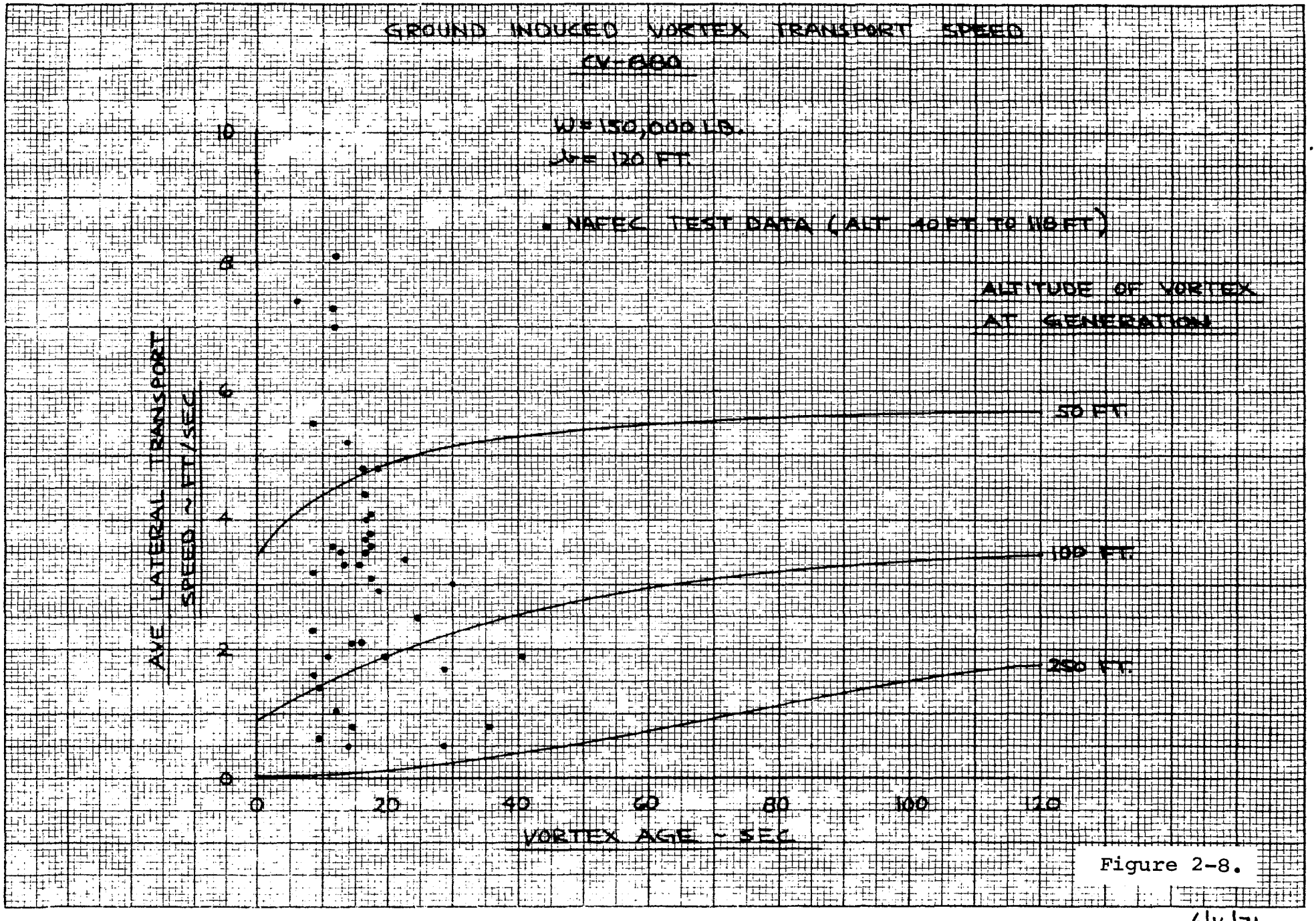

Figure 2-8.

6/16/71

at NAFEC. The particular data presented is for the CV-880 aircraft flying between altitudes of 40 and 118 feet. As shown, the data is widely scattered and several data points would fall outside of 40 and 118 feet altitude boundaries determined analytically.

One problem in reducing the measurements to obtain the ground induced transport speed is measuring the effective wind acting on the vortex. The wind must be measured close enough to the tower to represent the true wind speed in that area, but not so close as to be affected by either the flow field created by the vortex wake or the passage of the aircraft.

2.5 CONCLUSIONS

The characteristics of aircraft trailing vortex wakes have been examined in order to assess the adequacy of presently available theoretical models to represent actual vortex behavior and to determine which models best characterize vortex behavior for use in examining the performance requirements of a vortex monitoring system.

Considering the vortex characteristics separated into the following items: velocity distribution, decay and breakup, and vortex transport, the following conclusions can be made:

Considerable experimental data is available to define the expected peak velocities and approximate core radii for vortex wakes behind various aircraft with various flap configurations. However, none of the theoretical models available can adequately describe the velocity distribution over the same wide variation of conditions.

Considerable experimental data is available on vortex tangential velocity as a function of vortex age for various aircraft,

flap configurations, winds, etc. However, this data is widely scattered and atmospheric conditions were not adequately recorded. Moreover, when wind velocity was recorded, the data did not cover the high wind range for which vortex endurance is expected to be short. Finally, data was not taken at great enough vortex ages to determine when and how consistently vortex breakup occurs near the ground. Extrapolations using the data have been made which indicate that the McGowan vortex lifetime-in-wind curve is reasonably representative for commercial jets. However, when vortex data at greater age and/or wind speed are available, this curve may be found conservative.

Experimentally determined transport velocities when compared with theoretical values were found to be widely scattered about the boundaries defined analytically. The ground induced vortex transport velocity is very sensitive to vortex height at generation. The vortex transport velocities determined from experimental data may be in error due to inaccuracies in aircraft location and in knowledge of the true ambient wind acting on the vortex. It has been assumed that the theoretical vortex transport speed determined by summing vectorially the vortex, ground and wind induced motion adequately describes the actual motion and that the scatter in the data is due to the aforementioned uncertainties.

SECTION 3

VORTEX DRIFT

3.1 INTRODUCTION

This section presents curves showing the extent of vortex drift both in and out of ground effect for the Boeing 727 and 747 aircraft. The endurance of the vortices was based upon the McGowan lifetime curve presented in Section 2, which should be representative of lifetime under worst case environmental conditions for aircraft operating near the ground in either the take-off or landing configuration. Results are presented of a preliminary attempt to correlate these theoretical drift envelopes with experimental vortex test data taken at the FAA's NAFEC test facility.

3.2 RESULTS

A computer program formulated by Raytheon and programmed at TSC has been used to generate vortex drift envelopes for the Boeing 727 and 747 aircraft. This program includes the effects of vortex mutual induction, ground effect, and winds.

The aircraft characteristics assumed for input are listed in Table 3-I.

Aircraft	B-727	B-747
Weight (lb)	142,500	564,000
Span (ft)	108	195.67
Altitude (ft)	100, ∞	100, ∞
Speed (ft/sec)	225	240
$b\pi/8$ (ft)	42.4	76.8

TABLE 3-I. Aircraft Characteristics

The coordinate system used in the program is shown in Figure 3-1. For the series of runs presented herein the wind heading angle was varied in 10 degree increments from 0 to -90 degrees for each of the following wind magnitudes: (2.5, 3.45, 5.0, 7.5, 10, 15, 20, 25, 30, 35 miles/hour). For each wind magnitude the vortex endurance was obtained from the truncated McGowan lifetime curve discussed in Section 2 and repeated here as Figure 3-2. The initial aircraft altitude in all runs was 100 feet.

Figure 3-3 shows the locus of the decay points for the upwind vortex for the Boeing 747 aircraft. As shown, the upwind vortex starts from a point 76.8 feet ($\pi/8b$) down the minus y-axis and can drift to a point 1560 feet down the plus y-axis with a crosswind of 15 miles/hour and to a point 2080 feet down the x-axis with a downwind of 15 miles/hour. For zero wind the upwind vortex drifts due to ground effect to a point 1350 feet down the minum y-axis.

Figure 3-4 shows similar data for the downwind vortex of the B-747. In this case the vortex reaches a lateral distance of 2800 feet from the aircraft ground track with a crosswind speed of 7.5 miles/hour. The maximum drift distance in the downwind direction is identical to the upwind vortex or 2080 feet.

Figures 3-5 and 3-6 are similar to Figures 3-3 and 3-4 respectively, except the aircraft involved is the Boeing 727. In this case, the extent of the envelopes are somewhat smaller. The vortex induced motion is not as great since the aircraft parameter governing the magnitude of the self-induced motion (w/b^2) is less for the 727 than the 747 (see Section 2, Table 2-I).

Figure 3-7 presents the locus of the decay points for the

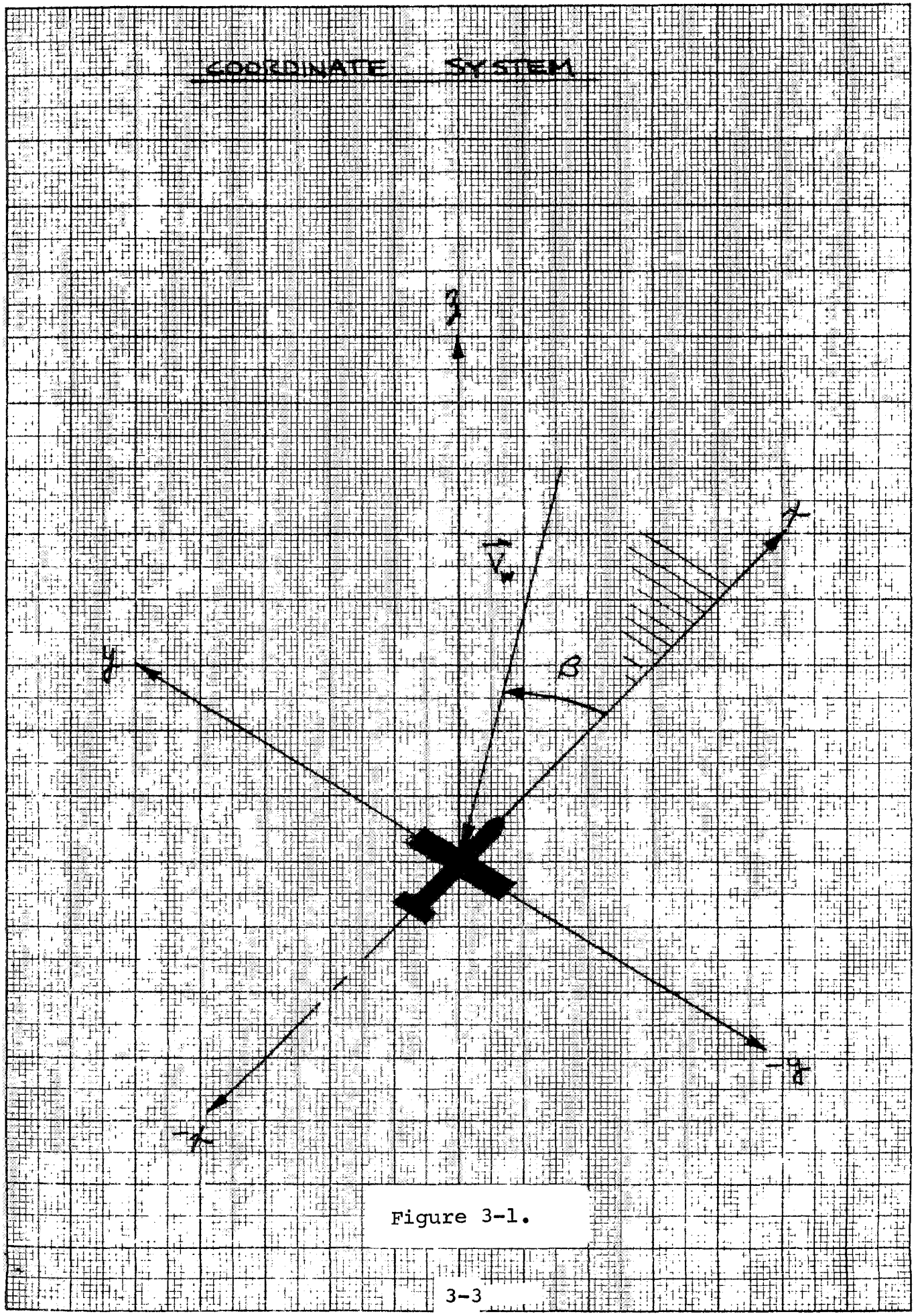

Figure 3-1.

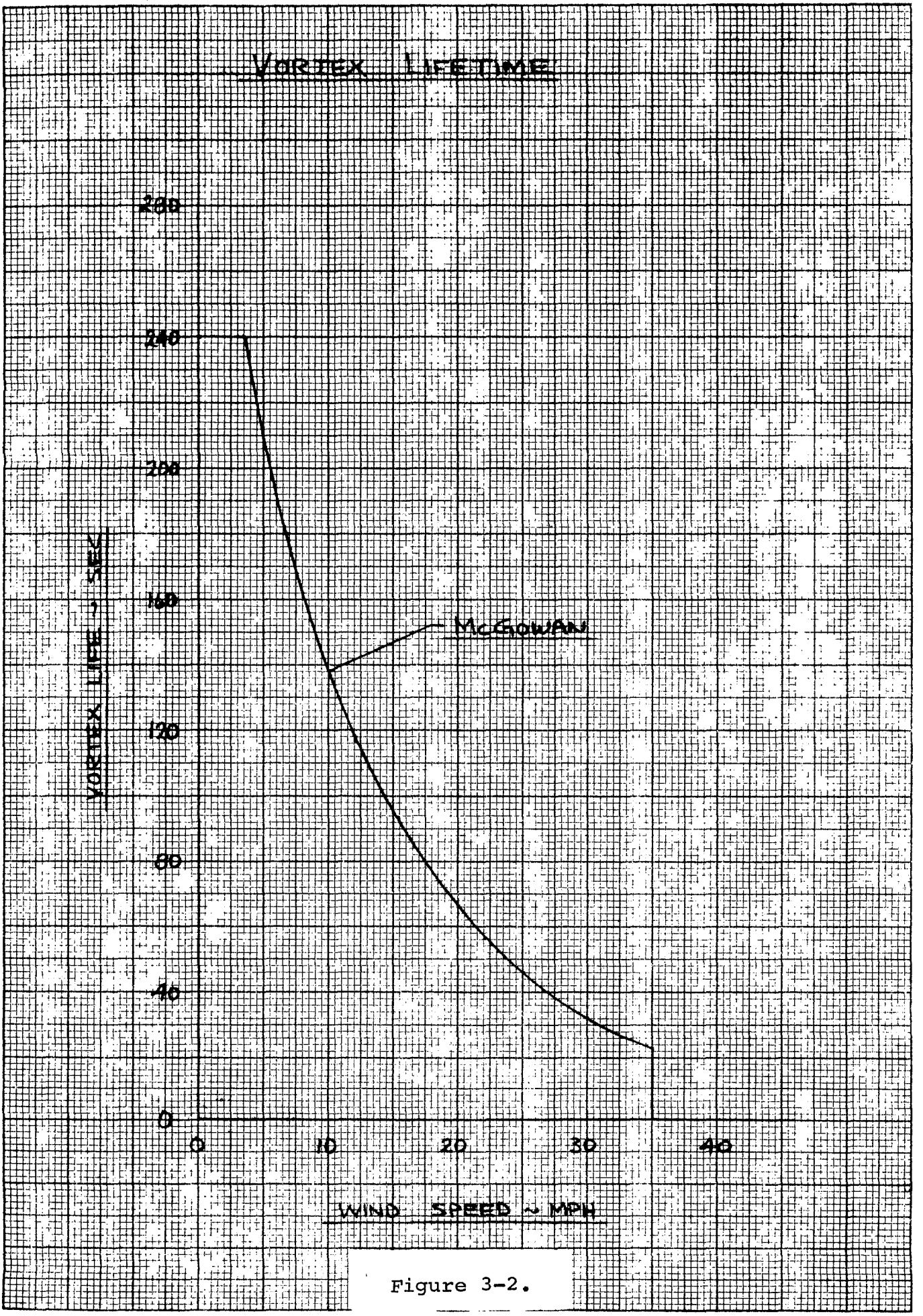
VORTEX LIFE TIME
280
240
200
160
120
80
40
0
VORTEX LIFE - SEC
McGOWAN
0
10
20
30
40
WIND SPEED ~ MPH

Figure 3-2.

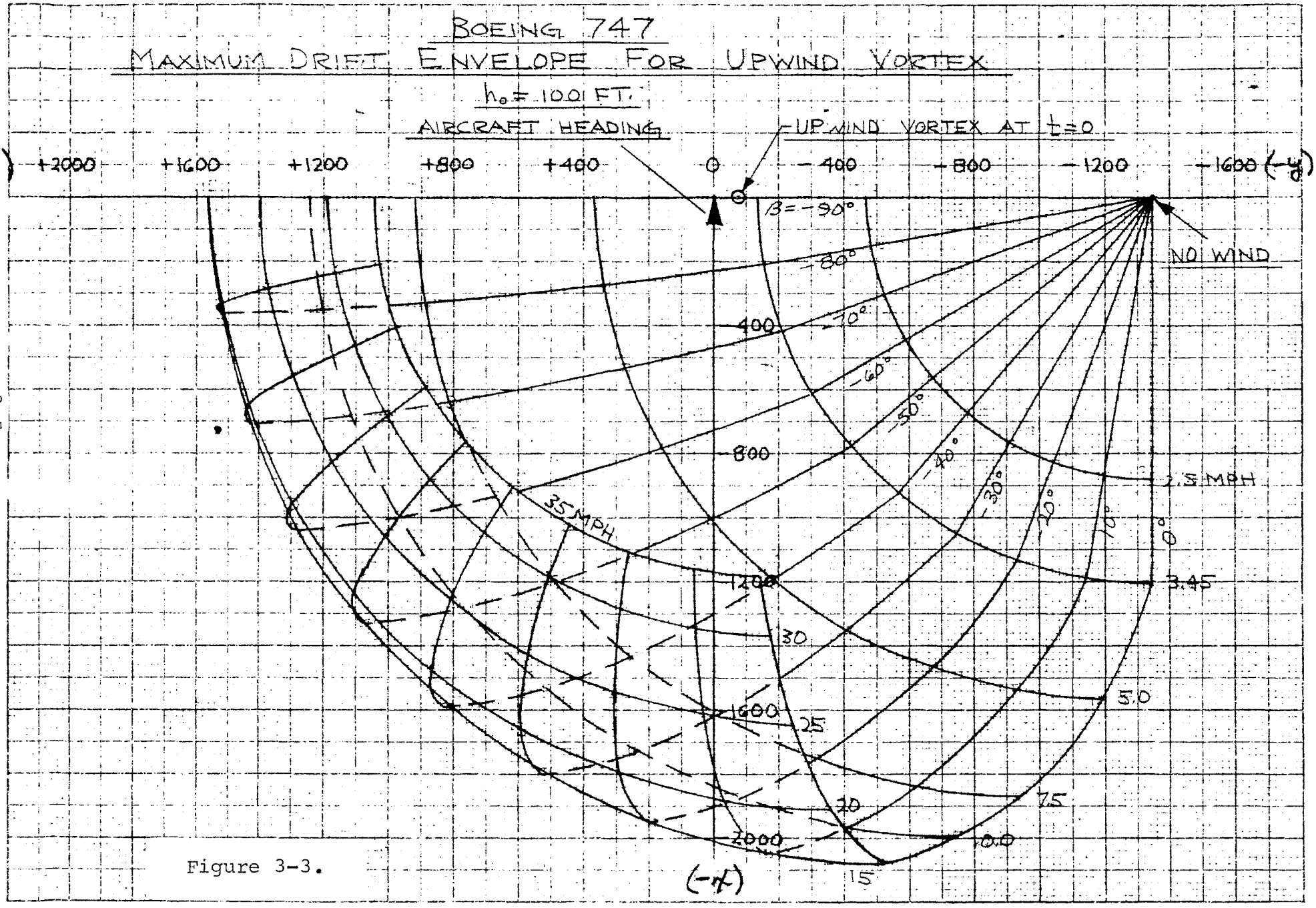
BOEING 747
MAXIMUM DRIFT ENVELOPE FOR UPWIND VORTEX
h_o = 1001 FT.
AIRCRAFT HEADING
UP WIND VORTEX AT t=0
(y)
+2000
+1600
+1200
+800
+400
0
-400
-800
-1200
-1600
(-y)
β=-90°
-80°
-70°
-60°
-50°
-40°
-30°
-20°
-10°
0°
NO WIND
400
800
1200
1600
2000
35 MPH
2.5 MPH
3.45
5.0
7.5
10.0
30
25
20
15
(-x)

Figure 3-3.

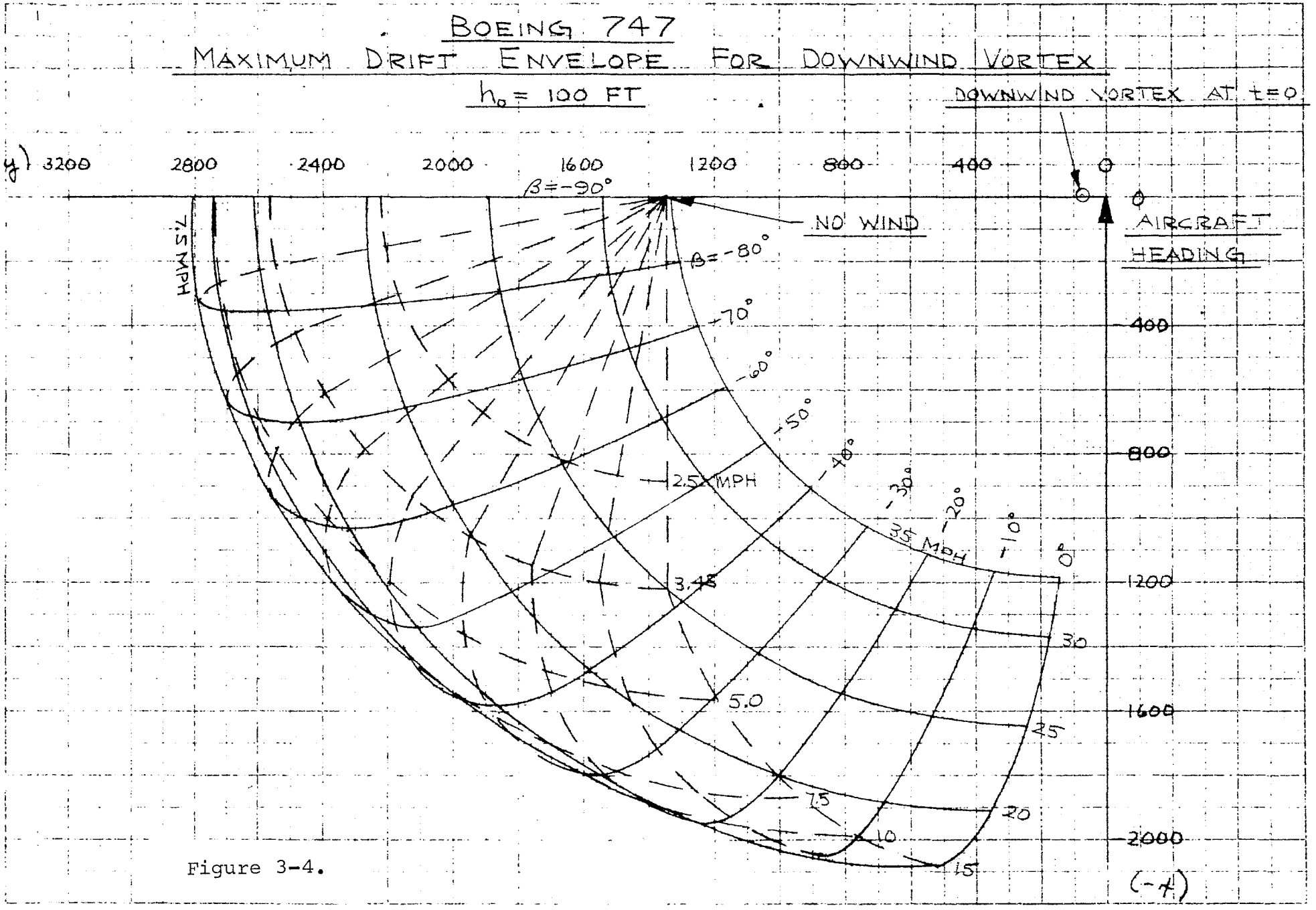
BOEING 747
MAXIMUM DRIFT ENVELOPE FOR DOWNWIND VORTEX
h_o = 100 FT
DOWNWIND VORTEX AT t=0
(y) 3200
2800
2400
2000
1600
1200
800
400
0
β=-90°
NO WIND
AIRCRAFT HEADING
7.5 MPH
β=-80°
-70°
-60°
-50°
-40°
-30°
-20°
-10°
0°
2.5 MPH
3.75
5.0
7.5
10
15
20
25
30
35 MPH
400
800
1200
1600
2000
(-y)

Figure 3-4.

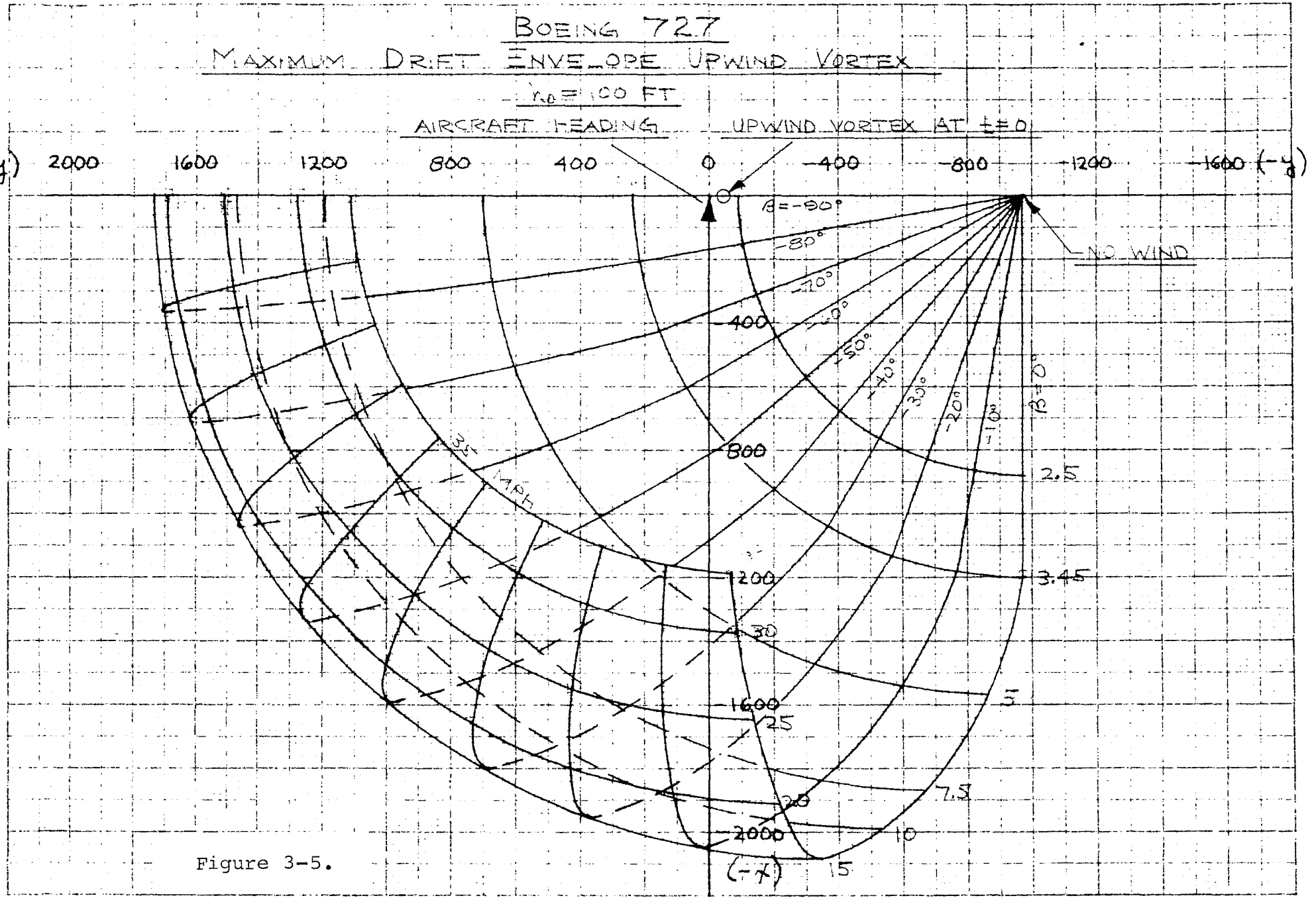
BOEING 727
MAXIMUM DRIFT ENVELOPE UPWIND VORTEX
h_0 = 100 FT
AIRCRAFT HEADING
UPWIND VORTEX AT ±=0
(y) 2000 1600 1200 800 400 0 -400 -800 -1200 -1600 (-y)
β=-90°
-80°
-70°
-60°
-50°
-40°
-30°
-20°
-10°
β=0°
NO WIND
400
800
1200
1600
2000
(-z)
35 MPH
2.5
3.45
5
7.5
10
15
20
25
30

Figure 3-5.

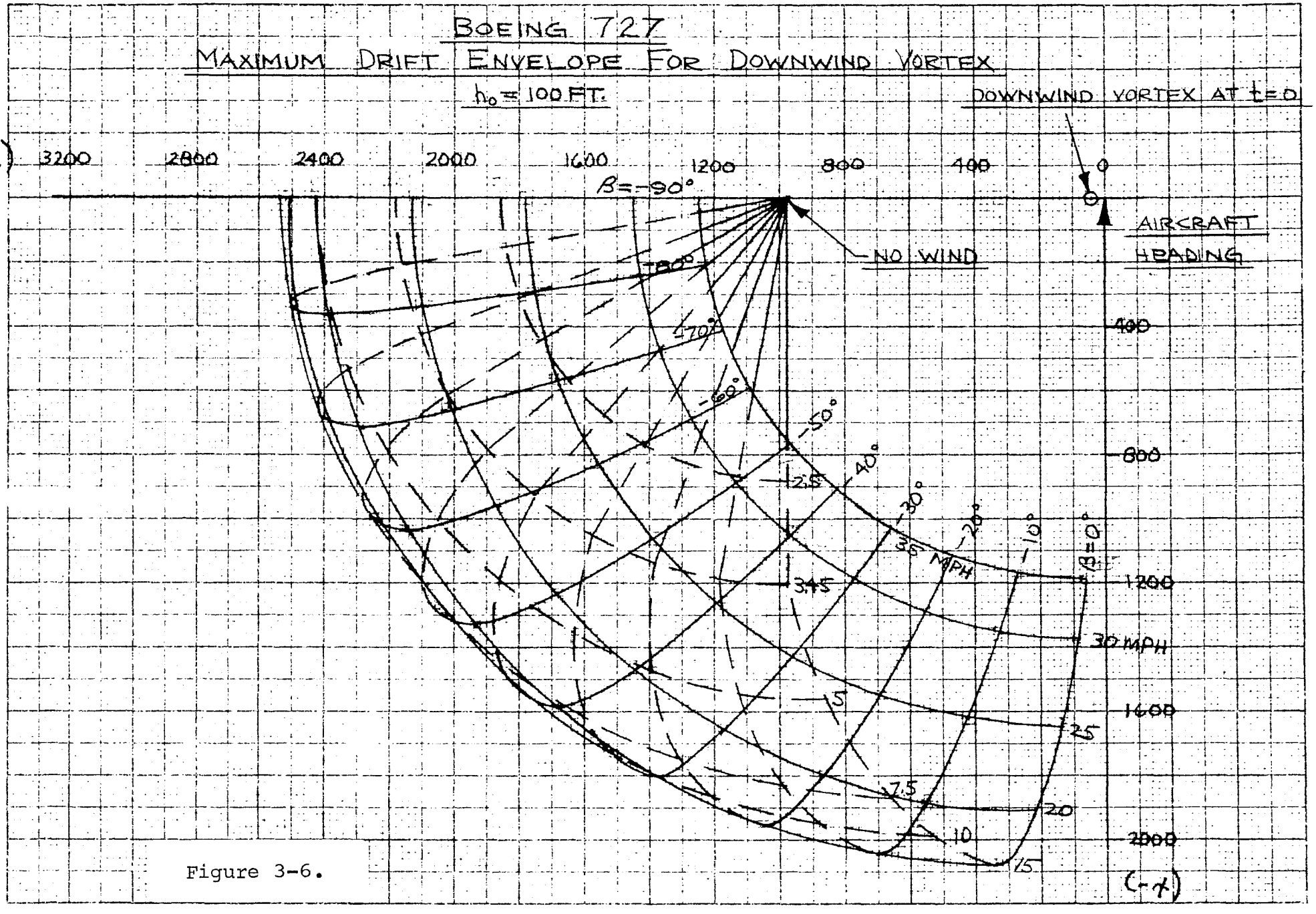
BOEING 727
MAXIMUM DRIFT ENVELOPE FOR DOWNWIND VORTEX
h_o = 100 FT.
DOWNWIND VORTEX AT t=0
(y)
3200
2800
2400
2000
1600
1200
800
400
0
β=-90°
-80°
-70°
-60°
-50°
-40°
-30°
-20°
-10°
β=0°
NO WIND
AIRCRAFT HEADING
400
800
1200
1600
2000
(-x)
2.5
3.5
7.5
10
15
20
25
30 MPH
35 MPH

Figure 3-6.

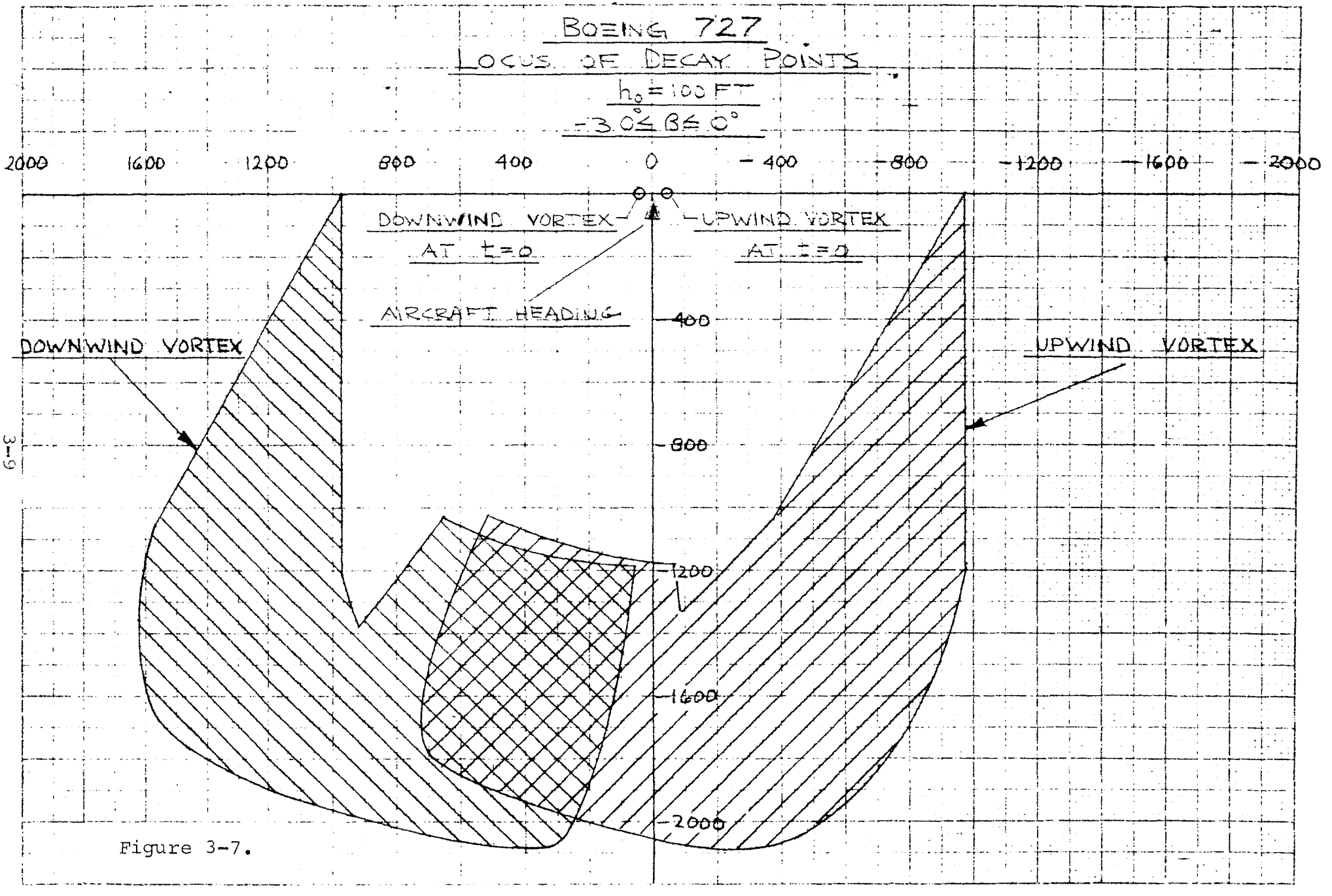
BOEING 727
LOCUS OF DECAY POINTS
h_o = 100 FT
-3.0° ≤ β ≤ 0°
2000
1600
1200
800
400
0
-400
-800
-1200
-1600
-2000
DOWNWIND VORTEX AT t=0
UPWIND VORTEX AT t=0
AIRCRAFT HEADING
DOWNWIND VORTEX
UPWIND VORTEX
400
800
1200
1600
2000

Figure 3-7.

B-727 aircraft, when the wind heading varies from 0 to 35 MPH and from a heading of -30^{o} to 0^{o}. The shaded region corresponds to the locus of positions of the vortices when they have decayed to a harmless tangential speed level.

Figure 3-8 shows the locus of decay points when the wind is allowed to vary from a heading of -30^{o} to $+30^{o}$ and can be obtained from Figure 3-7 by rotating the shaded regions around the aircraft heading axis.

Figure 3-9 shows the maximum drift data for the downwind vortex of the B-727 aircraft when flying out of ground effect where the entire vortex motion consists of wind drift. This data can be applied to the upwind vortex or to the B-747 aircraft simply by shifting the data with respect to the origin or shifting the initial position of the vortex.

Figure 3-10 shows the locus of decay points for the B-727 aircraft and is comparable to Figure 3-8 except here the aircraft is flying out of ground effect.

3.3 COMPARISON OF DRIFT ENVELOPES WITH EXPERIMENTAL DATA

The analysis of the performance requirements of a vortex monitoring system must be based on estimated vortex behavior as determined by idealized mathematical models. The degree to which these models represent actual vortex behavior is of major importance to the degree of authenticity afforded the results. Since comparisons between theoretical vortex models and measured data are few, an attempt was made in the present study to compare the drift envelopes presented for the B-727 with experimental data.

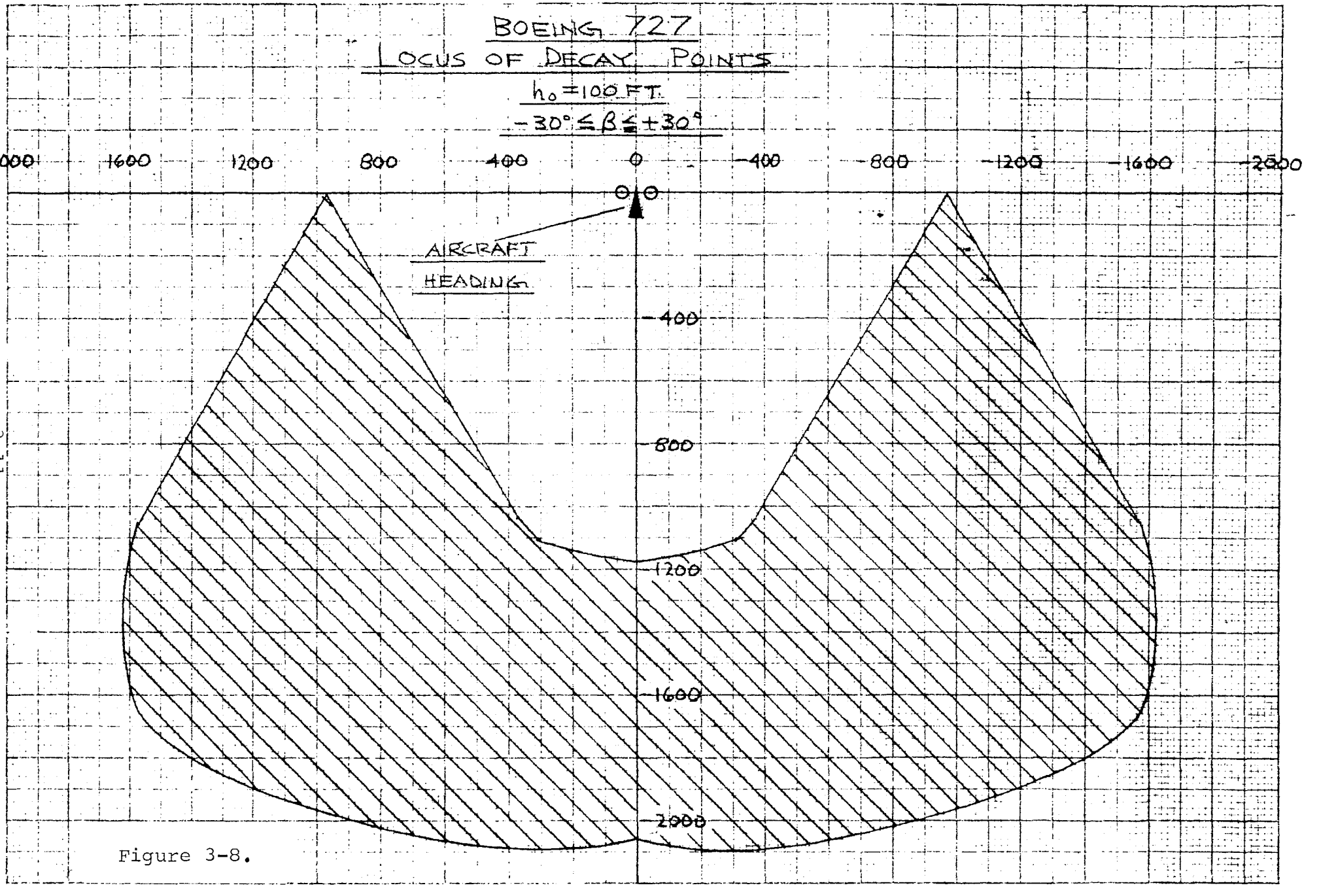
BOEING 727
LOCUS OF DECAY POINTS
h_o = 100 FT.
$-30° \leq \beta \leq +30°$
2000
1600
1200
800
400
0
-400
-800
-1200
-1600
-2000
AIRCRAFT HEADING
-400
-800
-1200
-1600
-2000

Figure 3-8.

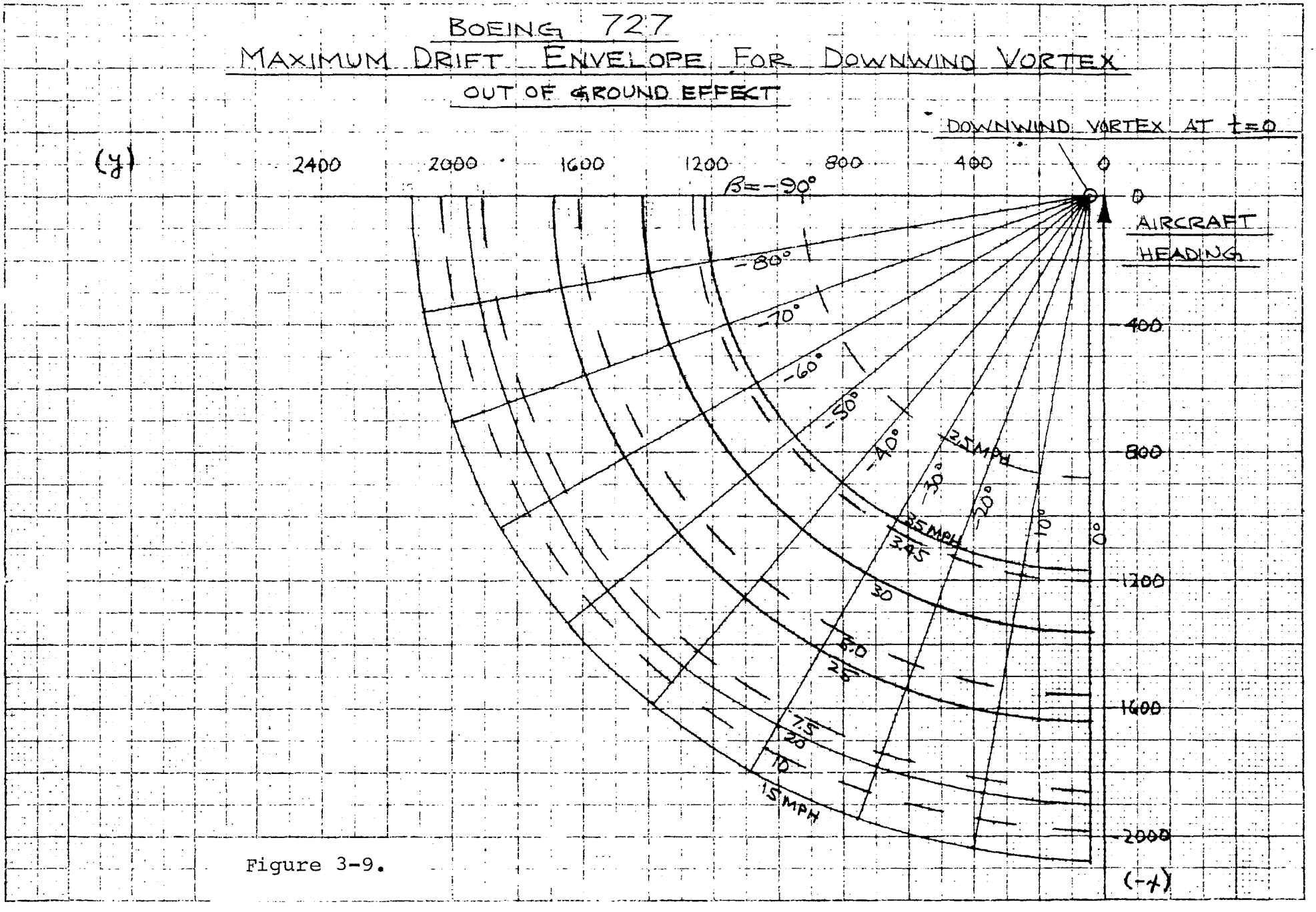
BOEING 727
MAXIMUM DRIFT ENVELOPE FOR DOWNWIND VORTEX
OUT OF GROUND EFFECT
DOWNWIND VORTEX AT t=0
(y)
2400
2000
1600
1200
800
400
0
β=-90°
-80°
-70°
-60°
-50°
-40°
-30°
-20°
-10°
0°
AIRCRAFT HEADING
400
800
1200
1600
2000
(-y)
25 MPH
35 MPH
30
20
15 MPH

Figure 3-9.

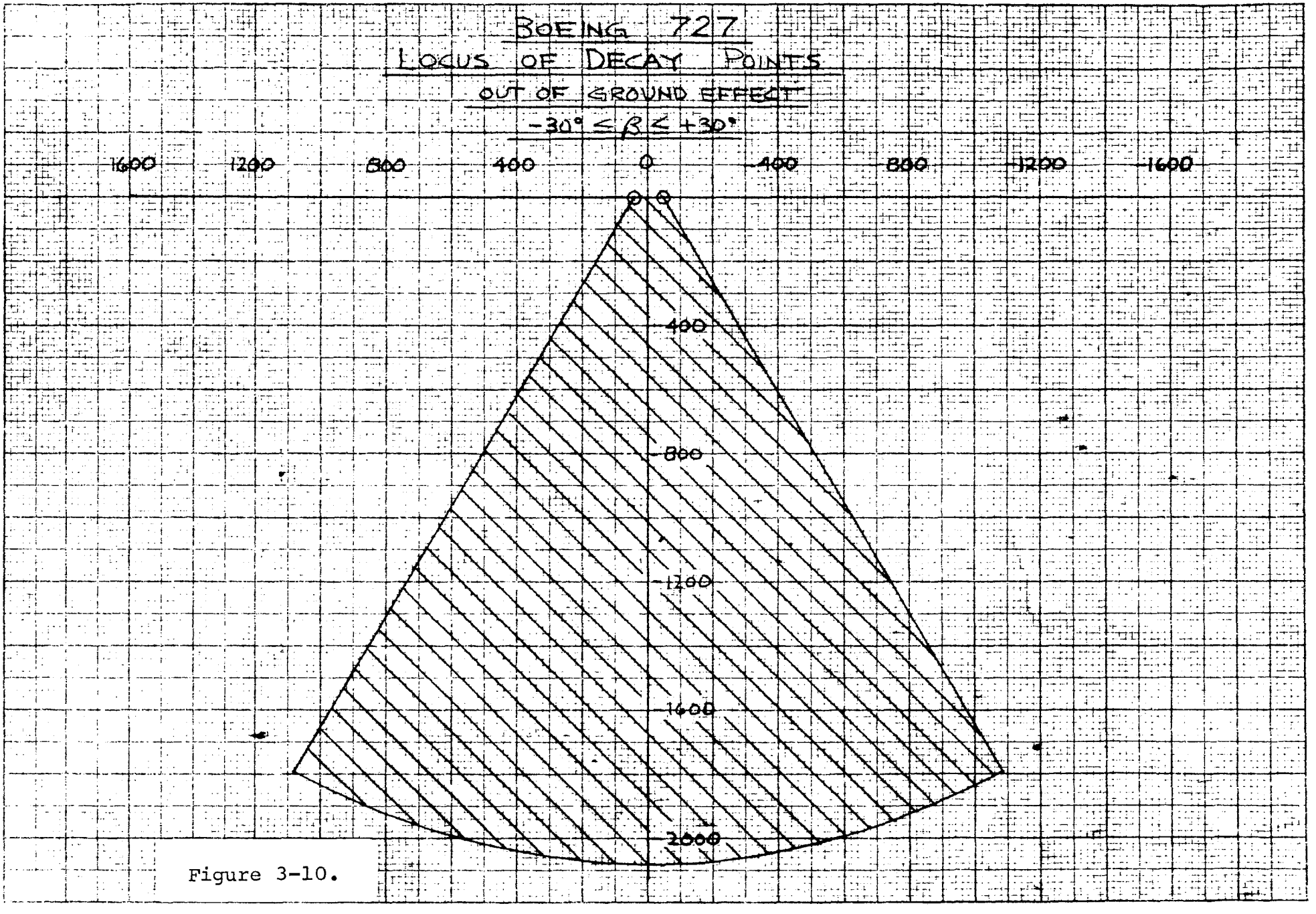
BOEING 727
LOCUS OF DECAY POINTS
OUT OF GROUND EFFECT
-30° ≤ β ≤ +30°
1600
1200
800
400
0
-400
-800
-1200
-1600
400
800
1200
1600
2000

Figure 3-10.

During tests conducted at NAFEC during May and June 1970 (Reference 5) some 42 flights were flown by a B-727 aircraft past a tower instrumented to record vortex information. In all passes except 34 and 35, the aircraft was in the landing configuration. Considerable data was recorded during these flybys, including aircraft heading, altitude, distance from tower, age of vortex when intercepting tower, wind direction, and wind velocity. The information recorded was sufficient to compare (in a very preliminary fashion) the theoretical drift envelopes with data extrapolated from the experimental tests. The manner in which this was accomplished and the results obtained are described below.

The geometry of the test site at NAFEC is shown schematically in Figure 3-11. The tests were conducted adjacent to Runway 22, which has a magnetic orientation of 220 degrees. Most flights were conducted with the aircraft in the landing configuration. Table 3-2 summarizes the pertinent data recorded and lists several calculated quantities. The relationship between the angle β, which was defined in Figure 3-1 and the angle θ_w, which is the wind direction measured from true North, is shown in Figure 3-12. Neglecting the magnetic compass variation at NAFEC, Atlantic City (less than 15 degrees) the angle β is given by

$$\beta = 220^{\circ} - \theta_w \qquad (3\text{-}1)$$

Since the drift envelopes are symmetrical, all experimental data points were referred to an equivalent β (β_{EFF}) lying between 0 and -90 degrees for which the absolute value of the lateral and downrange displacements are equivalent. This enabled all points to be plotted with the same format as the drift envelopes previously shown.

Using the data from Table 3-II, the average lateral drift velocity ($\dot{y}$) and the lateral distance at decay (y) were computed

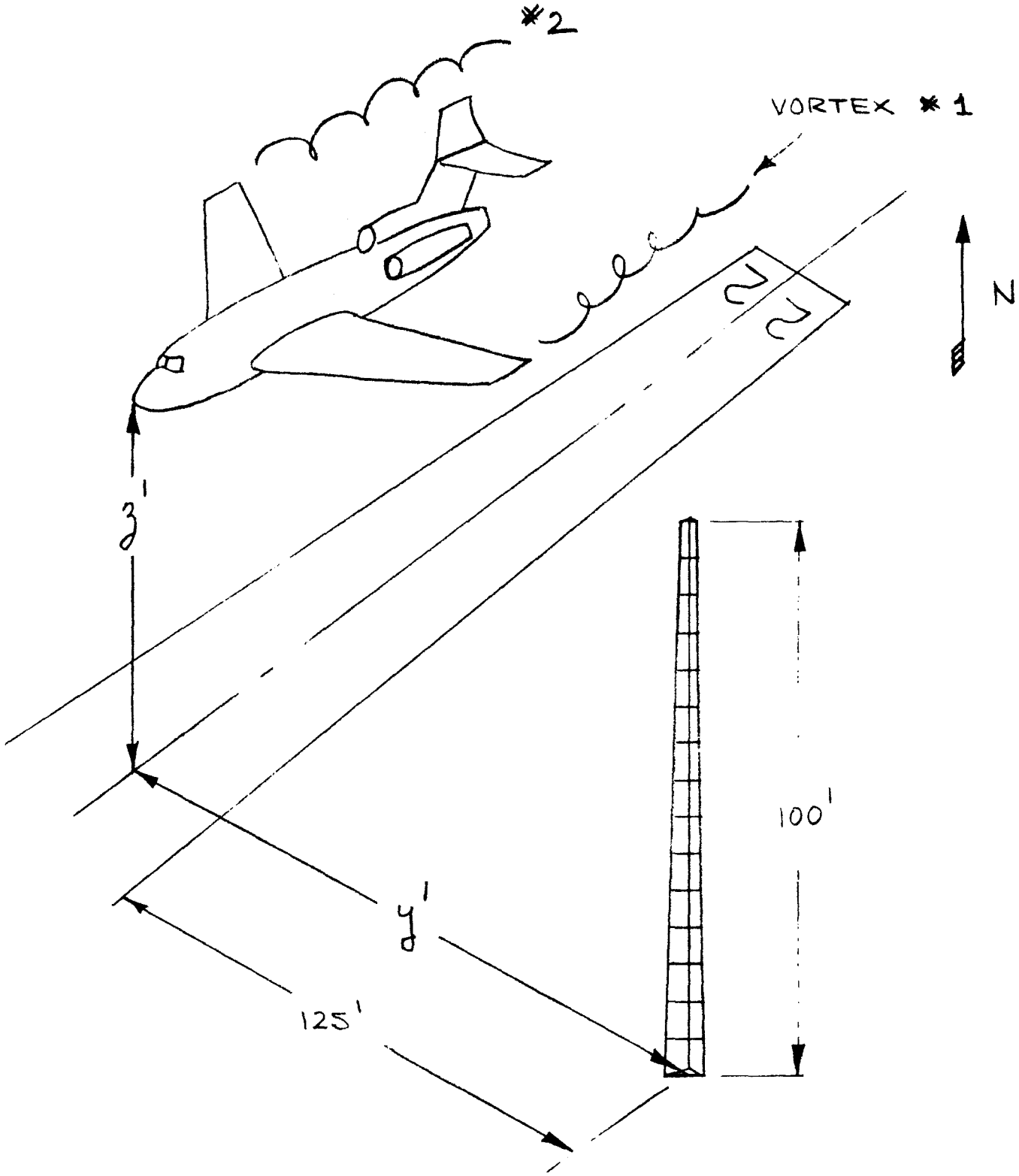

Figure 3-11. Geometry of NAFEC Test Site

NAFEC TEST DATA AND COMPUTED QUANTITIES

FOR B-727 AIRCRAFT

PASS	NO	Y^1	Z'	AGE	θ_w	V_w	t_{Max}	β	β_{Eff}	Δy	y
1	1	233	59	12.1	310	11	128	-90	-90	1894	1948
2		203	46	10.2	310	11	128	-90	-90	1869	1923
3		185	57	8.6	310	12	118	-90	-90	1794	1848
4		162	59	6.1	310	11	128	-90	-90	2266	2320
5		233	67	10.7	310	10	138	-90	-90	2304	2358
6		209	73	10.6	315	10	138	-95	-85	2015	2069
7		178	71	8.3	320	12	118	-100	-80	1758	1812
8		151	71	7.7	325	11	128	-105	-75	1613	1667
9		237	101	12.6	325	11	128	-105	-75	1856	1910
10		210	92	10.5	320	11	128	-100	-80	1907	1961
11		175	78	9.5	325	11	128	-105	-75	1626	1680
12		143	91	5.7	325	13	110	-105	-75	1716	1770
13		232	75	13.7	330	13	110	-110	-70	1430	1484
14		223	99	8.1	340	12	118	-120	-60	2466	2520
15		199	102	7.7	330	16	89	-110	-70	1673	1727
16		175	92	5.1	330	18	76	-110	-70	1801	1855
17		150	94	2.7	325	20	67	-105	-75	2385	2439
19		209	35	12.1	360	14	103	-140	-40	1318	1372
20		226	39	12.7	360	14	103	-140	-40	1391	1445
21		176	41	8.9	360	13	110	-140	-40	1507	1561
22		145	42	7.3	360	13	110	-140	-40	1375	1429
23		225	40	12.1	360	12	118	-140	-40	1664	1718
24		209	46	11.5	360	11	128	-140	-40	1728	1782
25		173	33	9.4	360	10	138	-140	-40	1753	1807
26		235	71	13.8	10	10	138	-150	-30	1808	1862
27		210	49	12.2	10	11	128	-150	-30	1638	1692
28		185	58	9.6	10	11	128	-150	-30	1741	1795
29		149	54	8.0	20	12	118	-160	-20	1404	1458

Table 3-II. (continued next page)

PASS	NO	Y	Z′	AGE	θ_w	V_w	t_{Max}	β	β_{Eff}	ΔY	Y
30	1	227	73	13.8	5	10	138	-145	-35	1725	1779
31		209	77	13.1	10	12	118	-150	-30	1392	1446
32		188	57	13.5	15	10	138	-155	-25	1366	1420
33		150	60	20.6	15	9	150	-155	-25	705	759
34		200	94	11.5	10	9	150	-150	-30	1905	1959
35		189	92	12.3	350	9	150	-130	-40	1650	1704
36		240	83	13.5	325	10	138	-105	-75	1904	1958
37		218	105	16.3	320	10	138	-100	-80	1394	1448
38		186	86	14.6	355	12	118	-135	-45	1062	1116
39		139	86	4.1	340	12	118	-120	-60	2443	2497
40		217	131	19.4	355	8	162	-135	-45	1361	1415
41		212	124	10.0	340	7	176	-120	-60	2781	2835
42		179	98	25.1	35	9	150	-175	-5	750	804
43		152	110	39.5	40	13	110	-180	0	275	329
4	2	162	59	31.0	310	11	128	-90	-90	896	842
6		209	73	38.0	315	10	138	-95	-85	952	898
7		178	71	31.0	320	12	118	-100	-80	885	831
8		151	71	25.9	325	11	128	-105	-75	1011	957
9		237	101	24.1	325	11	128	-105	-75	1549	1495
10		210	92	26.8	320	11	128	-100	-80	1267	1213
12		143	91	14.1	325	13	110	-105	-75	1540	1486
14		223	99	21.1	340	12	118	-120	-60	1546	1492
15		199	102	15.8	330	16	89	-110	-70	1424	1370
16		175	92	10.7	330	18	76	-110	-70	1626	1572
17		150	94	5.4	325	20	67	-105	-75	2533	2479
30		227	73	41.7	5	10	138	-145	-35	925	871
35		189	92	29.8	350	9	150	-130	-40	1230	1176
36		240	83	22.8	325	10	138	-105	-75	1780	1726
39		139	86	11.5	340	12	118	-120	-60	1982	1928
41		212	124	20.9	340	7	176	-120	-60	2235	2181

Table 3-II.(continued)

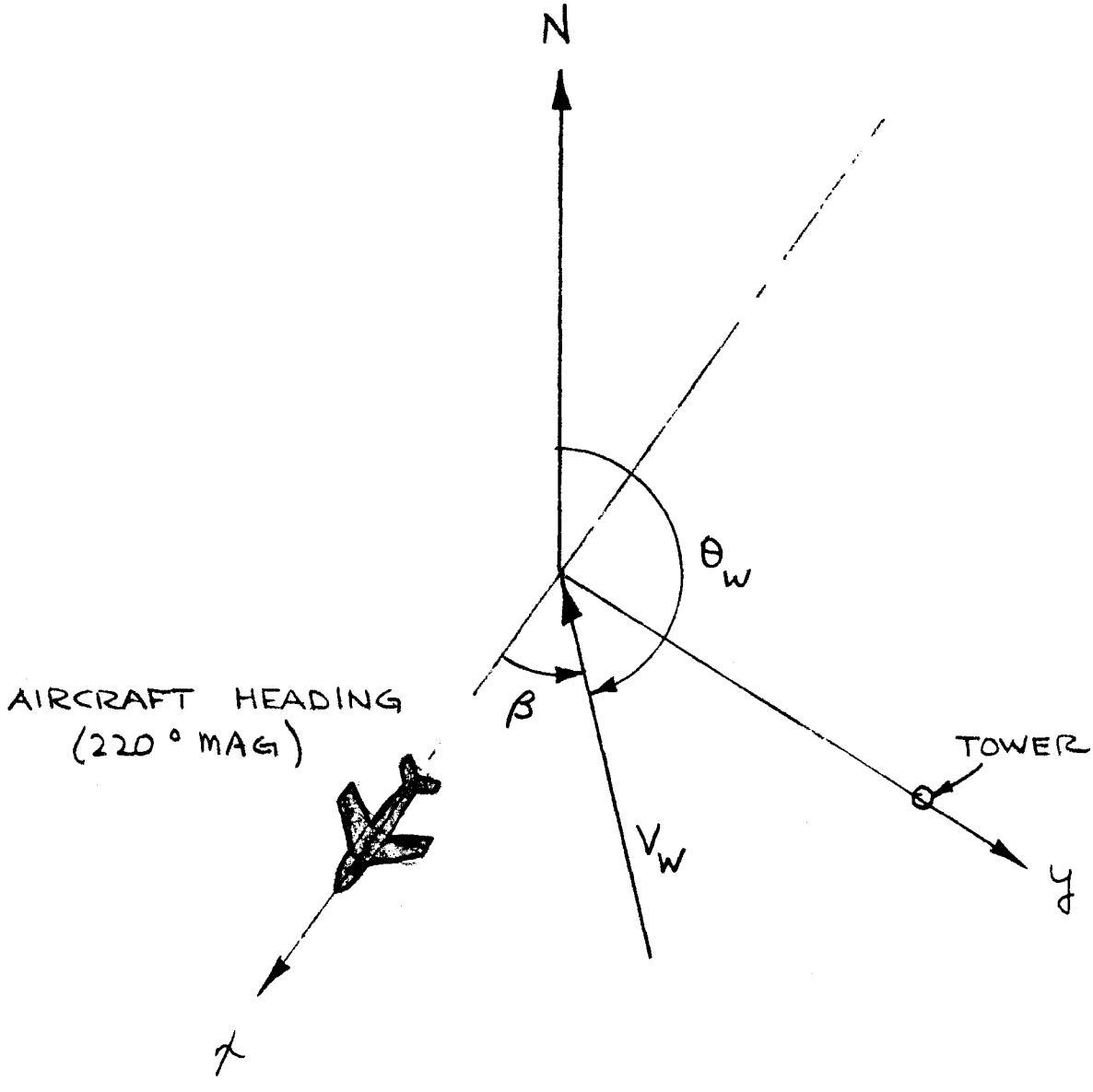

Figure 3-12. Angles Defining Wind Vector Orientation

from the following equations:

$$\dot{y}_1 = \frac{y' - b/2}{Age} \quad (3\text{-}2)$$

$$\dot{y}_2 = \frac{y' + b/2}{Age} \quad (3\text{-}3)$$

$$\Delta y_n = \dot{y}_n \, t_{Max} \quad (3\text{-}4)$$

$$n = 1,2 \quad (3\text{-}5)$$

$$y_1 = \Delta y_1 + b/2 \quad (3\text{-}6)$$

$$y_2 = \Delta y_2 - b/2 \quad (3\text{-}7)$$

where the subscript 1 refers to the vortex nearest the tower (the downwind vortex in all cases included herein) as shown in Figure 3-11, b is the wing span (108 feet for the B-727) and t_{Max} is the maximum vortex lifetime as defined in Figure 3-2 as a function of the wind speed.

The age of the vortex given in Reference 5 and listed in Table 3-2 is measured with respect to the time when the aircraft wing tip is abreast of the tower. This introduces an error whenever the wind direction departs from a heading of $\pm$90 degrees. Figure 3-13 illustrates the geometrical reason for this error. The figure shows the conditions existing with a tailwind. The vortex element which passes the tower originates upwind of the tower and drifts along the dotted line under the combined influence of the wind and ground effect. An interval of Δt elapses between the time the aircraft is in this first position (t_0) and when it passes abreast of the tower (t_1). The AGE recorded at NAFEC is the time from the tower abreast position (t_1) to the time when the vortex passes the tower (t_2). The true lateral drift rate is given by

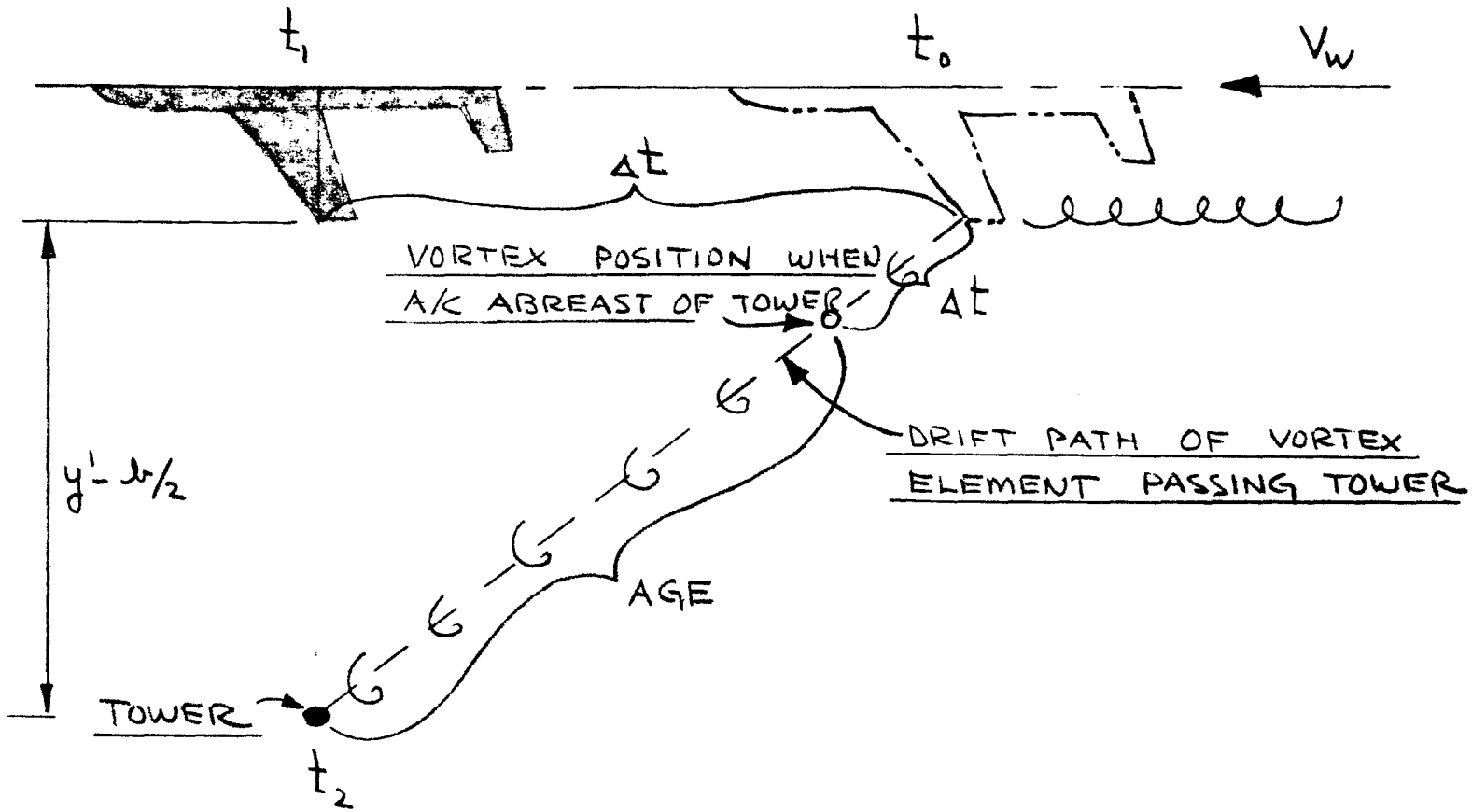

Figure 3-13. Geometry of Vortex Timing Error

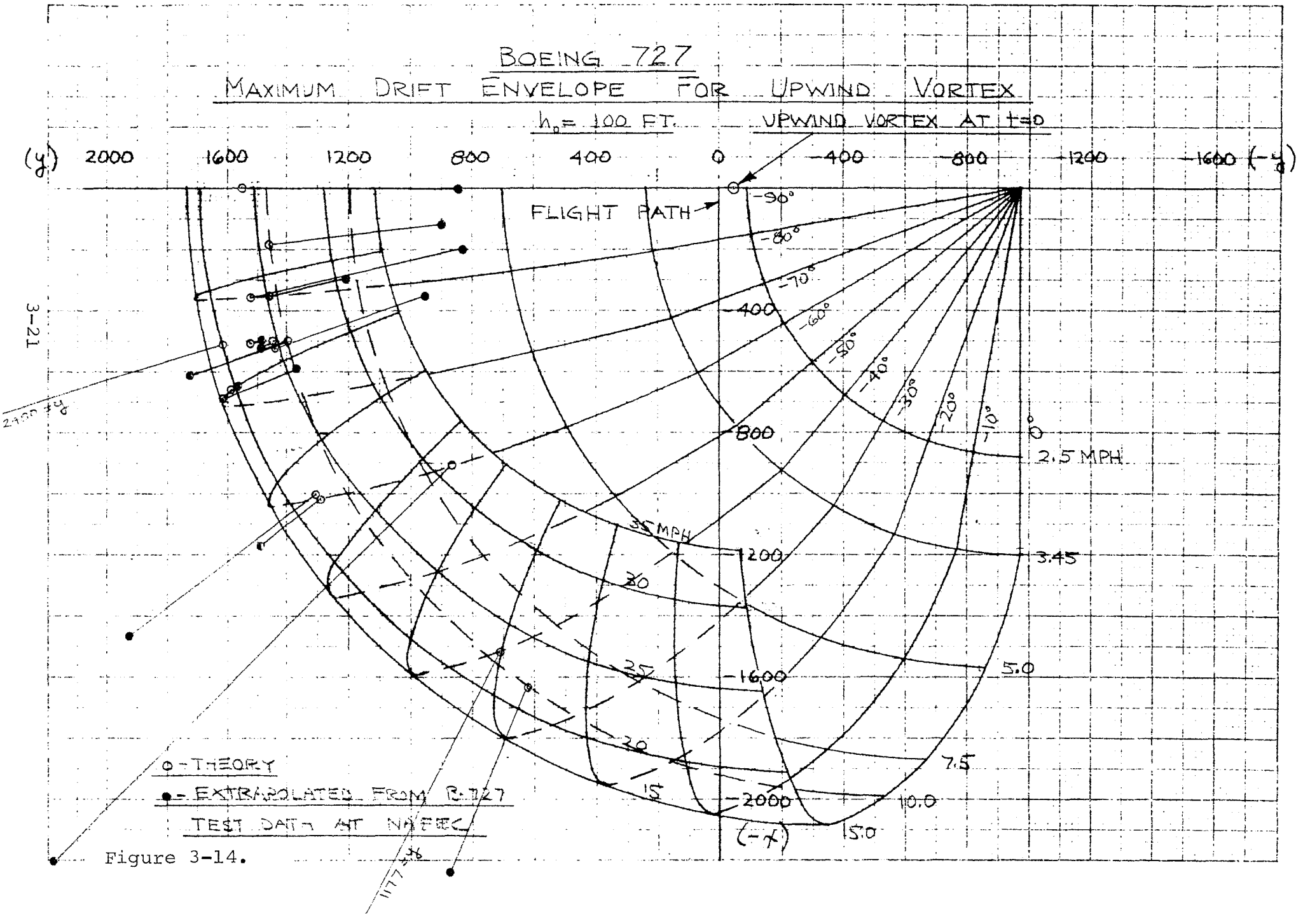
BOEING 727
MAXIMUM DRIFT ENVELOPE FOR UPWIND VORTEX
h_0 = 100 FT.
UPWIND VORTEX AT t=0
(y/b)
2000
1600
1200
800
400
0
-400
-800
-1200
-1600
(-y/b)
FLIGHT PATH
-90°
-80°
-70°
-60°
-50°
-40°
-30°
-20°
-10°
0°
400
800
1200
1600
2000
2.5 MPH
3.45
5.0
7.5
10.0
15.0
35 MPH
30
25
20
15
(-x)
o - THEORY
● - EXTRAPOLATED FROM B-727 TEST DATA AT NAFEC

Figure 3-14.

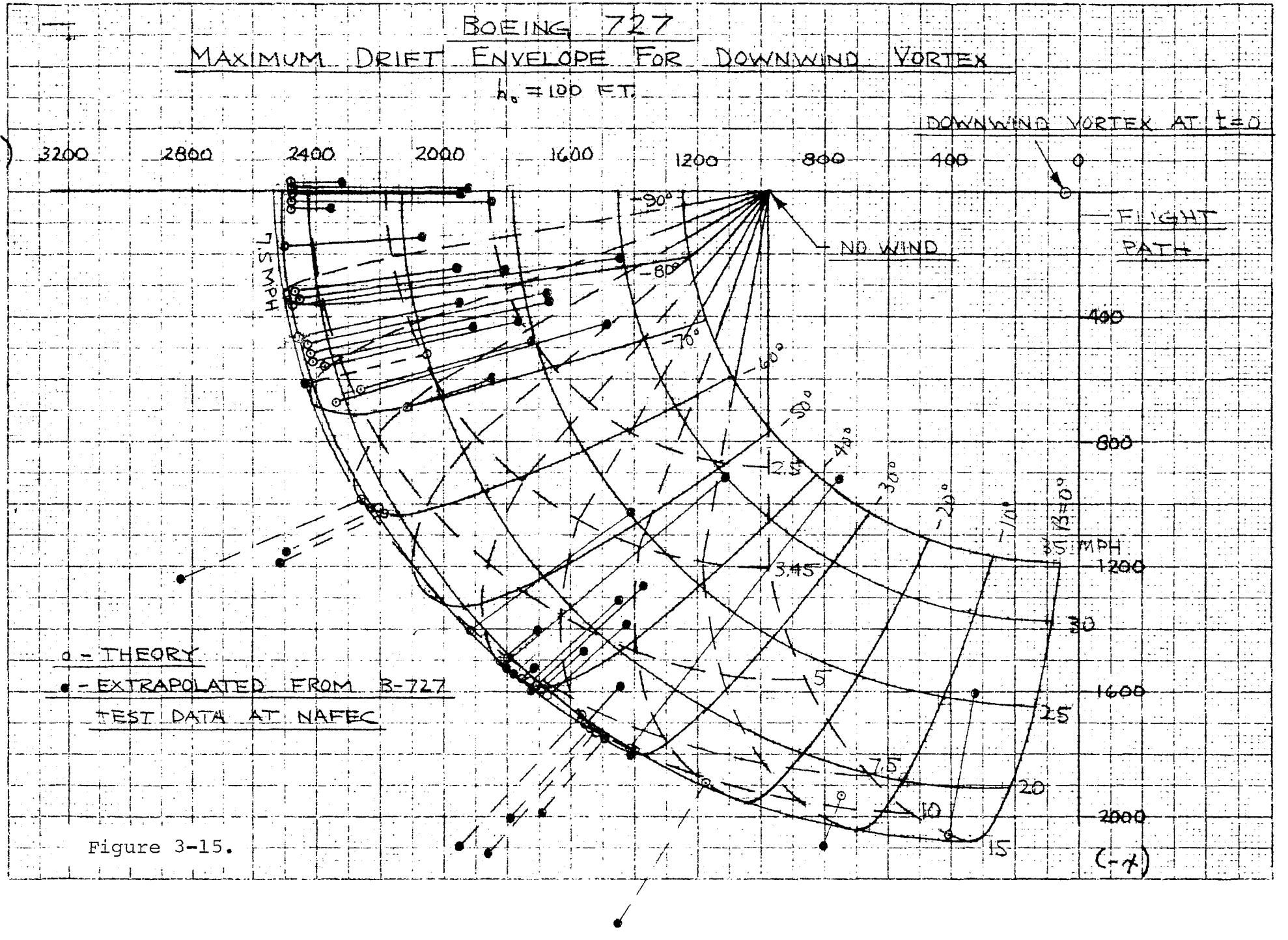
BOEING 727
MAXIMUM DRIFT ENVELOPE FOR DOWNWIND VORTEX
h_o = 100 FT.
DOWNWIND VORTEX AT t=0
(y)
3200
2800
2400
2000
1600
1200
800
400
0
FLIGHT PATH
NO WIND
-90°
-80°
-70°
-60°
-50°
-40°
-30°
-20°
-10°
β=0°
15 MPH
35 MPH
2.5
3.45
5
7.5
10
15
20
25
30
400
800
1200
1600
2000
(-y)
o - THEORY
● - EXTRAPOLATED FROM B-727 TEST DATA AT NAFEC

Figure 3-15.

$$\dot{y}_T = \frac{y' - b/2}{AGE \pm \Delta t} \qquad (3\text{-}7)$$

Since Δt is not included in the AGE of the vortex, an error that varies with the wind vector, the speed of the aircraft, and the ground effect speed is introduced. For a wind 5 degrees from a true tailwind, Reference 5 indicates that 26% over-estimation of the drift speed results. This error is usually less than a second and was ignored in the present study.

The extrapolated lateral drift distances given by Equations 3-5 and 3-6 were plotted (solid symbols) as a function of β on the drift envelopes for the B-727 aircraft (Figures 3-5 and 3-6) as shown in Figures 3-14 and 3-15 for the downwind and upwind vortices, respectively. The corresponding theoretical points for the same wind vector are shown by the open symbol and the two points are joined by a line which is dashed when the extrapolated test data point falls beyond the theoretical point.

In effect, the results indicate crudely the accuracy with which the lateral drift rate is being estimated, and indicate nothing specific about the endurance of the vortex. If the theoretical and experimental drift rates agreed both sets of decay points would agree. It appears from this simplified analysis that the actual drift rate is both over and underestimated by theory and that the average uncertainty is of the order of $\pm$30%.

It is recommended that a more thorough analysis of drift rate accuracy be performed. Initial aircraft conditions and wind vector from NAFEC test data could be used to compute theoretical vortex motion. Knowing the lateral distance from aircraft to tower the corresponding downrange vortex displacement can be determined and a time equivalent to the measured AGE of the vortex computed. The two vortex ages can then be compared to obtain the percentage error between theory and experiment for all test data points. This would provide statistical data for a reasonably sized sample on the accuracy with which a given theoretical model can duplicate experimental results.

SECTION 4

INTERACTION OF A VORTEX MONITORING SYSTEM WITH NAS ATC ELEMENTS

4.1 INTRODUCTION

The information presented in this section is not as comprehensive as originally intended because of the inability to obtain direct inputs from the FAA due to an outstanding proposal from Raytheon to the FAA of a conflicting nature.

Since the greatest hazard from wake turbulence occurs near the ground, a vortex monitoring system must concentrate on wake turbulence in the terminal area near the airport surface. This requires that the system integrate with other terminal ATC systems. Conversely, enroute vertical separation standards of 1,000 feet or greater generally preclude wake turbulence encounters. Therefore, it can be assumed that enroute VFR aircraft will continue to bear the responsibility for wake avoidance and ground based vortex monitoring systems will not be required for enroute traffic now or in the future.

Wake turbulence avoidance calls for consideration in the planning of airport/aircraft operations to increase airport capacity as well as in the direct avoidance of the hazard. Operational control must be spread among the elements of terminal air traffic control; namely, approach control, local control, and departure control. Surface traffic control may play an auxiliary role in clearing runways, but should not interface directly with a vortex monitoring system.

Key factors which affect the wake turbulence hazard are airport geometry, wind, and landing and departure patterns. In this section the significance of these factors will be reviewed, the automatic and manual facilities which terminal air traffic control has and will have at its disposal over the next ten years are described, present separation standards are reviewed,

and the manner in which a wake turbulence monitoring system might be integrated with these facilities is examined. Also discussed are operations under VFR conditions, the ARTS-III system, the ARTS-III system with automatic metering and spacing, and the possible impact of improved ILS and automatic data link capability on the wake turbulence system. Finally, runway layouts and wind rose data for major airports in the New England area are presented.

4.2 PRESENT SEPARATION STANDARDS

On 1 March 1970 the FAA implemented new separation standards because of the hazard imposed by wake turbulence from heavy jets. These standards affected traffic in the terminal area but had no effect on enroute traffic because the enroute separation standards in effect were already adequate.

The standards currently in use[1] are described below. A heavy jet is defined as an aircraft with a gross takeoff weight of greater than 300,000 lbs.

(1) When only radar separation is being applied, a minimum of five miles is required by any IFR aircraft following a heavy jet.

(2) When a VFR aircraft is being radar vectored or sequenced behind a heavy jet, provide a minimum of five (5) miles unless the VFR aircraft is known to be above the heavy jet or 1,000 feet or more below it.

(3) Use at least a two-minute interval behind a departing IFR or VFR heavy jet for aircraft departing on a parallel runway separated by 2500 feet or more if the succeeding departure flight path will converge with the path of the heavy jet.

---

(1) Krupinsky, E., "Wake Turbulence--Its Effect on the ATC System," FAA Symposium on Turbulence, Washington, D.C., March 22-24, 1971.

(4) Use at least a two-minute interval behind a VFR or IFR departing heavy jet for aircraft landing on a crossing runway if the arrival flight path will cross the take-off path behind the heavy jet and in front of the rotation point of the heavy jet.

(5) Use at least a two-minute interval behind a departing IFR or VFR heavy jet for aircraft departing on the same runway, parallel runways separated by less than 2500 feet or crossing runways if projected flight paths will cross.

When a heavy jet is operating behind another heavy jet, or for operations involving smaller jet aircraft, the limits are currently 3 miles and 1 minute respectively, or are unspecified.

For intersection take-offs a three-minute interval is used behind any turbojet aircraft.

4.3 RUNWAY GEOMETRY AND OPERATIONAL PROCEDURES

For wake turbulence considerations airport runway geometries fall into four major classifications; namely, single runway, dual runway, parallel runways, and crossing runways.

The present FAA separation standards, which require one minute between ordinary operations and two minutes after heavy jet operations, are inadequate. In most cases the two-minute separation is too conservative, resulting in lower runway utilization than necessary. Conversely, in the case where a slight crosswind is blowing, two-minute separation may be insufficient, resulting in following aircraft experiencing unacceptable disturbances when following at or below the approach path of the heavy jet. Clearly, separation procedures must be developed which take into account the surface wind information and vary the spacing accordingly.

A dual runway is a pair of parallel runways separated by less than 2500 feet. Operations on the two runways must be coordinated and separation minima between aircraft on the two approaches must be maintained. (The minimum separation is currently three miles.) Under certain wind conditions wake interference between runways can occur even when the runways are spaced as much as 2000 feet apart. Again, as in the single runway case, this is not cause for adopting standards that assume that wake interference will always exist. Rather the standard should vary with the surface wind.

Parallel runways separated by more than 2500 feet are independent of wake turbulence generated on the adjacent runway, but a problem may exist in the approach lanes. Normally the approach paths on these runways are parallel and at the same altitude-distance relationship from the ends of the runway. However, where this is not so, wake turbulence from aircraft on one approach path may intercept an aircraft following on the other approach path.

Vortex avoidance procedures (as opposed to separation standards) for crossing runway cases are discussed in FAA Advisory Circular Letter AC No. 9023B, 17 May 1971. When landing behind a heavy jet which is landing on a crossing runway, the pilot is instructed to cross above the heavy jet's flight path. When landing behind a heavy jet which is departing on a crossing runway, he is instructed to continue the approach provided that his rotation point is beyond the intersection. However, if the heavy jet rotates before the intersection, the pilot should cross above his flight path unless a landing is assured well before reaching the intersection.

Again, much of the time no hazard will exist in the crossing situation and the present separation standards are overly conservative. With a vortex monitoring system the wake location and surface wind conditions can be processed to predict hazard areas and allow the closer spacing of aircraft.

Airport operational procedures that affect runway selection must be considered in the development of wake avoidance systems. Present procedures will probably be modified as the significance of runway selection (as a function of wind vector) on the frequency of occurrence of vortex hazards is fully explored. Operational procedures vary from airport to airport such that no standard set of operational criteria can be assumed.

Choice of runway is usually based on the wind direction; the runway experiencing the maximum headwind (minimum crosswind) being the most desirable. If this were always true, choice of runway and system studies of vortex drift about the airport would be greatly simplified. However, this selection approach can be modified by a variety of other considerations; two significant ones are airport geometry and noise abatement procedures.

Airport geometry affects runway selection in subtle ways. For example, a runway may not possess suitable exits. This can result in exits being missed during landings involving minor overshoots, sometimes requiring aircraft to taxi to the end of the runway before exiting. This increase in runway occupancy may force a following aircraft into a missed approach. When a runway has this limitation, its capacity suffers and it is sometimes consciously or unconsicously avoided by controllers.

Airlines may also request the use of a particular runway because of its location relative to their terminal building. Runways may also be requested because of their length or because their orientation lies near to the approach or departure radial.

Noise abatement procedures have considerable impact on runway selection. At Logan Airport in Boston special anti-noise procedures[2] are in existence. These specify, primarily for take-off, the order of priority of runways to be used by traffic controllers. Runways are assigned in accordance with these priorities unless:

(2) "Anti-Noise Procedures Logan International Airport", Logan Tower Bulletin 68-1, July 18, 1968.

1) the wind exceeds 80 degrees from the runway heading; 2) the wind velocity exceeds 15 knots; or 3) the runway is not clear or is otherwise unsuitable. In the interest of safety a pilot may ask for and receive permission to depart from these priorities to the extent that air traffic and other conditions permit.

4.4 SIGNIFICANCE OF WIND IN A PREDICTION OR MONITORING ENVIRONMENT

Wake turbulence avoidance can be accomplished using a totally predictive approach relying solely on wind sensors and models of wake turbulence vortex transportation and decay, or, alternatively, it can utilize sensors which monitor the position of vortices at sampling locations and intervals. In either case it is necessary to predict the future location of the wake in order to determine possible conflicts between a vortex and an aircraft. The prediction accuracy will directly affect the runway capacity. Two factors affecting this accuracy are:

1) The prediction time interval. If arrival spacing is determined by vortex conflict prevention, then wind speed must be predicted three to ten minutes in advance to affect the manual or semi-automatic metering and spacing function performed by approach control which determines the arrival spacing. If no attempt is made to integrate wake conflict prevention into metering and spacing, then the prediction need only be one minute before touchdown in time for a decision to abort the landing if wind conditions cause a problem. Even if prevention is performed at the metering and spacing level, it will still be necessary to check for conflicts prior to landing to allow for wind variations beyond the limits assumed by the metering and spacing function.

2) The variation of the wind on the airport surface. If current wind sensors are used (typically one per airport except in the largest airports) the vortex transport rate would include a surface

wind velocity variation error. If vortex position can be measured directly by sensors, this source of error is eliminated.

The above error sources apply only to avoiding wake turbulence at or near the airport surface. Windspeed uncertainties will be even greater in the approach paths, unless wind data can be derived from comparisons of aircraft airspeed and groundspeed. Models of the variations of windspeed and heading with altitude are available and can be used to help correlate information received from aircraft and radar.

4.5 TERMINAL AIRSPACE AND RUNWAY UTILIZATION

In a busy single terminal area, arrivals and departures are normally assigned disjoint corridors so that interaction between them need not be considered. On the other hand, special coordination procedures must be invoked in multiple airport areas such as New York City. The complexity of effective dynamic conflict prevention in a multiple airport area is so great that it is anticipated that separation of arrivals and departures between airports will continue to be done procedurally in the time frame of interest. Therefore, wake turbulence monitoring systems need not be concerned with the interaction of arrival and departure streams of aircraft for single or multiple airports. Near the ground, however, there can be interaction between departures and arrivals.

Depending on load, a dual or single runway may be used for departures only, arrivals only, or operations may be mixed. Interaction between departures on a single or dual runway and interaction between two arrivals on a single or dual runway are the two most common situations of interest to a monitoring system. As facilities improve, aircraft touchdown and rollout times will become more predictable, aircraft will be spaced more closely, and it will become more critical to determine wake vortex hazards and plan operations to avoid these hazards.

4.6 VFR OPERATIONS

Under VFR operations the pilot is responsible for maintaining separation between himself and other aircraft and for avoiding wake turbulence. However, air traffic control does provide the pilot with advisories. At present these advisories can vary widely. In Houston, for example, a V/STOL runway is located just 1100 feet from a main runway used for heavy jets. During VFR conditions, these two runways are used independently. It is claimed that there has never been a wake turbulence encounter involving heavy jets. Since these runways are well within the drift limits of wake vortices, this may be the result of a prevailing wind which blows in a fortuitous direction. There are many such "lucky fields" in existence.

In a VFR advisory capacity, the wake turbulence monitoring system should determine when and where wind conditions and the resultant vortex drift will cause hazards on or near runways and approach paths. The controller can then advise the pilot via radio of the hazard on a particular runway or approach path and can hold, release, wave off or suggest modifications in flight path to avoid the hazard.

4.7 TOWER CAB CONSIDERATIONS

Controllers in the tower cab are concerned with the area within about five miles of the airport and below about 4000 feet. They are concerned with aircraft and other vehicles on the ground as well as those taking off and landing. At a typical major airport, the tower cab controllers do not establish the landing sequence of aircraft or the approach or departure patterns to be followed. They do establish departure sequencing and are responsible for runway utilization and sometimes for individual runway assignment (right or left). They are responsible for the safety of aircraft on or

near the ground and can direct aircraft to abort landings or perform other maneuvers in order to avoid safety hazards of any kind. Of principal concern is insuring that a preceding aircraft has cleared the runway before landing the next aircraft.

The tower cab controllers are supplied with two types of displays to aid them in performing these functions: an ASDE (Airport Surface Detection Equipment) and a BRITE (Bright Radar Indicator Tower Equipment) display repeater from the approach control radar.

The ASDE is a radar operating at 25-35 gigahertz, especially designed for showing details of the airport surface and its environs. It typically has a range of five miles. It has high resolution, a high prf (1-10 kHz) and a high rotation speed (1-15 revolutions per second). The ASDE display is provided with a hood so that it can be seen in daylight.

The BRITE display is a TV picture of the radar display as used in the IFR room (prior to ARTS). The TV presentation is on a CRT especially designed to give a bright picture that can be viewed in the tower cab during daylight. Since the display typically shows an area of 30-60 mile radius from the airport, detail of the airport itself is lacking. The display is used to give the local controller information about the sequence of arriving aircraft.

The function of aborting a landing because of a wake turbulence hazard belongs to the local controller in the cab. His ASDE display is of ideal scale to present wake turbulence information. This could be in the form of lines showing the location of the vortex wakes on the airport surface.

A single symbol could be attached to each line identifying it as wake turbulence. The Transportation Systems Center in Cambridge is expected to let a contract for a new ASDE display in the near fugure. This is an opportune time, therefore, to incorporate the requirements for wake turbulence monitoring into the ASDE display

design criteria if this has not already been done. The vectors and characters required could be generated by a stroke writing technique, and displayed in a time-shared mode between pulses of the ASDE PPI. In the worst case, the ASDE 10 kHz prf and five mile range leaves 38 microseconds between pulses. If only one character or one vector were displayed in each 38 microsecond interval at a refresh rate of 24 to 30 hertz it would be possible to display over three hundred characters and/or vectors. This should be more than sufficient. Within the interval it is required that the display deflect its beam from the outer edge of the display to the center, deflect to the position of the character or vector, draw the character or vector, and return to the center. In displays which are presently being produced, that are 20 inches in diameter, it is possible to perform this function for a character in 23 microseconds and for a one-inch vector in 29 microseconds.

An operational problem with the proposed intergrated display is that on a clear day the tower controller does not normally look at his ASDE display. The wake monitoring display should always be within the visual range of the controller. This may dictate a separate display or two displays, a separate one for fair days and an integrated one for "ASDE" days. A single display would have to be accessible to the controller both when he is looking at his ASDE display and when he is not.

4.8 ARTS-III

The FAA has introduced the Automated Radar Terminal System (ARTS) for automatically tracking and displaying radar targets. The Atlanta terminal is presently outfitted with ARTS-I and the common IFR room in New York has ARTS-1A. All other major terminal facilities under FAA jurisdiction are scheduled to receive ARTS-III. All of these systems perform essentially the same functions but are implemented with different hardware.

The ARTS system is a semi-automated system. Terminal traffic control requires a surveillance function which reports on the location of all targets of interest as well as their status (normal, emergency, radio failure, etc.). It also requires a control function which assembles the information presented by surveillance, integrates it with standard procedures, and transmits instructions of a procedural or tactical maneuvering nature. In ARTS the surveillance function is largely automatic; continuing location and altitude are acquired through the radar, beacon and tracking subsystems. Emergency and radio failure beacon codes are also recognized and processed. On the other hand, the control function in ARTS-III is centered in the controller. He makes the decisions and has the communications equipment at his disposal to instruct pilots to implement these decisions.

Vortex monitoring is a surveillance function and should be integrated into the ARTS-III system as an automatic function. The approach controller should have vortex information integrated into his displays to help him properly space aircraft. Because the approach controller's display covers an area that is 30-60 miles in radius, it is infeasible to show the current position of vortices on his display. Rather, it will be necessary to process the vortex data and extrapolate useful information from it. Information as to the time required for a vortex to clear a runway and the time required for a vortex to reach and clear an adjacent (dual) runway might be generated.

Some computation will be necessary to develop the information to be displayed from the monitoring sensors. These computations will be done, at least initially, in a processor separate from ARTS. The information may be input to the ARTS computer or sent directly to a display where a multiplexer would accept inputs from both ARTS and the wake turbulence monitoring computer. This latter approach is being taken in the initial stages to integrate metering

and spacing (Section 4.9) into the ARTS system. (The ARTS-1A system in Atlanta has hardware particularly suitable to this approach.)

It is envisioned that the information displayed to the approach controller will be tabular in nature, and since the ARTS-III displays already have tabular capability, no difficulty in implementation is foreseen.

4.9 METERING AND SPACING

When an airport is operating near maximum capacity, it is the responsibility of the approach controller to maximize the landing rate consistent with separation standards. To accomplish this objective, the controller uses holding stacks, speed change commands, and path stretching maneuvers. At the ARTS-III level of automation, the controller does this manually using only a limited portion of the possible options because it is mentally impossible to keep track of all of the possibilities.

A Metering and Spacing System is presently being procured by the FAA. This sytem is expected to be operational in initial form in the 1972-1973 time period. By the 1974-1975 time period more advanced versions will be delivered and should be installed in most of the major airports under FAA jurisdiction. The metering and spacing system will calculate optimum path stretching, speed change and holding maneuvers, and display commands to the approach controllers. The approach controllers will relay these commands to the pilots. The controller will still have manual override capability, but choosing alternatives, a significant part of the control function, will become automated.

More advanced versions of the system are expected to display to the departure controller the time slots between arrivals available for takeoff.

The automatic metering and spacing system and the vortex monitoring system must interface on a computer-to-computer basis. The intervals available for landing without hazard must be input to the metering and spacing system on a dynamic basis. (Currently the Metering and Spacing System is expected to accept wake turbulence data in terms of the minimum separation interval permissible between different classes of aircraft. No surface wind information is expected to be used.)

Again, when metering and spacing takes up departure scheduling, wake turbulence information must be included in the computation of departure intervals.

The Metering and Spacing System receives aircraft position information from ARTS. It also uses groundspeed and airspeeds received from ARTS to compute wind information to be used in connection with later flights. This wind information could also be used by the wake turbulence monitoring system. Such information could supplement the wind information received from other sources.

An important relationship exists between the metering and spacing of aircraft on approach and a vortex monitoring system. If a monitoring system is introduced, present separation standards will be modified. The actual separation will be determined by the prevailing atmospheric conditions and the expected vortex drift behavior. Since metering and spacing is done many minutes before touchdown, atmospheric conditions during final approach may differ from those assumed to exist.

The function of the vortex monitoring system would be basically two-fold. First, to define the separation standards for metering and spacing based on the aircraft involved and the predicted vortex behavior and, second, to monitor the actual vortex behavior near touchdown in order to provide the controller with information to instruct pilots to perform missed approaches or other avoidance maneuvers when a hazard exists near touchdown due to abnormal vortex behavior and/or unexpected wind shifts.

4.10 IMPROVED ILS AND DATALINK

Present ILS (Instrument Landing Systems) provide landing guidance on a fixed vertical glide scope (usually three degrees) at a fixed azimuth heading. Development programs are being initiated which are expected to provide ILS systems with improved performance and flexibility beginning approximately in 1978. The newer systems will provide accuracies of 0.05 degrees in glide slope in both vertical and azimuth directions. They will also allow variable glide slopes and curved approach paths for aircraft suitably equipped.

Multiple glide slopes will have a significant effect on the vortex hazard. Heavy aircraft may be required to descend at relatively steep descent angles (as steep as 6 degrees). If a light aircraft follows a heavy one at a conventional slope of three degrees, its approach path would lie beneath the path of the heavy aircraft and in a position to intercept its wake. The same consideration applies to aircraft approaching on dual runways at different glide slopes.

Beyond 1980 digital data link capability will be installed in many aircraft. This will allow the metering and spacing system controller to communicate commands directly to aircraft thus reducing the communication interval (the controller monitors but does not relay the instructions) and allow aircraft to touchdown very accurately in time. This, in turn, will make possible reduced standards for aircraft separation on approach and landing. This development will increase the need for an accurate vortex monitoring system in order to take advantage of the closer spacings permissible.

4.11 RUNWAY GEOMETRY AND WIND ROSE DATA

The geometry of four of the major airports in the New England area are shown in Figures 4-1, 4-3, 4-5, and 4-6. These figures

show the geometry for Logan Airport in Boston, Massachusetts, T. F. Green Airport near Providence, Rhode Island, Bangor International Airport in Bangor, Maine, and Windsor Locks serving the Hartford, Connecticut area. Figures 4-2 and 4-4 show wind rose data for Logan and T. F. Green Airports respectively.

Wind rose data shows the percentage of time that the wind lies in a particular sector as a function of wind velocity. The data is based on Weather Bureau information covering a particular time interval.

This data can be used to examine vortex drift between runways and the probability of vortex hazard occurrence.

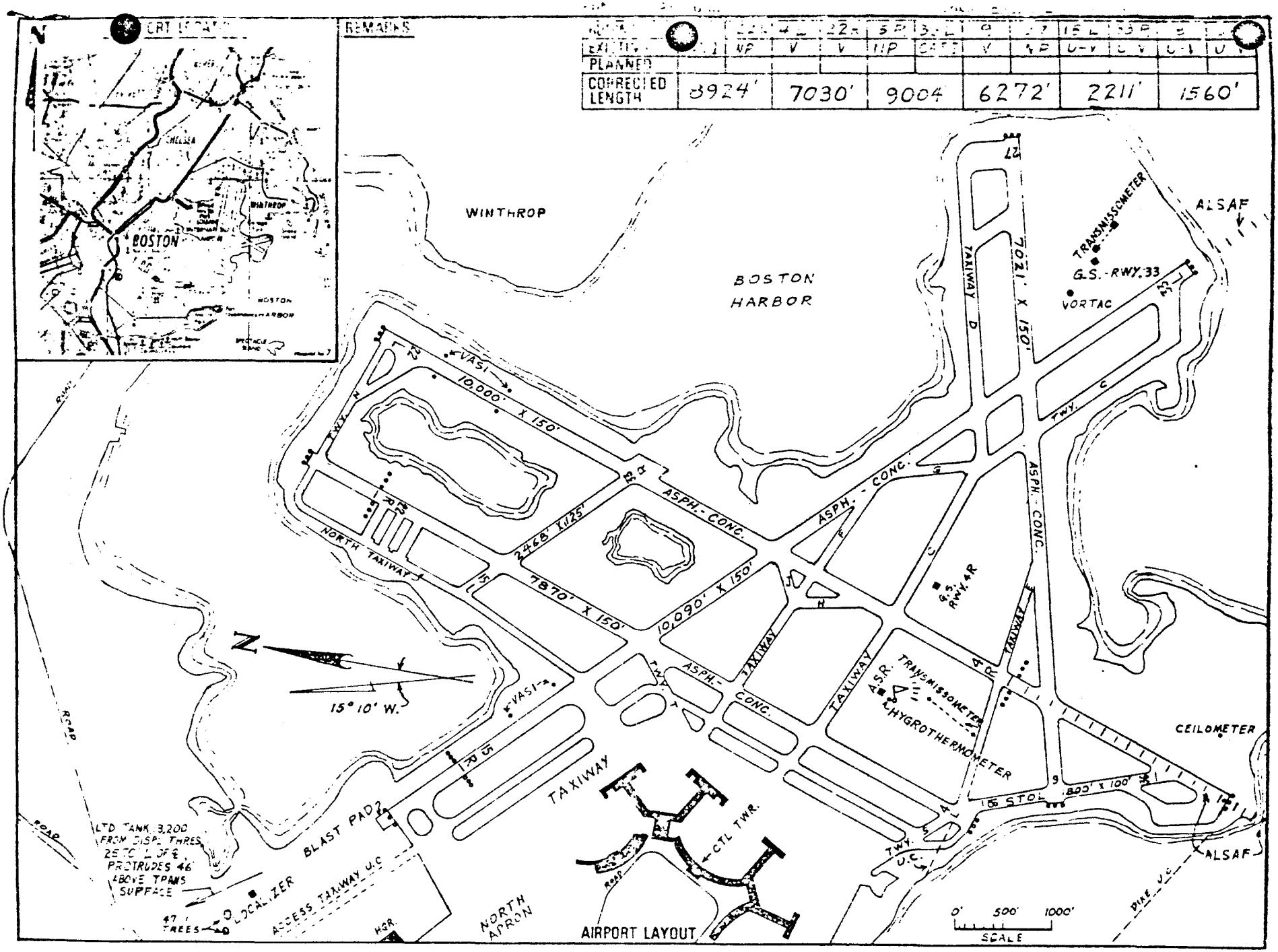

Figure 4-1.

LOGAN AIRPORT
BOSTON, MASS

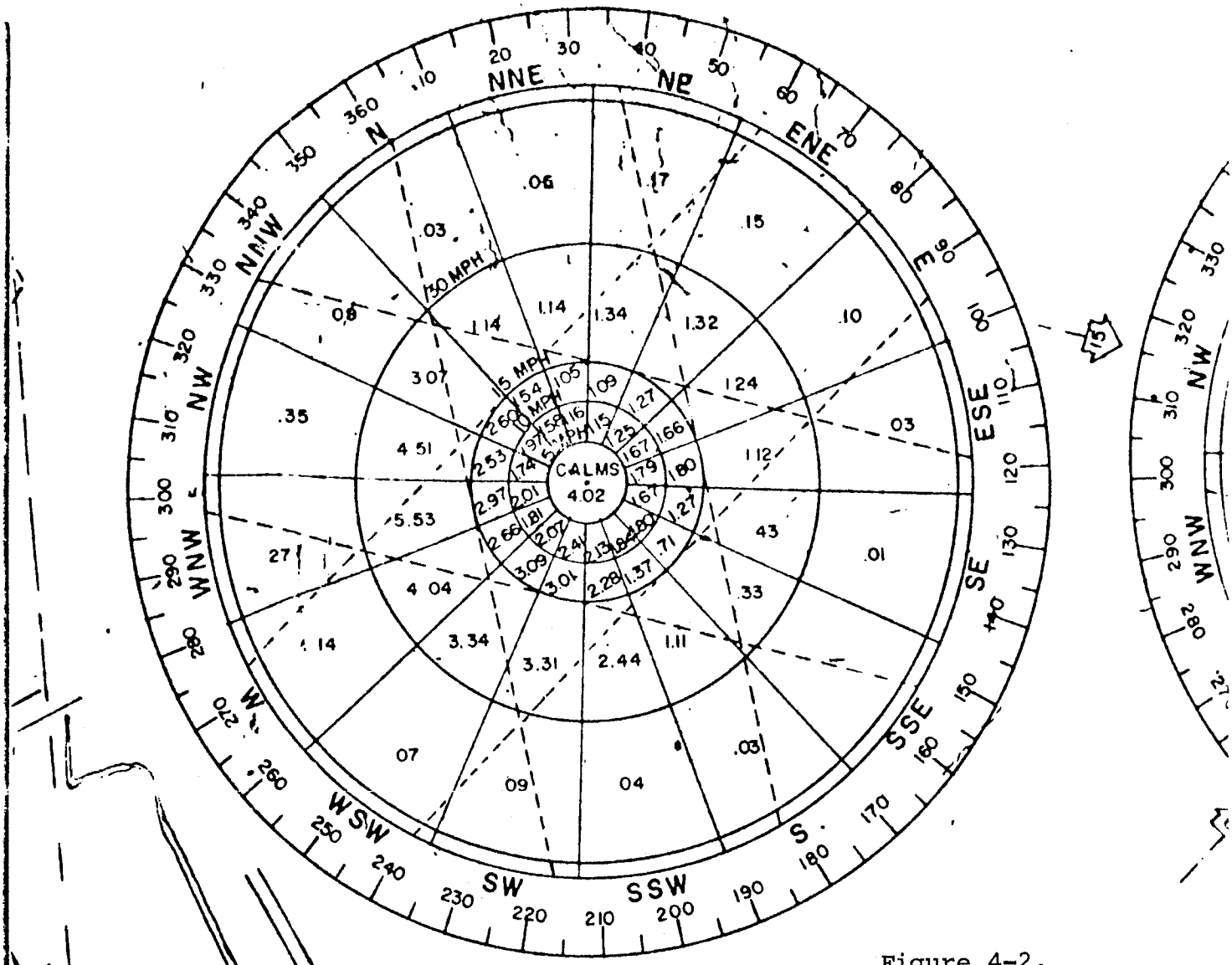

Figure 4-2.

Page 4-17

WIND ROSE

STATION: LOGAN INTERNATIONAL AIRPORT

PERIOD OF RECORD: JAN, 1959 - DEC, 1963

NOTE: VFR COVERAGE 15 MPH CROSS WIND

4-22	77.16 %
15-33	81.65 %
9-27	83.51 %
4-22, 15-33	92 20 %
15-33, 9-27	94.28 %
4-22, 15-33, 9-27	99 60 %

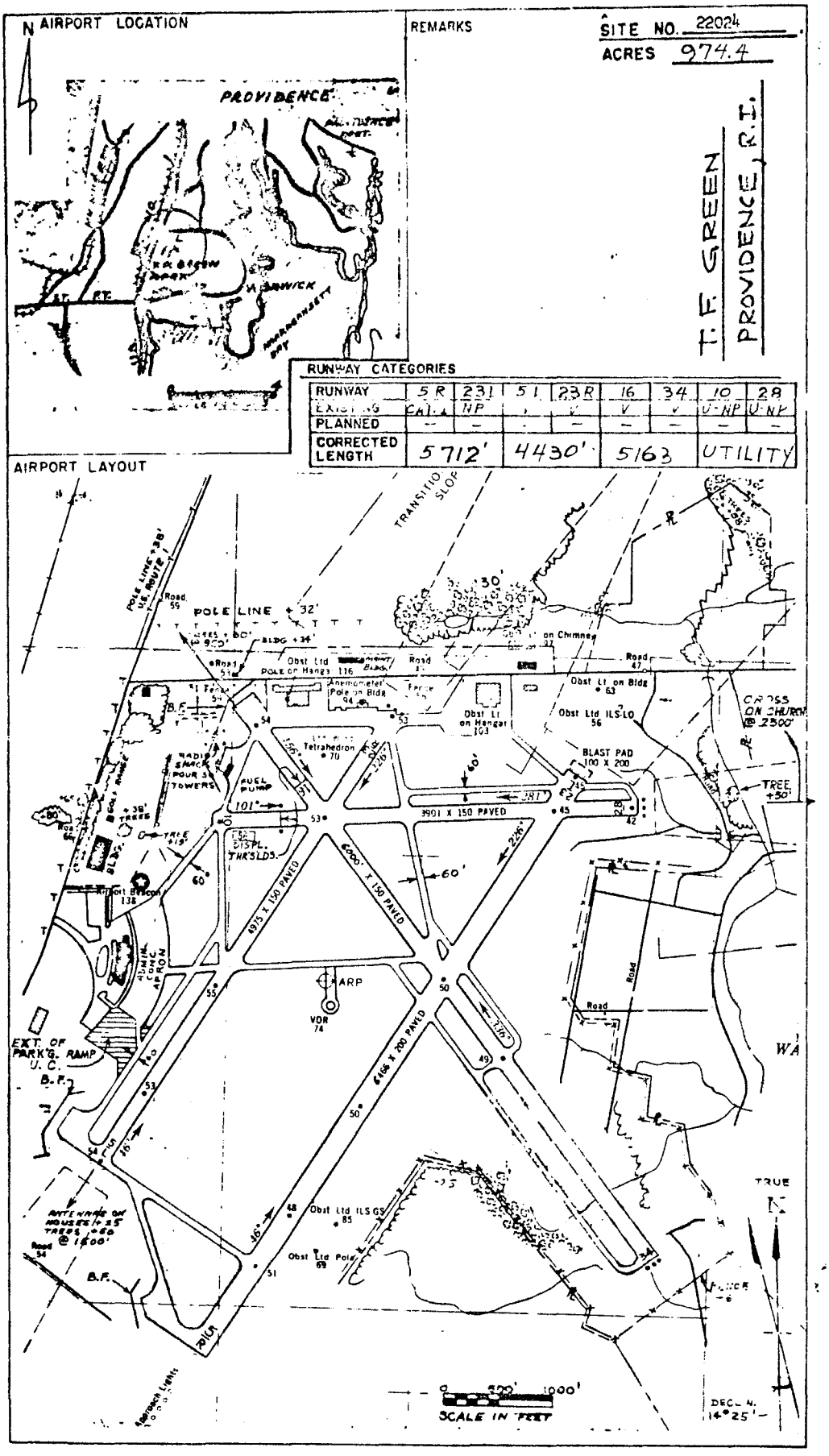
N AIRPORT LOCATION
PROVIDENCE
REMARKS
SITE NO. 22024
ACRES 974.4
T.F. GREEN
PROVIDENCE, R.I.
RUNWAY CATEGORIES
RUNWAY | 5R | 23L | 5L | 23R | 16 | 34 | 10 | 28
EXISTING | CAT. A | NP | | V | V | V | U-NP | U-NP
PLANNED | – | – | – | – | – | – | – | –
CORRECTED LENGTH | 5712' | 4430' | | | 5163 | | UTILITY
AIRPORT LAYOUT
TRANSITIO SLOP
POLE LINE +32'
POLE LINE +38' U.S. ROUTE 1
Road 55
Road 51
Road 47
Obst Ltd Pole on Hangs 116
Anemometer Pole on Bldg 94
Obst Lt on Hangar 103
Obst Lt on Bldg 63
Obst Ltd ILS-LO 56
Tetrahedron 70
BLAST PAD 100 X 200
3901 X 150 PAVED
6300' X 150 PAVED
4975 X 150 PAVED
6165 X 200 PAVED
ARP
VOR 74
EXT. OF PARK'G. RAMP U.C.
ANTENNAS ON HOUSES +25 TREES +60 @ 1800'
Obst Ltd ILS GS 85
Obst Ltd Pole 69
CROSS ON CHURCH @ 2300'
TREE +50'
Road
TRUE N
SCALE IN FEET
DECL'N. 14°25'

Figure 4-3.

T. F. GREEN AIRPORT
PROVIDENCE, R.I.

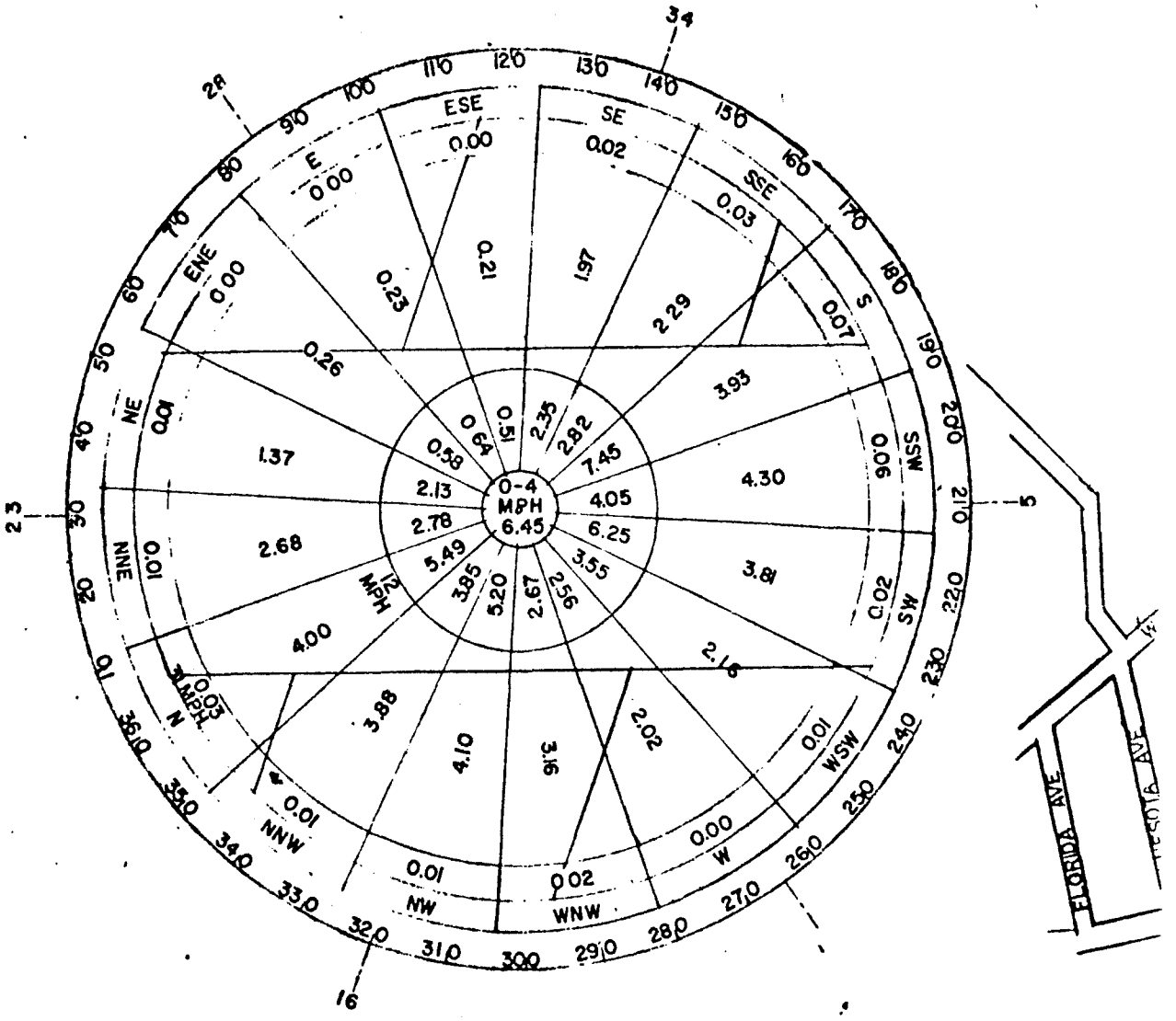

WIND COVERAGE
15 M. P. H. ALLOWABLE CROSS WIND COMPONENTS

RUNWAY	% COVERAGE
16-34	79 5
5-23	80 8
16-34 AND 5-23	95 1

SOURCE NATIONAL WEATHER RECORDS CENTER
PERIOD JUNE 1956 — MAY 1961

Figure 4-4.

EFFECTIVE

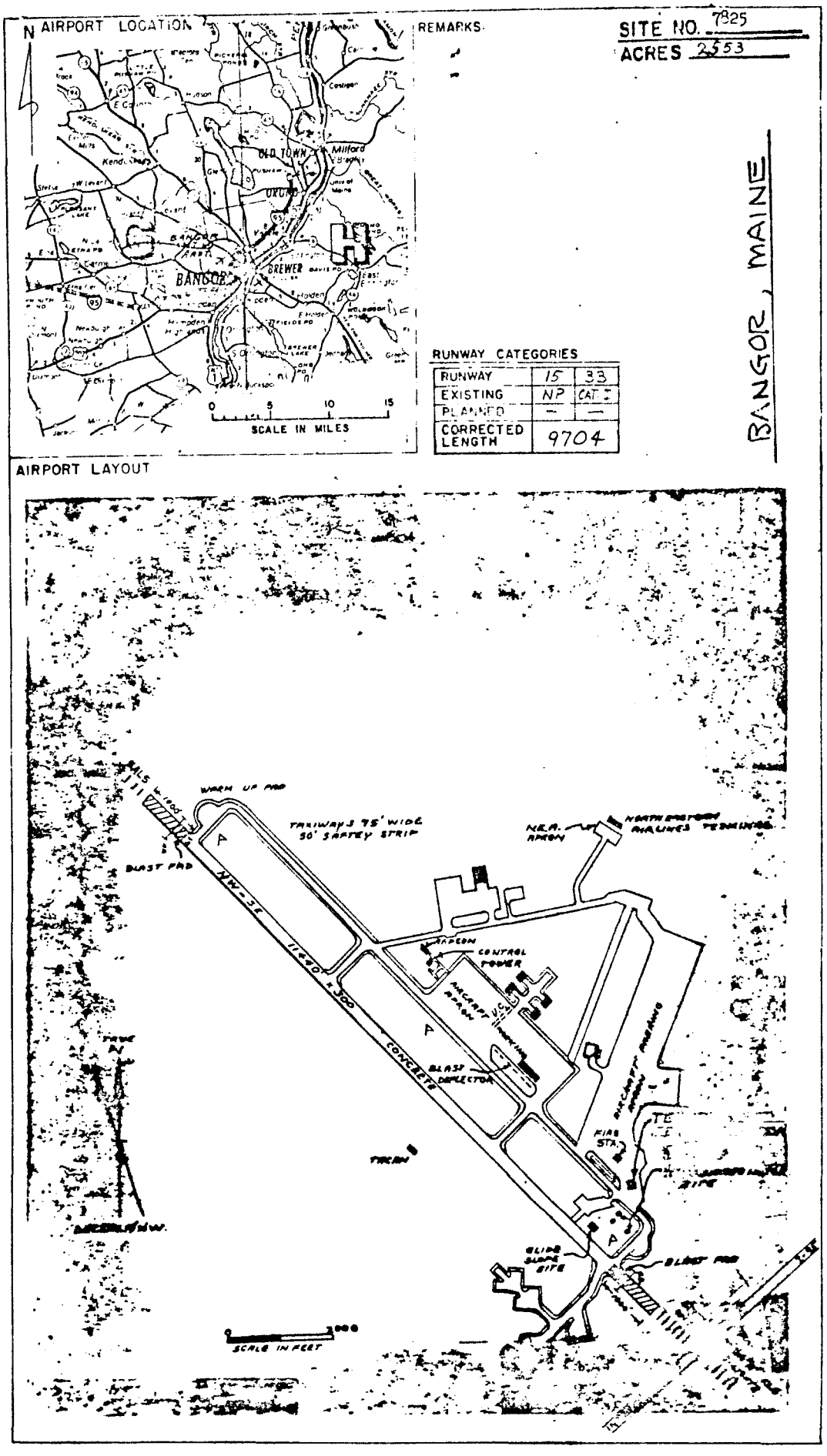
AIRPORT LOCATION
N
REMARKS
SITE NO. 7825
ACRES 2553
BANGOR, MAINE
OLD TOWN
Milford
Orono
BANGOR
BREWER
0 5 10 15
SCALE IN MILES
RUNWAY CATEGORIES
RUNWAY 15 33
EXISTING NP CAT. I
PLANNED — —
CORRECTED LENGTH 9704
AIRPORT LAYOUT
WIND CONE
TAXIWAY 75' WIDE 50' SAFETY STRIP
N.E.A. APRON
NORTHEASTERN AIRLINES TERMINAL
BLAST PAD
RW-15
RW-33
11,290 x 300
CONCRETE
CONTROL TOWER
APRON
AIRCRAFT PARKING
FIRE STA.
GLIDE SLOPE SITE
BLAST PAD
SCALE IN FEET

Figure 4-5.

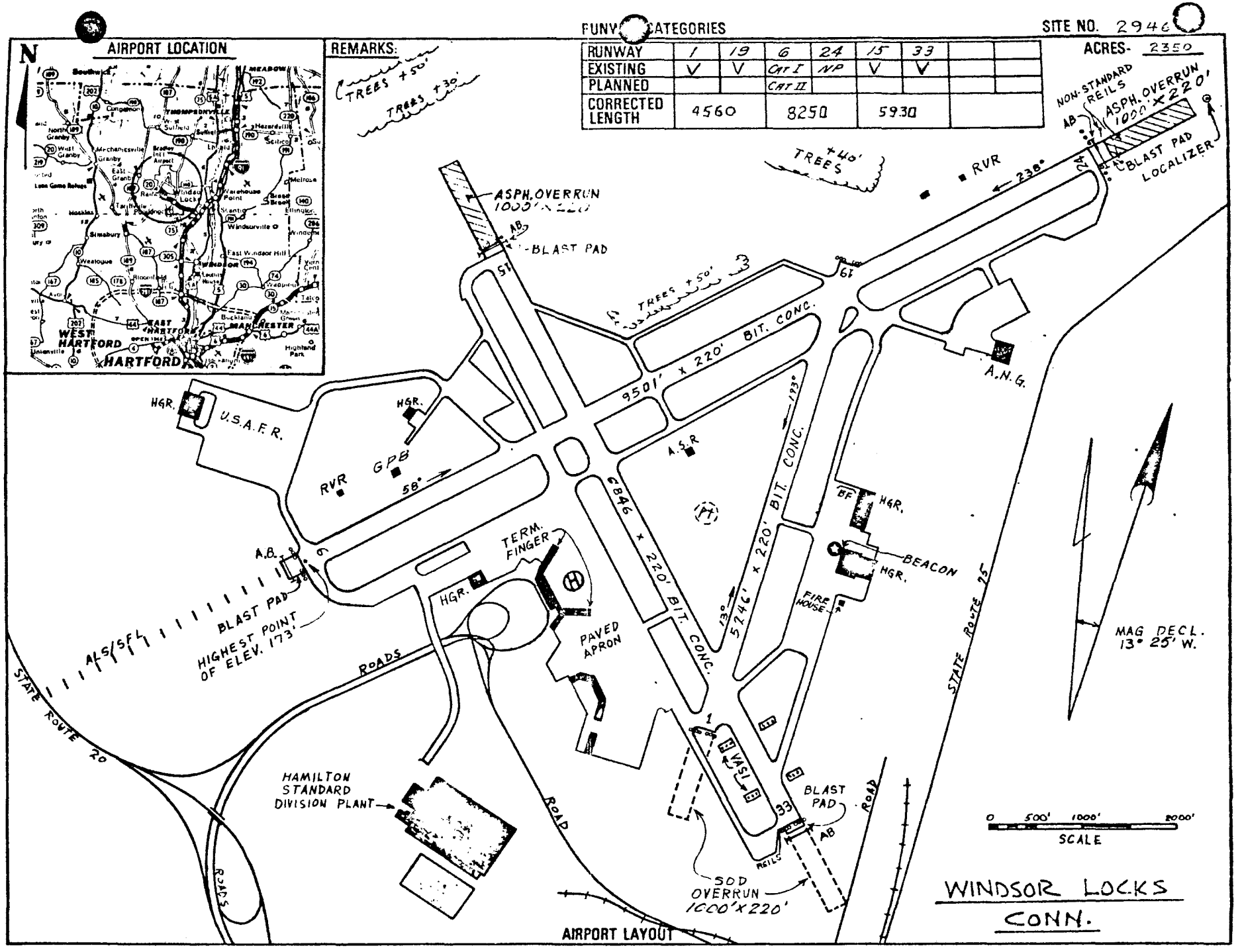
AIRPORT LOCATION
N
HARTFORD
WEST HARTFORD
EAST HARTFORD
MANCHESTER
REMARKS:
TREES +50'
TREES +30'
RUNWAY CATEGORIES
SITE NO. 2946
ACRES- 2350
RUNWAY | 1 | 19 | 6 | 24 | 15 | 33
EXISTING | V | V | CAT I | NP | V | V
PLANNED | | | CAT II | | | |
CORRECTED LENGTH | 4560 | | 8250 | | 5930 |
NON-STANDARD REILS
ASPH. OVERRUN 1000' x 220'
BLAST PAD
LOCALIZER
TREES +40'
RVR
238°
ASPH. OVERRUN 1000' x 220'
AB
BLAST PAD
TREES +50'
9501' x 220' BIT. CONC.
A.N.G.
HGR.
U.S.A.F.R.
RVR
GPB
58°
A.S.R.
6846' x 220' BIT. CONC.
193°
5246' x 220' BIT. CONC.
BF
HGR.
BEACON
HGR.
FIRE HOUSE
A.B.
BLAST PAD
HIGHEST POINT OF ELEV. 173'
ALS/SFL
TERM. FINGER
HGR.
PAVED APRON
ROADS
STATE ROUTE 20
HAMILTON STANDARD DIVISION PLANT
ROAD
ROADS
VASI
BLAST PAD
AB
REILS
SOD OVERRUN 1000' x 220'
STATE ROUTE 75
MAG DECL. 13° 25' W.
0 500' 1000' 2000'
SCALE
WINDSOR LOCKS
CONN.
AIRPORT LAYOUT

Figure 4-6.

SECTION 5

APPLICATION OF DATA TO AIRPORT MONITORING REQUIREMENTS

5.1 INTRODUCTION

In this section, work in two basic areas is described. The vortex drift predicted by a computer program developed for generating drift envelopes was compared with experimental data measured at the FAA's test flight facility in Atlantic City, New Jersey. This involved a comparison of the vortex arrival times at the test tower predicted by theory with the actual measured arrival times. The results of this analysis are presented in Section 5.2.

Also examined and described herein are the vortex monitoring requirements for a particular runway combination commonly used at Logan Airport in Boston during IFR operations. The results, which are presented in Section 5.3, show the search volumes and the frequency of occurrence of vortex hazards for parallel runway, intersecting runway, and preceding traffic operations.

The author wishes to acknowledge the assistance of Bob Pinnock and Bob Bianculli of the FAA Logan Airport Control Tower, who provided valuable inputs related to the operational use and runway selection procedures at Logan Airport and to Bob Montinari of the Service Technology Corporation, the computer services subcontractor at the Transportation Systems Center, for his excellent computer programming efforts.

5.2 COMPARISON OF THEORETICAL AND EXPERIMENTAL DRIFT RATES

As suggested in Section 3, an analysis has been conducted to determine the accuracy with which a theoretical model predicts the experimental drift rate measured at the FAA's NAFEC Test Center in Atlantic City, New Jersey. A series of 165 cases were examined,

109 cases involving the drift of the downwind vortex and 56 involving the drift of the upwind vortex. The aircraft involved were the B-727, B-707, DC-9, and CV-880. The experimental data used in this analysis was taken from Reference 5.

5.2.1 COMPUTER PROGRAM

A computer program was formulated to calculate the theoretical vortex behavior and to compare the theoretical and measured results.

The program was developed from the program summarized briefly in Section 2, which computes the motion of an incremental element of a vortex filament due to the combined influence of winds, mutual induction, and ground effect. A more complete description of this program is contained in Appendix A.

The NAFEC test setup and the measurements made are described in Section 3.3. In the comparison made in that section, the vortex behavior was restricted to the B-727 aircraft flying at a fixed altitude, speed, and weight. Variations in these factors can have a significant effect on the resultant vortex motion; in particular, the initial vortex height has a pronounced effect on the lateral transport speed as shown in Section 2, Figure 2-7. The present analysis has included as many variables as the theoretical model permitted to provide a comprehensive comparison between theory and experiment.

In Reference 5 the average lateral transport speed is determined by taking the distance of the aircraft wing tip to the tower; $(y' + b/2)$ for the upwind vortex and $(y' - b/2)$ for the downwind vortex and dividing these quantities by the vortex AGE. Vortex

AGE is measured from the time the wingtip is abreast of the tower to the time the vortex passes the tower.

The experimental drift rate determined in this manner is not exact for two reasons: 1) the vortex element triggering the tower sensors is not always generated at the instant the aircraft is abreast of the tower and 2) the vortex is not formed at the wing tip but more nearly at a distance from the aircraft centerline of $\pm \pi/8$ b.

For the present analysis, either the experimental drift rates had to be corrected to obtain the true vortex age or the equivalent AGE had to be extracted from the theoretical model. The latter approach was selected for simplicity.

The theoretical and experimental transport velocities are given by

$$v_T = \frac{d}{AGE_T} \tag{5-1}$$

$$v_E = \frac{d}{AGE_E} \tag{5-2}$$

The percentage by which the experimental transport velocity differs from the theoretical $\epsilon(v)$ is given by

$$\epsilon(v) = \frac{v_E - v_T}{v_T} \times 100\% \tag{5-3}$$

Substituting Equations 1 and 2 into 3 gives

$$\epsilon(v) = \left(\frac{AGE_T}{AGE_E} - 1 \right) \times 100\% \tag{5-4}$$

where AGE_E is the vortex age measured at NAFEC and reported in Reference 5.

The method used to compute the theoretical vortex age (AGE_T) is described below. In order to compute AGE_T the program calculates the path of the vortex based on the particular initial conditions for that case. The initial conditions upon which the subsequent motion depends are the altitude, weight, span, and speed of the aircraft and the wind velocity, wind heading and air density. The program computes the position of the vortex element at time increments Δt. At each time step the lateral position of the vortex element measured from the aircraft centerline is compared with the actual lateral distance to the tower determined at NAFEC for that particular run. By interpolation the position of the vortex and the corresponding time are determined for the point where the computed lateral distance of the vortex equals the actual. This time is the true vortex age (t_T).

From the downrange drift of the vortex (x) a correction is made to the true vortex age to obtain AGE_T.

$$AGE_T = t_T - \frac{x}{V_{AC}\left(\frac{6076.1}{3600}\right)} \qquad (5\text{-}5)$$

where V_{AC} is the aircraft speed in knots. The reason for this correction is discussed in Section 3.

5.2.2 RESULTS

Significant quantities of the cases that were examined are tabulated in Table 5-I. These include the vortex number (where 1

Table 5-I. Experimental and Computed Data
B-727

Case	Pass No.	Vortex No.	V_{AC} (knots)	y (ft)	z (ft)	W_{AC} (lbs)	V_W (mph)	β_W (deg)	AGE_E (sec)	AGE_T (sec)	$\epsilon(v)$ 1%
1	1	1	134	233	59	136,000	11	- 90	12.1	9.93	-17.9
2	2		128	203	46	134,000	11	- 90	10.2	7.81	-23.4
3	3		128	185	57	133,000	12	- 90	8.6	6.98	-18.8
4	4		126	162	59	131,000	11	- 90	6.1	6.41	5.1
5	5		126	233	67	130,000	10	- 90	10.7	11.03	3.1
6	6		125	209	73	128,000	10	- 95	10.6	9.97	- 6.0
7	7		125	178	71	126,000	12	-100	8.3	7.04	-15.2
8	8		124	151	71	125,000	11	-105	7.7	6.21	-19.3
9	9		124	237	101	123,000	11	-105	12.6	11.56	- 8.3
10	10		124	210	92	122,000	11	-100	10.5	9.79	- 6.8
11	11		123	175	78	120,000	11	-105	9.5	7.69	-19.0
12	12		122	143	91	118,000	13	-105	5.7	5.14	- 9.8
13	13		122	232	75	117,000	13	-110	13.7	9.39	-31.4
14	14		133	223	99	138,000	12	-120	8.1	10.68	31.9
15	15		132	199	102	136,000	16	-110	7.7	6.66	-13.5
16	16		130	175	92	132,000	18	-110	5.1	4.98	-22.7
17	17		130	150	94	130,000	20	-105	2.7	3.59	33.1
18	19		138	209	35	138,000	14	-140	12.1	7.96	-34.2
19	20		138	226	39	137,000	14	-140	12.7	9.10	-28.4
20	21		138	176	41	134,000	13	-140	8.9	7.35	-17.5
21	22		136	145	42	133,000	13	-140	7.3	5.79	-20.7
22	23		137	225	40	132,000	12	-140	12.1	10.29	-15.0
23	24		138	209	46	131,000	11	-140	11.5	10.67	- 7.2
24	25		134	173	33	130,000	10	-140	9.4	7.78	-17.2
25	26		134	235	71	135,000	10	-150	13.8	17.28	25.2
26	27		134	210	49	137,000	11	-150	12.2	12.30	0.8
27	28		134	185	58	135,000	11	-150	9.6	11.57	20.5
28	29		128	149	54	134,000	12	-160	8.0	9.93	24.1
29	30		126	227	73	132,000	10	-145	13.8	15.28	10.7
30	31		130	209	77	131,000	12	-150	13.1	13.88	6.0
31	32		130	188	57	129,000	10	-155	13.5	13.66	11.7
32	33		128	150	60	128,000	9	-155	20.6	11.52	-44.1

(continued)

Table 5-I. Experimental and Computed Data (continued)

B-727

Case	Pass No.	Vortex No.	V_{AC} (knots)	y (ft)	z (ft)	W_{AC} (lbs)	V_W (mph)	β_W (deg)	AGE_E (sec)	AGE_T (sec)	$\epsilon(v)$ 1%
33	34	1	150	200	94	126,000	9	-150	11.5	18.83	63.8
34	35		150	189	92	125,000	9	-130	12.3	12.81	- 4.1
35	36		132	240	83	124,000	10	-105	13.5	12.39	- 8.2
36	37		130	218	105	123,000	10	-100	16.3	11.44	-29.8
37	38		128	186	86	122,000	12	-135	14.6	9.91	-32.1
38	39		128	139	86	120,000	12	-120	4.1	5.77	40.8
39	40		138	217	131	138,000	8	-135	19.4	18.57	- 4.3
40	41		136	212	124	137,000	7	-120	10.0	17.09	70.9
41	42		138	179	98	136,000	9	-175	25.1	31.30	24.7
42	43		134	152	110	135,000	13	-180	39.5	34.22	-13.4
43	4	2	126	162	59	131,000	11	- 90	31.0	17.14	-44.7
44	6		125	209	73	128,000	10	- 95	38.0	22.71	-40.2
45	7		125	178	71	126,000	12	-100	31.0	14.95	-51.8
46	8		124	151	71	125,000	11	-105	25.9	14.82	-42.8
47	9		124	237	101	123,000	11	-105	24.1	19.75	-18.0
48	10		124	210	92	122,000	11	-100	26.8	17.72	-33.9
49	12		122	143	91	118,000	13	-105	14.1	10.43	-26.0
50	14		133	223	99	138,000	12	-120	21.1	19.21	- 9.0
51	15		132	199	102	136,000	16	-110	15.8	11.02	-30.3
52	16		130	175	92	132,000	18	-110	10.7	8.75	-18.2
53	17		130	150	94	130,000	20	-105	5.4	6.73	24.7
54	30		126	227	73	132,000	10	-145	41.7	47.0	15.0
55	35		150	189	92	125,000	9	-130	29.8	28.03	- 5.9
56	36		132	240	83	124,000	10	-105	22.8	24.30	6.6
57	39		128	139	86	120,000	12	-120	11.5	12.60	9.5
58	41		136	212	124	137,000	7	-120	20.9	40.54	94.0

(continued)

Table 5-I. Experimental and Computed Data (continued)

B-707

Case	Pass No.	Vortex No.	V_{AC} (knots)	y (ft)	z (ft)	W_{AC} (lbs)	V_W (mph)	β_W (deg)	AGE_E (sec)	AGE_T (sec)	$\epsilon(v)$ 1%
59	1	1	128	224	39	201,000	15	-120	7.3	6.27	-14.1
60	2		126	224	58	199,000	14	-110	7.7	7.10	- 7.83
61	3		132	230	50	196,000	17	-120	6.7	6.37	- 4.9
62	4		128	237	42	193,000	15	-120	6.1	6.98	14.3
63	5		133	251	41	220,000	10	-140	12.1	11.36	- 6.1
64	6			235	50	219,000	10	-140	12.5	11.51	- 7.9
65	7			236	74	217,000	9	-140	14.9	14.73	- 1.1
66	8			225	68	216,000	10	-140	12.9	12.51	- 3.1
67	9			228	39	215,000	9	-140	10.9	10.58	- 2.9
68	10		150	226	59	190,000	11	-145	11.6	13.02	12.2
69	11		145	225	56	188,000	9	-130	11.5	12.07	5.0
70	2	2	126	224	58	199,000	14	-110	16.7	18.54	11.0
71	3		132	230	50	196,000	17	-120	19.2	16.37	-14.8
72	7		133	236	74	217,000	9	-140	62.3	93.88	50.6
73	8		133	225	68	216,000	10	-140	54.5	69.03	26.7
74	11		145	225	56	188,000	9	-130	55.7	50.62	- 9.1
						DC-9					
75	1	1	155	150	100	76,000	12	- 90	8.3	6.45	-22.3
76	2		156	250	80	75,300	12	- 85	21.6	11.90	-44.9
77	3		140	177	86	74,700	11	- 85	7.9	8.63	9.2
78	4		140	188	93	74,000	11	- 90	8.2	9.26	12.9
79	5		200	204	92	73,500	13	- 95	11.2	8.75	-21.9
80	6		200	219	106	72,700	13	- 95	8.5	9.56	12.5
81	7		200	202	108	72,400	14	- 95	8.4	8.07	- 4.0
82	8		200	357	101	72,100	13	- 95	14.6	16.66	14.1
83	9		125	247	89	71,700	13	-100	9.8	10.77	9.9
84	10		126	239	127	70,900	14	-100	9.4	9.84	4.6
85	11		125	258	35	70,400	13	-100	13.0	9.56	-26.4
86	12		129	233	33	69,900	15	-100	6.6	7.57	14.6

(continued)

Table 5-I. Experimental and Computed Data (continued)

DC-9

Case	Pass No.	Vortex No.	V_{AC} (knots)	y (ft)	z (ft)	W_{AC} (lbs)	V_W (mph)	β_W (deg)	AGE_E (sec)	AGE_T (sec)	$\epsilon(v)$ 1%
87	1	2	155	150	100	76,000	12	- 90	15.4	10.70	-30.5
88	2		156	250	80	75,300	12	- 85	27.5	17.28	-37.2
89	3		140	177	86	74,700	11	- 85	13.6	13.91	2.3
90	4		140	188	93	74,000	11	- 90	13.8	14.35	4.0
91	5		200	204	92	73,500	13	- 95	16.0	12.71	-20.6
92	7		200	202	108	72,400	14	- 95	11.8	11.61	- 1.6
93	9		125	247	89	71,700	13	-100	14.6	15.55	6.5
94	10		126	239	127	70,900	14	-100	12.9	13.47	4.4
95	12		129	233	33	69,900	15	-100	18.6	15.70	-15.6
						CV-880					
96	6	1	155	218	50	156,000	14	- 35	14.0	11.85	-15.3
97	7		148	177	40	153,000	15	- 35	12.9	8.07	-37.5
98	9		142	178	58	147,000	15	- 30	16.8	10.31	-38.6
99	12		142	186	50	141,000	15	- 40	9.9	8.61	-13.1
100	14		132	176	67	136,000	15	- 30	18.6	10.73	-42.3
101	15		132	187	67	134,000	15	- 30	17.2	11.61	-32.5
102	16		132	192	69	132,000	16	- 30	15.7	11.60	-26.1
103	17		141	-222	82	155,000	15	70	16.6	14.74	-11.2
104	18		143	-222	116	152,000	17	60	14.5	13.49	- 7.0
105	19		142	-293	100	149,000	18	80	9.2	13.85	50.6
106	20		143	-310	86	147,000	19	75	16.4	14.43	-12.0
107	22		140	-409	102	143,000	16	80	30.8	21.33	-30.7
108	23		165	-383	116	141,000	18	75	12.1	17.65	45.8
109	24		165	-379	122	140,000	18	80	18.5	16.94	- 8.4
110	25		170	133	118	156,000	10	- 75	12.0	6.01	-49.9
111	26		170	232	104	153,000	9	- 70	14.8	14.35	- 3.0
112	27		162	236	86	151,000	9	- 70	18.5	14.11	-23.7
113	28		160	324	97	145,000	10	- 65	24.4	19.67	-19.4
114	31		150	246	114	137,000	7	-165	40.5	42.05	3.8

(continued)

Table 5-I. Experimental and Computed Data (continued)

CV-880

Case	Pass No.	Vortex No.	V_{AC} (knots)	y (ft)	z (ft)	W_{AC} (lbs)	V_W (mph)	β_W (deg)	AGE_E (sec)	AGE_T (sec)	$\epsilon(v)$ 1%
115	33	1	144	192	100	133,000	6	-145	28.9	22,24	-23.0
116	34		142	158	100	131,000	6	-160	19.8	24.27	22.6
117	36		190	-302	75	152,000	13	145	35.6	39.69	11.5
118	40		185	-285	104	142,000	14	150	28.8	35.05	21.7
119	45		144	162	40	148,000	7	- 40	8.4	10.30	22.5
120	46		145	166	61	143,000	9	- 25	11.5	14.95	30.0
121	47		140	200	50	141,000	8	- 25	11.4	17.62	54.6
122	50		148	230	68	135,000	10	- 30	11.9	19.84	66.7
123	51		138	252	64	134,000	12	- 30	13.7	18.86	37.7
124	53		138	165	65	130,000	12	- 35	6.0	10.44	74.0
125	54		145	245	100	160,000	16	- 25	17.4	19.03	9.4
126	55		148	215	100	158,000	15	- 50	6.8	10.07	48.1
127	56		146	185	90	156,000	10	- 35	6.6	14.76	123.7
128	60		138	185	100	148,000	11	- 20	17.0	20.99	23.5
129	63		142	215	40	142,000	13	- 20	7.8	15.43	97.8
130	64		144	185	30	141,000	13	- 15	7.8	12.61	61.6
131	66		148	200	100	160,000	11	- 50	10.9	12.01	10.2
132	67		142	200	100	144,000	13	- 55	11.0	9.80	-10.9
133	68		140	200	90	142,000	13	- 55	11.8	9.67	-18.1
134	69		134	200	100	140,000	15	- 55	7.2	8.63	19.9
135	70		133	200	90	138,000	15	- 60	8.8	8.05	- 8.5
136	72		142	163	61	148,000	6	- 90	8.6	10.21	18.7
137	73		145	189	55	147,000	7	- 75	10.9	11.06	1.4
138	75		143	248	51	144,000	8	- 70	13.1	13.85	5.8
139	87		140	190	76	136,000	6	- 25	17.3	23.96	38.5
140	17	2	141	-222	82	155,000	15	70	8.5	8.23	- 3.1
141	18		143	-222	116	152,000	17	60	8.4	8.35	- 0.6
142	19		142	-293	100	149,000	18	80	14.0	9.38	-33.0
143	20		143	-310	86	147,000	19	75	9.5	9.67	1.8
144	21		140	-418	95	145,000	18	70	17.3	14.83	-14.3
145	22		140	-409	102	143,000	16	80	15.2	15.29	0.6

(continued)

Table 5-I. Experimental and Computed Data (continued)
CV-880

Case	Pass No.	Vortex No.	V_{AC} (knots)	y (ft)	z (ft)	W_{AC} (lbs)	V_W (mph)	β_W (deg)	AGE_E (sec)	AGE_T (sec)	$\epsilon(v)$ 1%
146	23	2	165	-383	116	141,000	18	75	12.1	13.28	9.7
147	24		165	-379	122	140,000	18	80	18.5	12.81	-30.8
148	25		170	133	118	156,000	10	- 75	12.0	13.31	10.9
149	27		162	236	86	151,000	9	- 70	18.5	27.89	50.8
150	29		160	-331	103	144,000	5	125	30.1	35.72	18.7
151	36		190	-302	75	152,000	13	145	17.3	19.26	11.3
152	37		195	-290	118	150,000	13	140	16.0	18.27	14.2
153	38		195	-295	96	147,000	12	145	17.0	21.51	26.6
154	39		200	-285	96	145,000	11	145	16.0	22.54	40.9
155	40		185	-285	104	142,000	14	150	16.4	20.38	24.3
156	41		185	-321	89	140,000	13	155	22.7	27.36	20.5
157	53		138	165	65	130,000	12	- 35	18.0	33.65	86.88
158	55		148	215	100	158,000	15	- 50	11.0	17.74	61.24
159	56		146	185	90	156,000	10	- 35	13.0	48.88	276.0
160	66		148	200	100	160,000	11	- 50	26.0	24.36	- 6.30
161	67		142	200	100	144,000	13	- 55	18.0	17.84	- 0.9
162	68		140	200	90	142,000	13	- 55	28.0	18.34	-34.5
163	69		134	200	100	140,000	15	- 55	13.0	15.36	18.1
164	70		133	200	90	138,000	15	- 60	14.0	14.60	4.3
165	72		142	163	61	148,000	6	- 90	48.0	52.07	8.5

refers to the vortex generated by the wing nearest the tower); V_{AC}, the aircraft speed in knots; y, the lateral distance between the aircraft path and the tower; z, the aircraft height; W_{AC}, the aircraft weight in lbs; V_W, the wind speed in mph; β_W, the wind heading measured with respect to the aircraft path; AGE_E, the vortex age measured experimentally; AGE_T, the vortex age determined analytically; $\epsilon(v)$, the percentage error in vortex transport speed where a positive value indicates the experimental speed exceeds the theoretical.

One error source which was inadvertently not accounted for was the wind heading angle (β_W). This angle was determined from the following expression:

$$\beta_W = \theta_{AC} - \theta_W \qquad (5\text{-}6)$$

where θ is the angle measured from North. In the tabulated data of Reference 5, the wind direction is a true reading, whereas the aircraft track was a magnetic reading. Therefore, the wind heading angles are biased by the amount of the local variation (less than 15 deg.). To change the aircraft compass heading (θ_{AC}) to a true heading the local variation is subtracted which means that the values of β_W were approximately 15 degrees too large in each case.

The percentage error data has been plotted as a function of the experimental age in Figure 5-1. The percentage errors obtained can be summarized as follows: The average error of all the runs computed by taking the "average value" of all of the percentage errors and dividing by the total number of runs was ±24.6%. The average error for the downwind vortex (No. 1) was ±22.6% and for

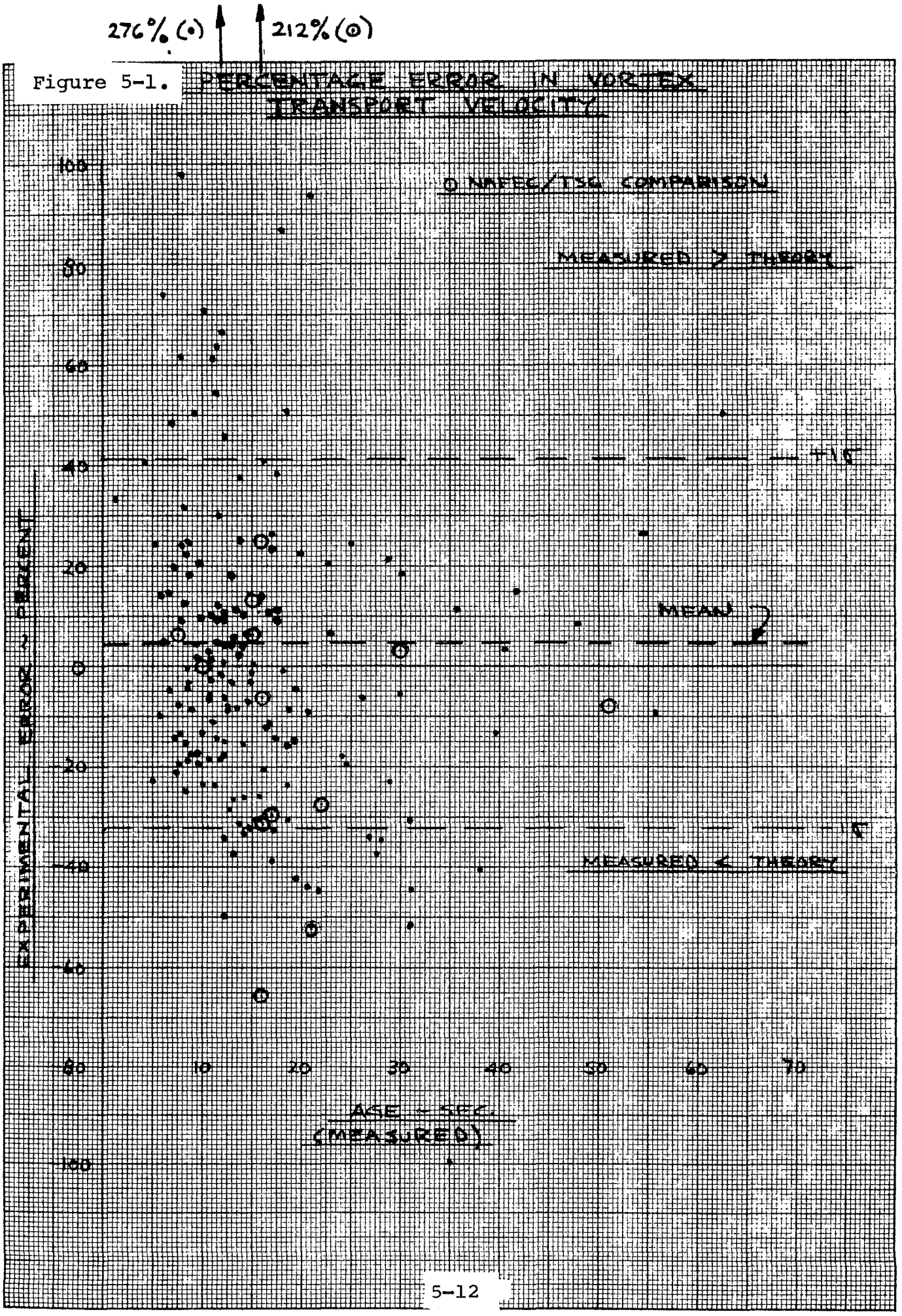

Figure 5-1.

the upwind vortex (No. 2) was ±28.4%. The mean of all errors was +4.5% and the standard deviation was 36.8%. By aircraft, the lowest average error was obtained with the B-707, with an average error of ±12.0% out of 16 runs; next was the DC-9 with an average error of ±15.2% out of 21 runs; the B-727 with ±23.0% out of 58 runs; and the CV-880 with ±31.7% out of 70 runs. The resultant errors are summarized by aircraft, vortex number, and sign in Table 5-II.

Although the data is widely scattered, several points are encouraging. First, all data points were included in the sample including the positive point of 276%; the deletion of this one point from the sample would reduce the standard deviation to below 30%. Second, the correction of the wind heading angles by the compass variation might reduce uncertainties. Third, in an analysis of 14 cases contained in Reference 2, where vortex arrival time was measured by the NAFEC tower and by an acoustic system, developed by the Transportation Systems Center, the average difference in arrival time was 34.8%. This result was obtained by taking (for each case) the absolute value of the difference in arrival time determined by the NAFEC tower techniques, dividing by the NAFEC tower arrival time, and dividing the sum of these percentage errors by the number of cases. The points obtained are shown in Figure 5-1 by the circular symbols. This result indicates that the agreement between theory and the NAFEC tower data is at least as good as the agreement between two independent experimental measurements of arrival time! This fact lends credibility to predictive techniques for vortex hazard assessment. Additional improvements in the vortex model, such as, allowance for wind shear and inclusion of three-dimensional effects, might further improve the results. It is recommended that future work consider these factors.

Table 5-II. Summary of Percentage Errors

AIRCRAFT	VORTEX NO.	POSITIVE ERROR	NEGATIVE ERROR	AVERAGE ERROR
B-727	1	376.5/16 = 23.5%	- 484.2/26 = -18.6%	860.7/42 = ±20.5%
	2	149.8/ 5 = 30.0%	- 320.8/11 = -29.2%	470.6/16 = ±29.4%
				1331.3/58 = ±23.0%
B-707	1	31.5/ 3 = 10.5%	- 47.9/ 8 = - 6.0%	79.4/11 = ± 7.2%
	2	88.3/ 3 = 29.4%	- 23.9/ 2 = -12.0%	112.2/ 5 = ±22.4%
				191.6/16 = ±12.0%
DC-9	1	77.8/ 7 = 11.1%	- 119.5/ 5 = -23.9%	197.3/12 = ±16.4%
	2	17.2/ 4 = 4.3%	- 105.5/ 5 = -21.1%	122.7/ 9 = ±13.6%
				320.0/21 = ±15.2%
CV-880	1	900.1/24 = 37.5%	- 431.2/20 = -21.6%	1331.3/44 = ±30.3%
	2	761.9/18 = 42.3%	- 123.5/ 8 = -15.4%	885.4/26 = ±34.1%
				2216.7/70 = ±31.7%
TOTALS	1	1385.9/50 = 27.7%	-1082.8/59 = -18.4%	2468.7/109= ±22.6%
	2	1017.2/30 = 33.9%	- 573.7/26 = -22.1%	1590.9/ 56= ±28.4%
			TOTAL	4059.6/165= ±24.6%

MEAN ERROR = $\frac{746.6}{165}$ = +4.5%

STANDARD DEVIATION = ±36.8%

5.3 AIRPORT VORTEX MONITORING REQUIREMENTS

Investigations conducted under the present study contract have indicated the significance of various factors regarding the performance requirements of a vortex monitoring system. While, in general, bounds can be established for the range capability and coverage required of a particular vortex sensor, specific sensor locations depend primarily upon the particular airport geometry, prevailing winds, and the runway selection and operational procedures.

To show the significance of these factors on sensing requirements, an evaluation of the vortex hazards at Logan Airport in Boston was conducted. To limit the scope of this investigation only one runway combination was investigated, namely, runways 4L, 4R, and 9. This combination is used when the weather is poor and the wind from the northeast and is the primary runway combination used under IFR conditions. This combination contains both parallel and intersecting runways and was used to investigate vortex hazards for these situations as well as those existing due to preceding traffic. The procedures developed can be used to analyze the vortex hazards for any airport where the runway geometry, operational usage, runway selection procedures, and wind vector information is known.

5.3.1 RUNWAY SELECTION AT LOGAN AIRPORT

Vortex hazards in the terminal area arise when other aircraft are flying within the drift range of the vortices generated by heavy aircraft. Since flight paths in the terminal area are dictated by the landing and departure flight patterns and the

latter by the runways in use, the vortex hazards at any given time depend upon the runway or runway combinations selected by the controller.

At most airports and at Logan Airport in particular, there are three basic considerations in selecting the runway combination; the wind vector, noise abatement procedures, and the capacity of the runway combination. In addition runways may be closed for repairs or snow removal, etc., but this simply limits the combinations available to the controller.

Noise abatement procedures in use at Logan Airport are described in Reference 8. These procedures specify the order of priority of runways in terms of noise abatement. For departures, the order of priority is

Runway 15R - most desirable
Runway 9
Runways 22R, 22L
Runways 4R, 33L, 27, 4L - in that order

For landings all runways are equal in priority except runway 22R which is used last. An addition to the reference memo also states that between the hours of 10 P. M. and 7 A. M., runway 4R is to be used exclusively over runway 4L for all departures and landings.

In addition to these stated priorities but also for noise abatement, runway 4L is restricted to departures under 12,500 lbs. and runway 22R to arrivals under 12,500 lbs.

At Logan Airport controllers are supposed to assign runways in accordance with the above priorities unless 1) the crosswind

exceeds 80 degrees from the runway direction and (or) 2) the wind velocity exceeds 15 knots. In application, this schedule is not rigidly adhered to because of capacity limitations with certain runways.

An obvious factor in runway selection is the wind vector. Neglecting other considerations the most desirable runway maximizes the headwind (also minimizing the crosswind). This runway choice is desirable from an aircraft performance standpoint, since it minimizes the takeoff or landing roll of the aircraft. However, if sufficient runway length is available, pilots can ask for and do receive permission to land or depart on runways with tailwinds.

Controllers often select one runway over another (even when wind vector dictates otherwise) to maximize traffic handling capacity. This third factor is a primary consideration used by controllers in selecting a particular runway combination. During periods of peak traffic, in particular, a controller is strongly influenced by the ability of a runway(s) to handle traffic. For this reason, controllers will stay with or shift to a combination of runways which has greater traffic capacity.

Because the controller is faced with these conflicting demands, runway selection cannot be defined uniquely as a function of wind vector. Overlaps in usage occur due to individual controller preferences.

The basic runway combinations in use at Logan Airport are:

1) 4L, 4R, and 9: For winds less than 15 knots 4L is used for arrival of both heavy and light aircraft, but for departures is restricted to aircraft under 12,500 lbs. (noise abatement); 4R is used for arrival of both heavy and light aircraft and is occasionally used for departure of a heavy aircraft for the additional runway length; 9 is used exclusively for departures of both light and heavy aircraft. Departures of light aircraft are fed to runways 9 or 4L as a function of their destination. For winds over 15 knots runway 9 is dropped.

2) 33L, 33R: 33L is used for arrival and departure of both heavy and light aircraft; 33R is restricted to aircraft under 12,500 lbs., and is undesirable for departures since they must cross 33L.

3) 22L, 22R, 27: For winds less than 15 knots 22L is used for arrival and departure of both heavy and light aircraft; 22R is used for departures of both heavy and light aircraft but for arrivals is restricted to aircraft under 12,500 lbs. (noise abatement); 27 is used exclusively for arrivals of both heavy and light aircraft. For winds over 15 knots 27 is dropped.

4) 22L, 22R, 15R: For winds less than 15 knots 22L and 22R are used for arrivals exclusively; 22R is restricted to aircraft less than 12,500 lbs; 15R is used exclusively for departures of both heavy and light aircraft. For winds greater than 15 knots all operations are on 15R.

5) 4L, 4R, 9, 15R: For winds less than 15 knots 4L and 4R are used for arrival of all aircraft; 9 and 15R are used for departure of all aircraft.

6) 15L, 15R, 9: For winds less than 15 knots 15L is used for arrivals of light aircraft; 15R is used for arrivals and departures of both heavy and light aircraft; 9 is used for departures of both heavy and light aircraft.

The approximate wind vectors corresponding to the use of the above runways is shown in Figure 5-2. In this diagram, the wind vector points to the origin and the angles are measured from true North. The orientation of the various runways at Logan is shown by the circular symbol. The three most commonly used combinations are

1) most used during IFR weather (wind from the northeast)
2) most used during the winter
3) most used during the summer

Of these three combinations, the first was chosen to examine the location of possible vortex hazards and to assess vortex monitoring requirements. The geometry of this runway combination and the normal operational usage are shown in Figure 5-3. Runways 4L and 4R are parallel runways, 1500 feet apart, used primarily for arrivals. Runway 4L is used for the arrival of both heavy and light aircraft, but is restricted to aircraft under 12,500 lbs. for departures. Runway 4R is used for the arrival of both heavy and light aircraft, with IFR traffic using the displaced threshold to avoid shipping traffic in Boston Inner Harbor. Runway 4R is also used occasionally for a departing heavy jet desiring the additional runway length. Runway 9 in this combination is the departure runway and is used for the majority of departures of both heavy and light aircraft. Noted on the diagram are the last touchdown points (4500 feet from the threshold) and the

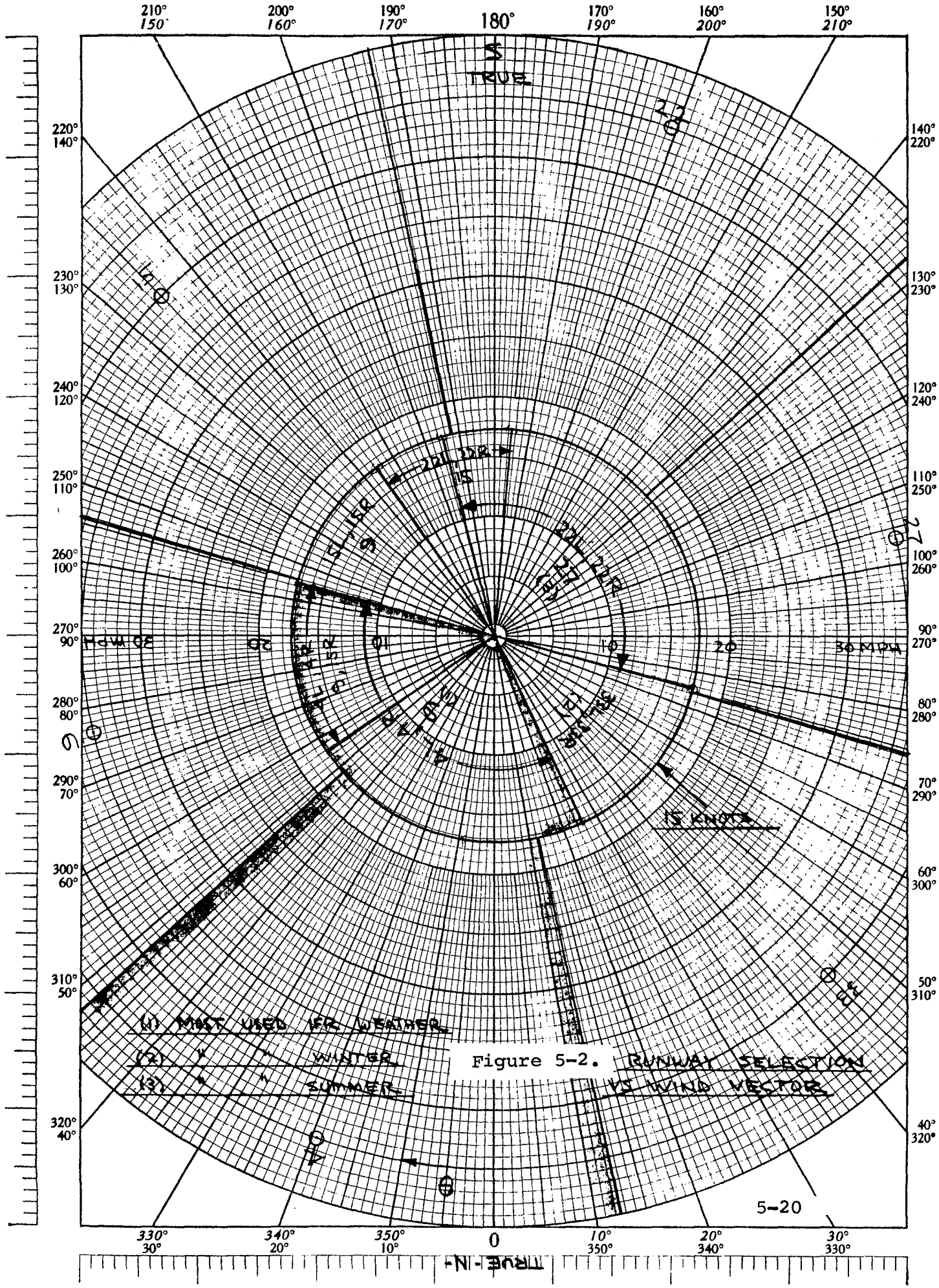

Figure 5-2. RUNWAY SELECTION VS WIND VECTOR

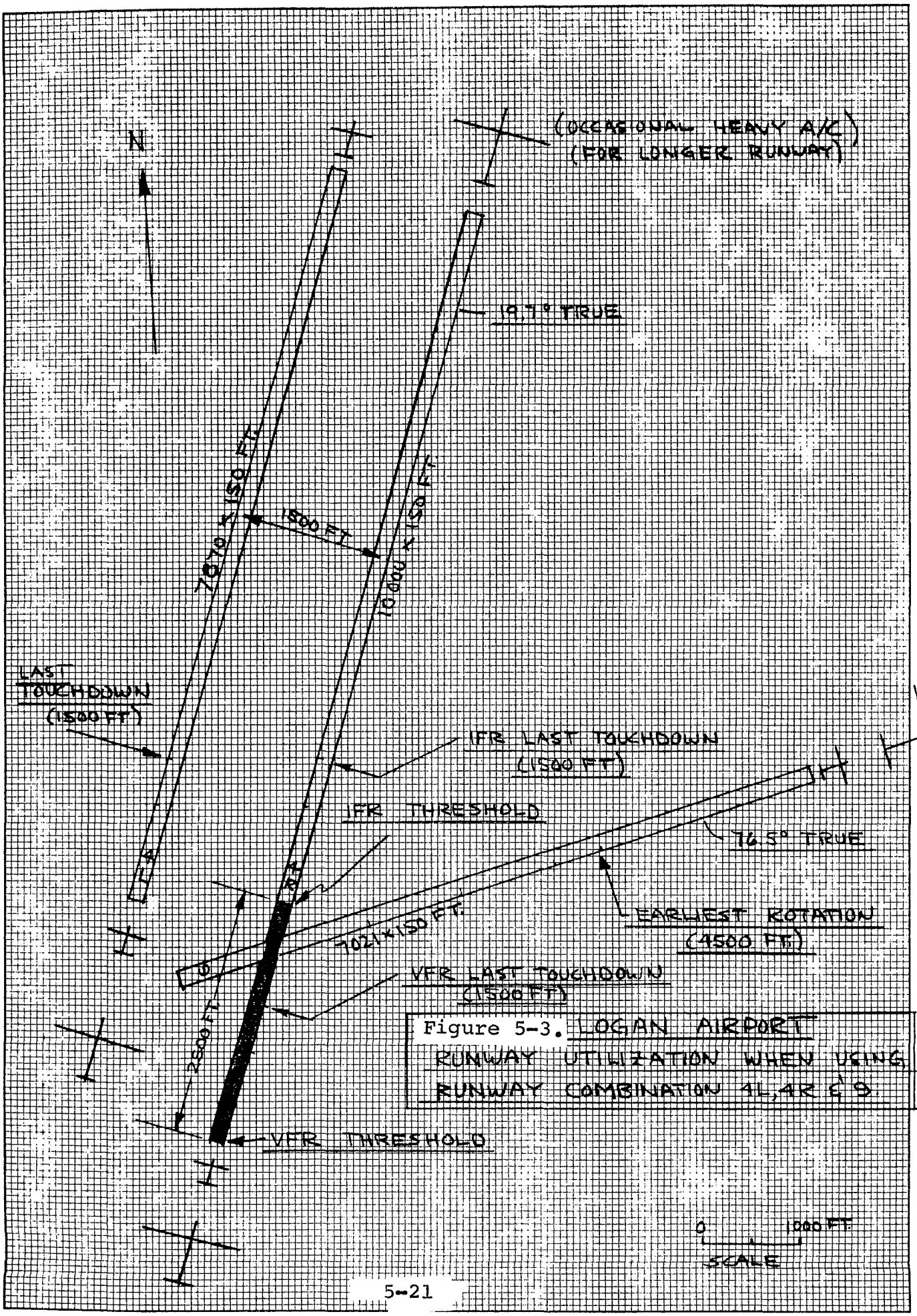

Figure 5-3. LOGAN AIRPORT RUNWAY UTILIZATION WHEN USING RUNWAY COMBINATION 4L, 4R & 9

earliest rotation points (1500 feet from the threshold) assumed for heavy jet operations.

The runway orientations are: θ = 19.7 deg. true (35.0 deg. magnetic) for runway 4 and θ = 76.5 deg. true (91.8 deg. magnetic) for runway 9; the local compass variation is 15.3 degrees West.

5.3.2 PARALLEL RUNWAY OPERATIONS (4L AND 4R)

Parallel operations on runways 4L and 4R affect each other if the vortices generated on one reach the adjacent runway in a region where an aircraft is airborne. This occurrence depends upon the drift capability of the vortices under the wind vector conditions that exist when both runways are simultaneously in use. The vortex drift envelopes for a heavy jet were presented in Section 3. This data in combination with Figure 5-2 can be used to analyze the vortex interaction between runways 4L and 4R. In Figure 5-2 the wind vectors corresponding to the use of runway 4L, 4R and 9 are shown. This runway combination is used for wind headings $334.7^{\circ} < \theta < 104.7^{\circ}$ true when the wind is less than 15 knots and for $347.7^{\circ} < \theta < 48.1^{\circ}$ true when the wind is over 15 knots. The drift data from Section 3 is reproduced in Figures 5-4 and 5-5. These figures show the drift envelopes for the port and starboard vortices respectively. A vortex is assumed to represent a hazard when its axis reaches to within 125 feet of the edge of the adjacent runway. Since runways 4L and 4R are 1500 feet apart and each is 150 feet wide, the critical lateral drift distance is 1300 feet. Provided the wind vector lies within the limits shown on Figure 5-2 that correspond to the use of runways 4L and 4R, a vortex which drifts laterally more than this distance

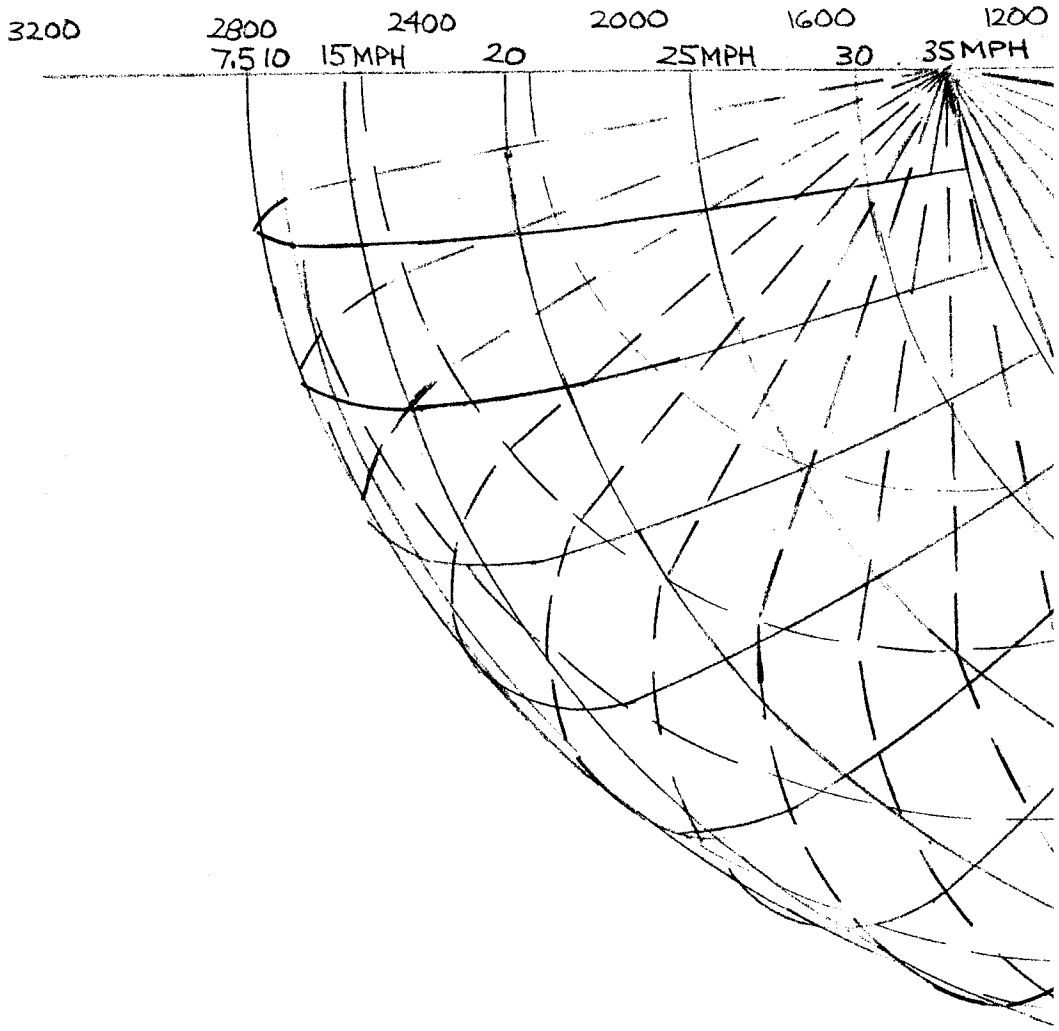
3200
2800
2400
2000
1600
1200
7.5
10
15MPH
20
25MPH
30
35MPH

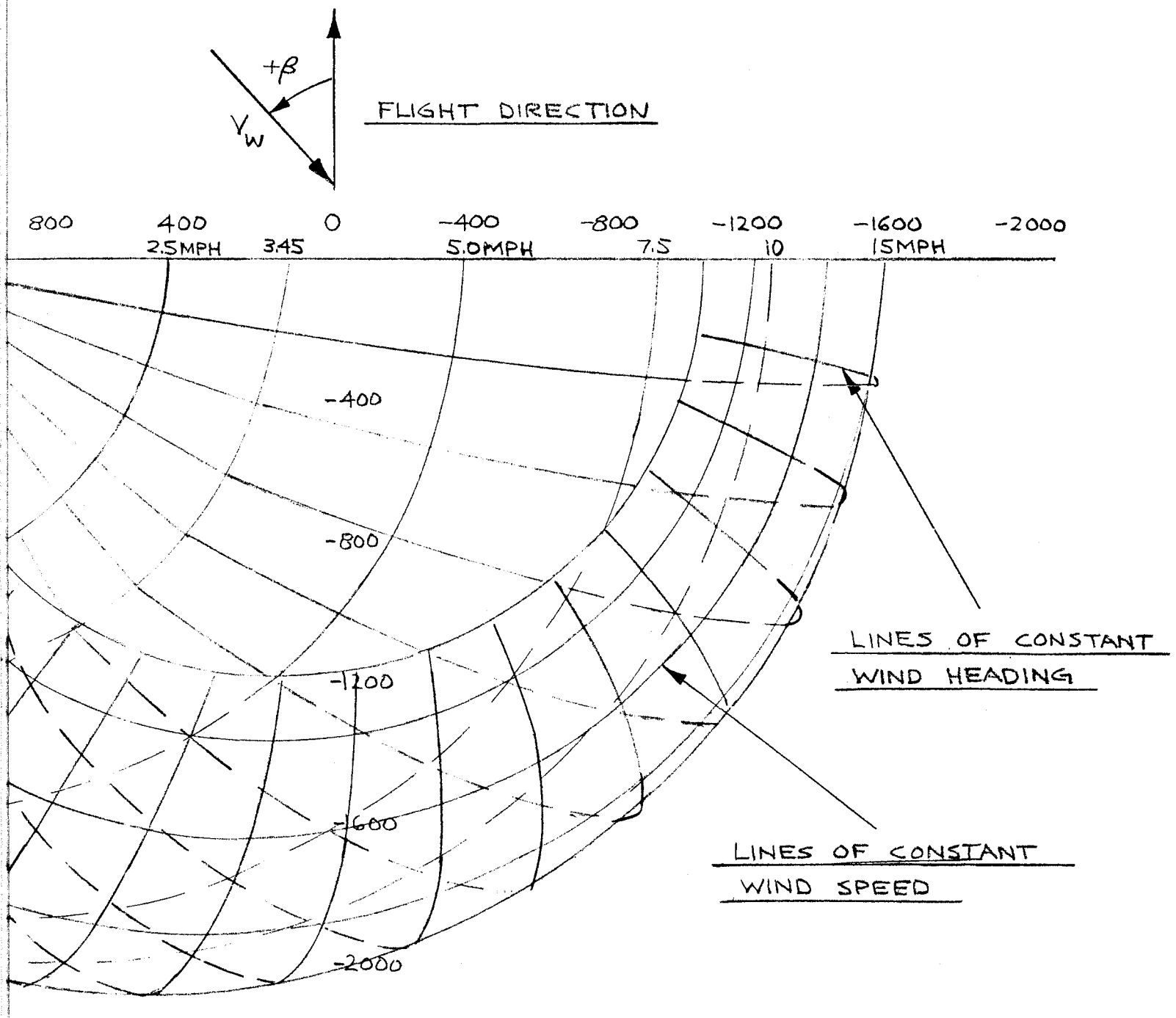

-2400 Figure 5-4. DRIFT ENVELOPE FOR PORT VORTEX OF HEAVY JET (h_o = 100 FT.)

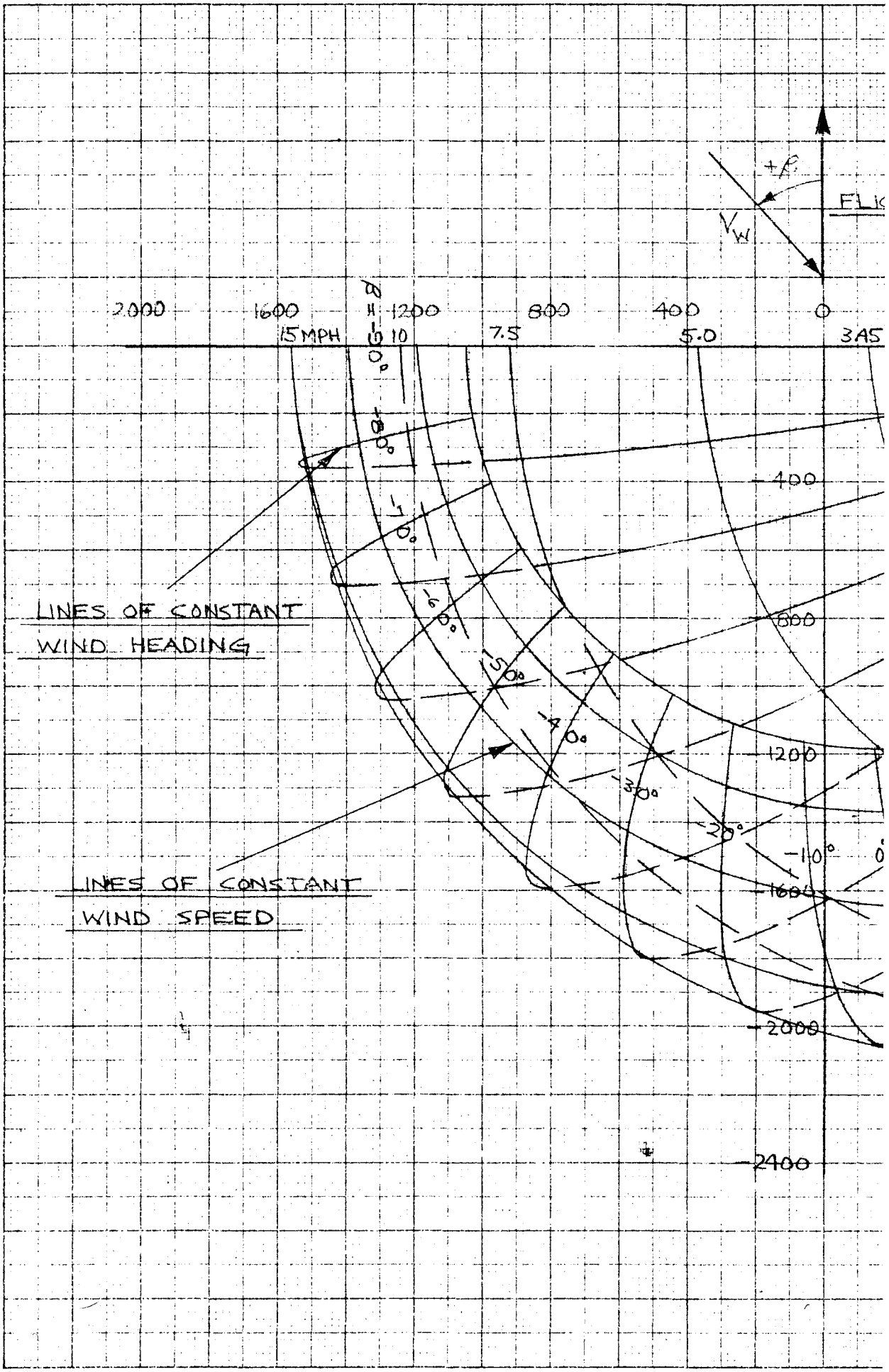
+β
V_W
2000
1600
1200
800
400
0
15 MPH
10
7.5
5.0
3.45
0°
-30°
-60°
-90°
-120°
-150°
-180°
-210°
-240°
-270°
-300°
-330°
400
800
1200
1600
2000
2400
-20°
-10°
LINES OF CONSTANT WIND HEADING
LINES OF CONSTANT WIND SPEED

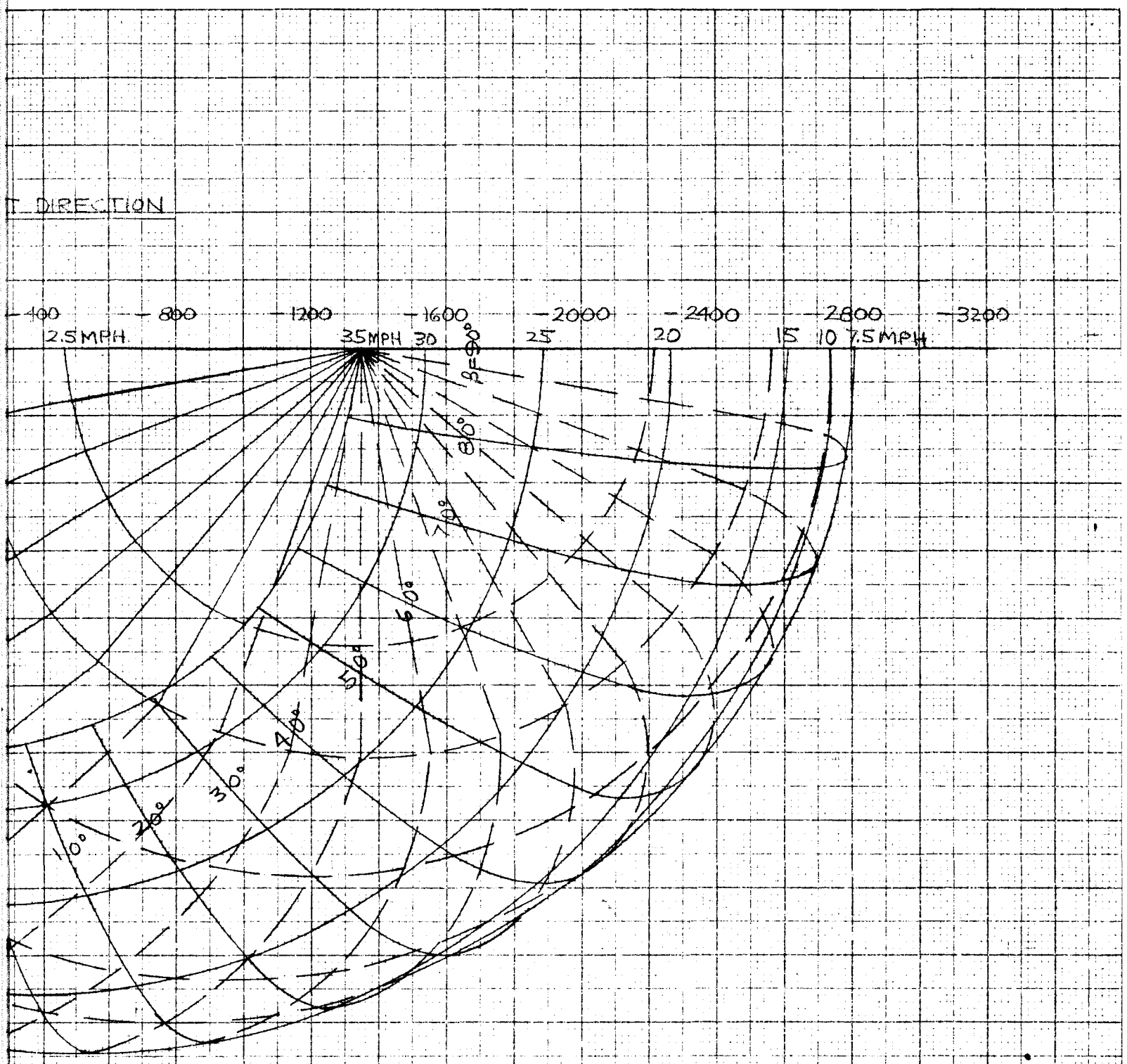

Figure 5-5. DRIFT ENVELOPE FOR STARBOARD VORTEX OF HEAVY JET (h_o = 100 FT)

constitutes a vortex hazard. To apply the wind vector data from Figure 5-2 to the drift envelope data, the wind heading angles must be converted from angles measured from true North (θ) to angles relative to the runway heading (β). This relationship is given by

$$\beta = \theta_R - \theta_W \qquad (5\text{-}7)$$

where θ_R is the runway heading and θ_W the wind heading. With respect to the runway heading the wind headings corresponding to the use of runways 4L, 4R, and 9 are

4L, 4R: <15 knots, $-85^\circ < \beta < +45^\circ$
>15 knots, $-28.4^\circ < \beta < +32^\circ$

9: <15 knots, $-28.2^\circ < \beta < 101.8^\circ$
>15 knots, (not used)

The range of wind headings (as limited by either usage or drift) for which vortex interactions occur from 4R onto 4L were examined for both the port and starboard vortices using Figures 5-4 and 5-5 The wind heading limits obtained are listed in Table 5-III as a function of wind speed.

Identical information corresponding to operations on runway 4L affecting 4R are listed in Table 5-IV.

If the relative wind heading angles are converted back to true headings they can be used in conjunction with the wind rose diagram for Logan Airport to obtain an estimate of the frequency of occurrence of the hazard. If the data listed in Tables 5-III and 5-IV is converted using Equation 5-7 and plotted on the wind

Table 5-III. Wind Headings for Which Operations on 4R Affect 4L

Port Vortex		Starboard Vortex
Wind Speed (mph)	β	β
2.5	$-85^{o} \rightarrow +2^{o}$	
3.5	$-85^{o} \rightarrow +2.5^{o}$	
5.0	$-85^{o} \rightarrow -4^{o}$	Starboard vortex never reaches runway 4L.
7.5	$-85^{o} \rightarrow -11^{o}$	
10.0	$-85^{o} \rightarrow -17^{o}$	
15.0	$-85^{o} \rightarrow -23^{o}$	
17.3 (15 knots)	$-85^{o} \rightarrow -27^{o}$	
>15 knots, vortex never reaches adjacent runway because of usage.		

Table 5-IV. Wind Headings for Which Operations on 4L Affect 4R

Port Vortex		Starboard Vortex
Wind Speed (mph)	β	β
2.5		$-3^{o} \rightarrow +45^{o}$
3.5		$-2^{o} \rightarrow +45^{o}$
5.0	Port vortex	$+4^{o} \rightarrow +45^{o}$
7.5	never reaches	$11^{o} \rightarrow +45^{o}$
10.0	runway 4R.	$17^{o} \rightarrow +45^{o}$
15.0		$23^{o} \rightarrow +45^{o}$
17.3		$27^{o} \rightarrow +45^{o}$
	<15 knots	
17.3	>15 knots	$27^{o} \rightarrow +32^{o}$
20.0		$30^{o} \rightarrow +32^{o}$
21.2		32^{o}

rose for Logan Airport (presented in Section 4), Figure 5-6 is obtained. This figure shows two cross-hatched regions; the region on the right represents the locus of wind vectors when operations on 4R affect 4L and the region on the left represents the locus of wind vectors when operations on 4L affect 4R.

The values shown in each sector of the wind rose represent the percentage of time that the wind vector originates from that direction and magnitude. Summing the individual percentages for the two regions gives approximately 10.6% for the percentage of time that operations on 4R will affect 4L and 5.1% for the percentage of time operations on 4L will affect 4R. These percentages are the frequency of occurrence if operations on the two runways were continuous. To obtain a true indication of the frequency of hazard, these percentages should be reduced by an amount which compensates for the frequency with which the phasing necessary to produce a hazard exists between operations on the two runways. This would considerably reduce the hazard frequency.

Of interest in the development of a vortex monitoring system are the regions through which vortices of potential hazard drift on their path to an adjacent runway. For parallel runways (4L and 4R) of the runway combination under analysis, search regions are shown in Figures 5-7 and 5-8. Figure 5-7 shows the monitoring regions due to operations on runway 4L which affect traffic on 4R. Under the assumed usage of this runway combination, runway 4L is used by heavy aircraft for landing only. Therefore, vortices are only generated up to the last touchdown point of these aircraft. This point was assumed to be 1500 feet from the runway threshold. The figure shows the vortex decay region for

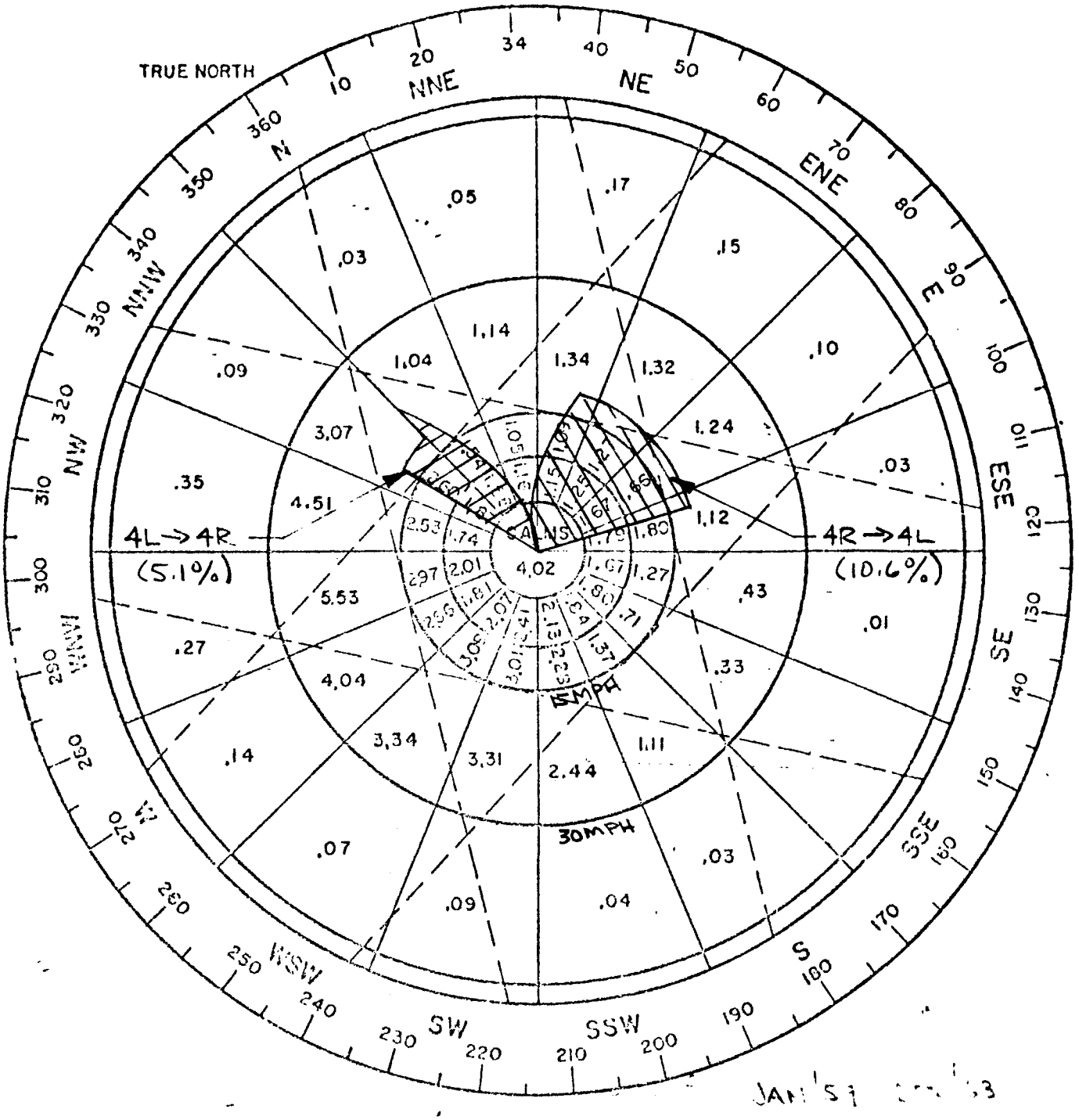

Figure 5-6. WIND ROSE FOR LOGAN AIRPORT SHOWING WIND VECTORS CAUSING VORTEX HAZARDS TO IFR PARALLEL OPERATIONS ON 4L & 4R

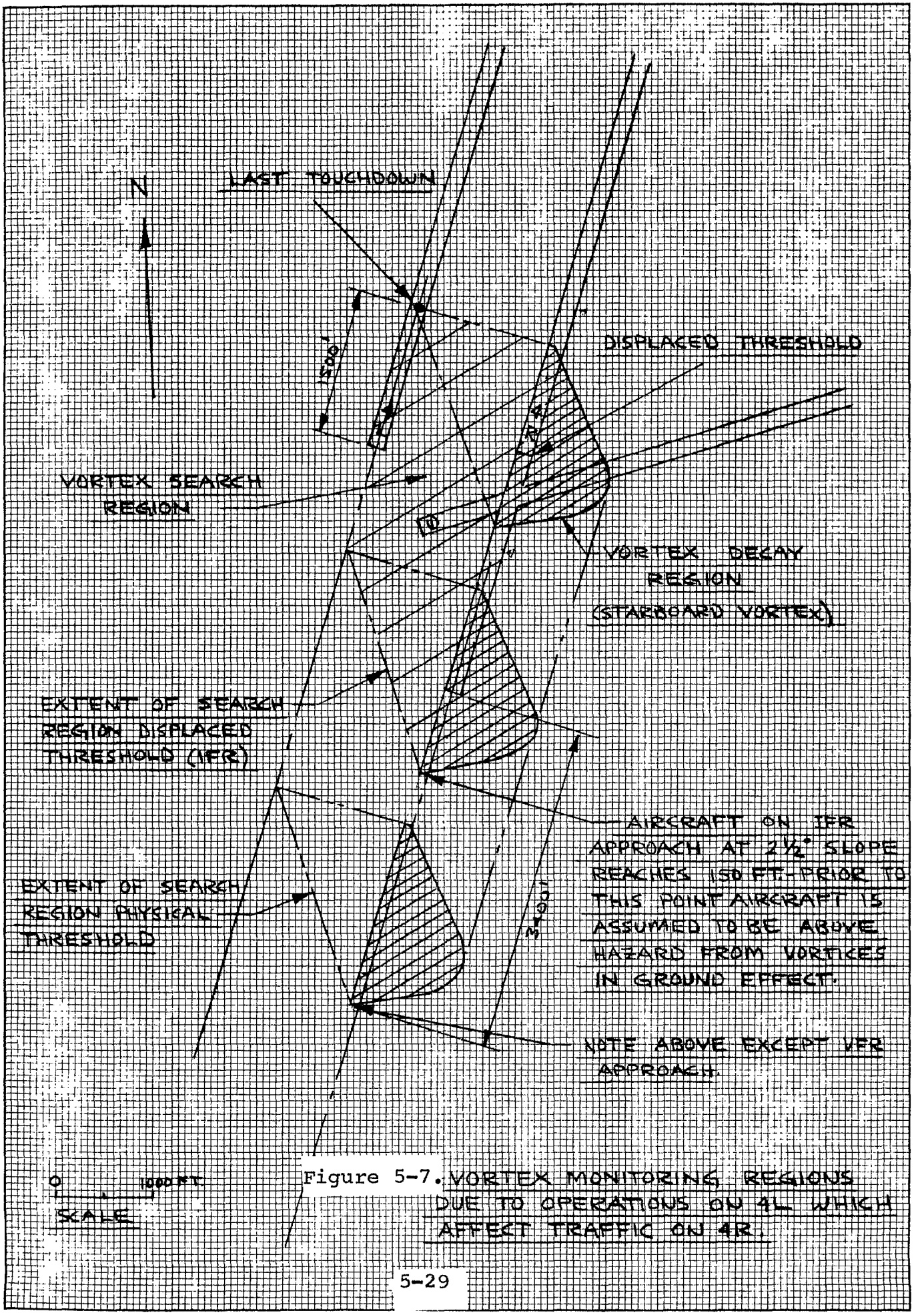

Figure 5-7. VORTEX MONITORING REGIONS DUE TO OPERATIONS ON 4L WHICH AFFECT TRAFFIC ON 4R.

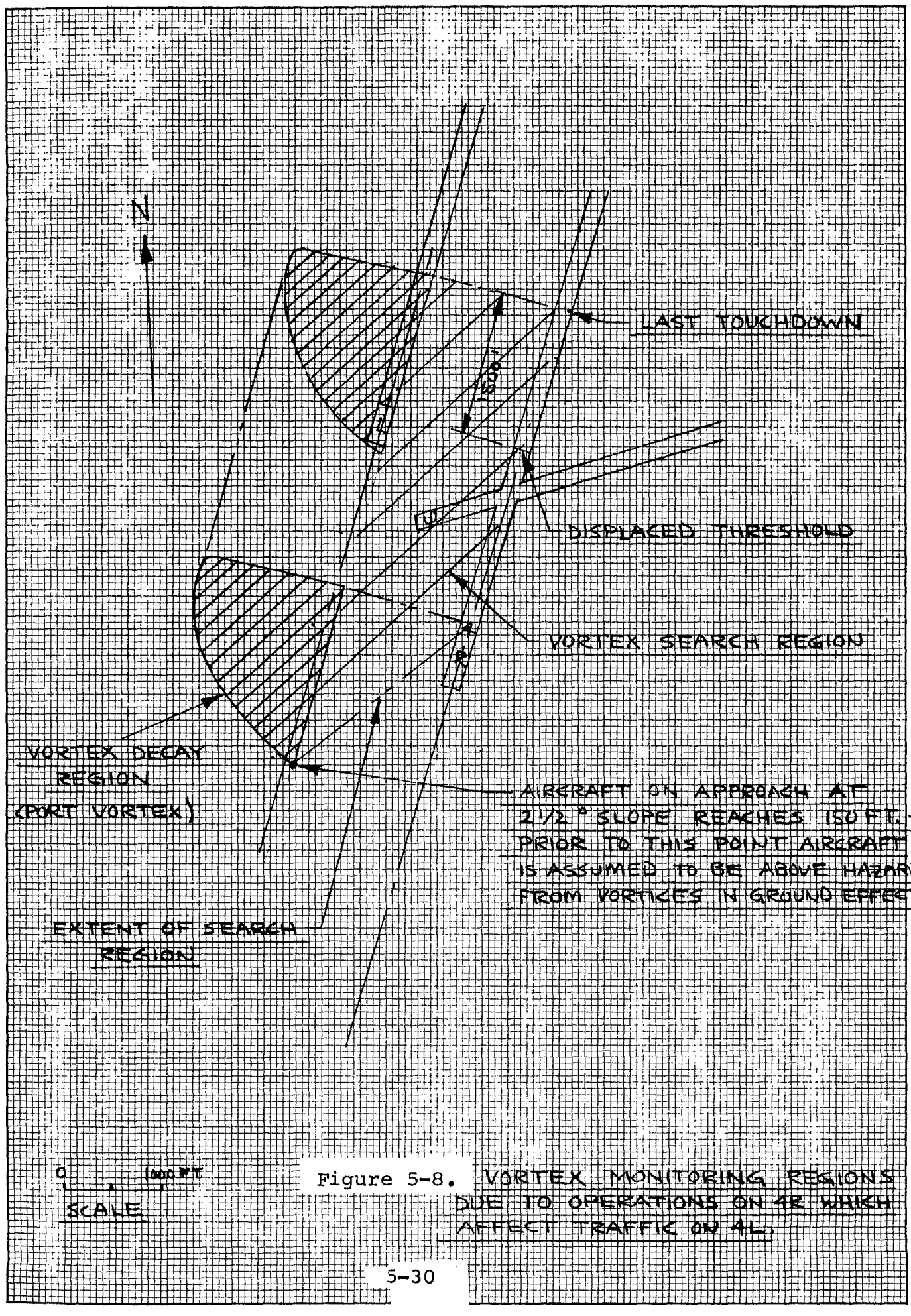

Figure 5-8. VORTEX MONITORING REGIONS DUE TO OPERATIONS ON 4R WHICH AFFECT TRAFFIC ON 4L.

the starboard vortex superimposed on the runway geometry. (The port vortex never reaches runway 4R.) Only that portion of the decay region from Figure 5-5 which is applicable to the usage restrictions is shown.

The first point at which a heavy jet aircraft landing on runway 4L generates vortices hazardous to operations on 4R, is at the point where aircraft landing on 4R have descended to an altitude comparable to ground effect height. (During their path between runways, vortices under consideration will have reached ground effect altitude.) The altitude assumed hazardous was 150 feet. At a minimum approach slope of $2\frac{1}{2}$ deg., this altitude is reached approximately 3400 feet from the earliest touchdown point (assumed to be the runway threshold). Because runway 4R has two effective thresholds, one physical, used during VFR operations, and one displaced, used during IFR operations, the extent of the search region is shown for both. The monitoring region lies between the two runways and extends longitudinally an average of 3500 feet for the displaced threshold and 6000 feet for the physical threshold. The former is less than the distance to the middle marker on approach to runway 4R and, therefore, sensors could be located to cover this region. In the case of VFR operations, the distance at this point almost spans Boston Inner Harbor and location of sensors would constitute a problem.

Figure 5-8 presents vortex monitoring information due to operations on runway 4R which affect runway 4L. Only landing operations are considered, although runway 4R is also used for an occasional departure of heavy aircraft. The infrequency of this occurrence was assumed to negate this as a potential hazard.

However, if an operation on 4L is properly phased with the departure of a heavy aircraft using 4R, a hazard can occur. The applicable drift envelope was obtained from Figure 5-4 for the port vortex. (The starboard vortex never reaches runway 4L.) The vortex search region extends between the runways from a maximum distance of 1000 feet off the end of runway 4R to 1500 feet down runway 4L. The region off the end of runway 4L is located in Bird Island Flats, an area which is currently being filled for expansion purposes at Logan Airport. Since all vortices passing through these regions will be in ground effect, the vertical extent of the search region is 150 feet.

5-3-3 INTERSECTING RUNWAY OPERATIONS (4R AND 9)

Runways 4R and 9 intersect within several thousand feet of their thresholds. Using the runway combination 4L, 4R, and 9, runway 9 is used exclusively for departures. It is conceivable that vortices generated by landing operations on runway 4R can affect aircraft departing on 9 and that vortices from aircraft departing on 9 can affect aircraft arriving or departing on runway 4R.

As previously noted, runway 9 is used when winds are less than 15 knots for $-28.2^{o} < \beta < 101.8^{o}$ and runway 4 is used for $-85^{o} < \beta < 32^{o}$, when the wind is less than 15 knots and for $-28.4^{o} < \beta < 32^{o}$ when the wind is greater than 15 knots. The drift envelopes assuming these limits for the starboard vortex of an aircraft using runway 4R and the port vortex for an aircraft using runway 9 are shown in Figure 5-9. The envelopes are located at the last touchdown point on 4R and the earliest rotation

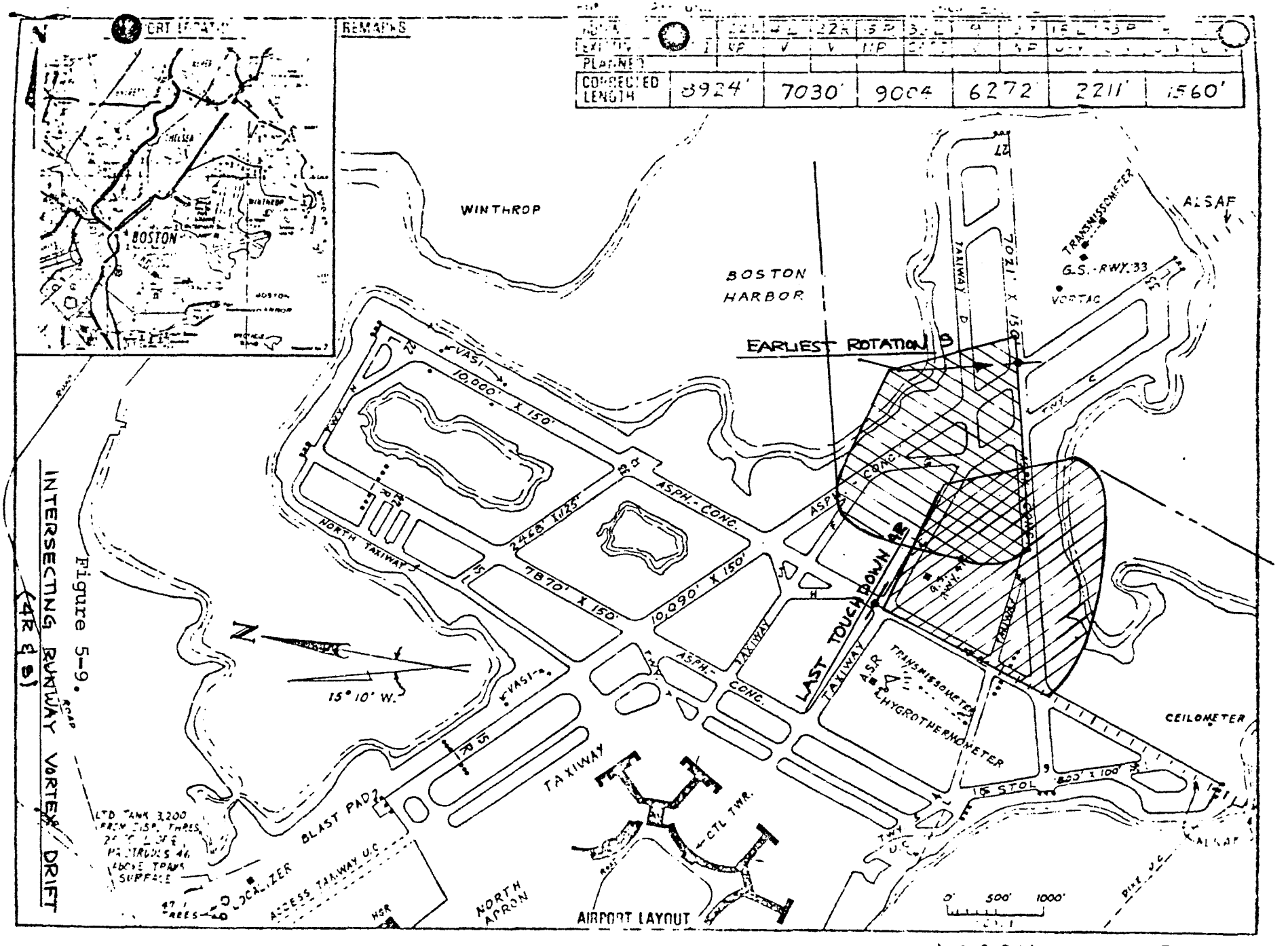

Figure 5-9. INTERSECTING RUNWAY VORTEX DRIFT (4R & 9)

LOGAN AIRPORT
BOSTON, MASS

point on 9. As shown, neither envelope overlaps the other runway in a region where aircraft will be airborne and hence for the runway combination under investigation, no vortex hazard exists due to operations on the intersecting runways, 4R and 9.

5.3.4 PRECEDING TRAFFIC OPERATIONS (4L, 4R, AND 9)

The final area to be examined is the vortex hazard due to preceding traffic operating on the same runway. Normally in these operations, if aircraft are following the same flight path as the preceding aircraft or above it and the altitude is above ground effect, no hazard will occur due to the natural tendency of the vortices to sink due to mutual induction. In the present analysis, since we are dealing with the terminal area, we have assumed a hazard to exist whenever the center of the trailing aircraft lies within a lateral distance B = 200 feet of the center of the generating aircraft. If the generating aircraft is assumed to be flying down the center of the runway, this distance corresponds to the lateral separation distance used in the parallel runway study.

Similar to the parallel and intersecting runway operations, wind vectors which result in vortex hazards can be defined for the preceding traffic case. Figure 5-10 presents the pertinent geometry. The quantity d_{V_t} represents the lateral distance from the runway centerline reached by the vortex with zero crosswind in time t. This distance is obtained from the vortex drift computer program for a heavy jet aircraft operating at 100 feet altitude. When d_{V_t} is greater than B (as in the example shown in Figure 5-10), a crosswind blowing from right to left, which reduces

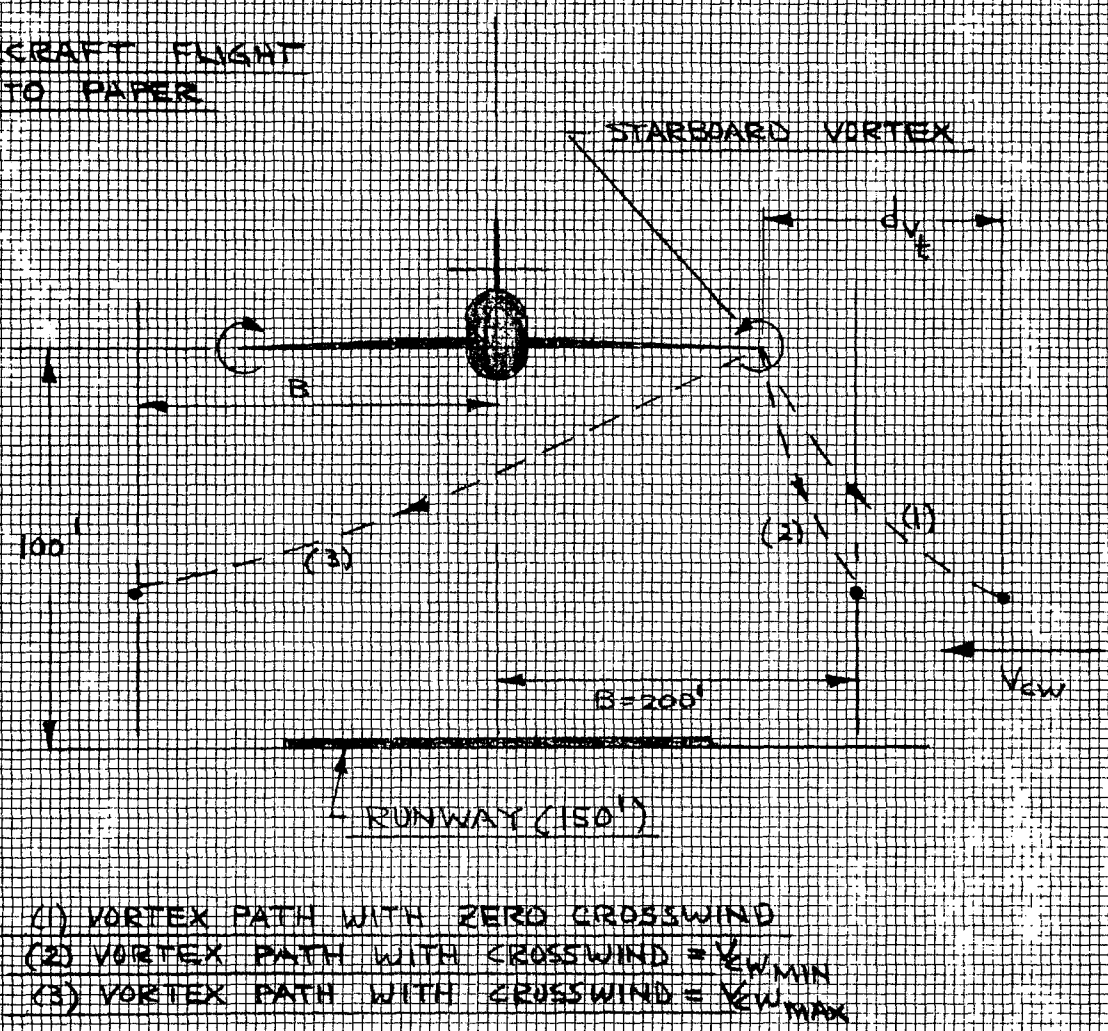

Figure 5-10. GEOMETRY FOR PRECEDING TRAFFIC VORTEX HAZARD EVALUATION

the drift velocity of the vortex, causing it to reach the hazard boundary in time t, is acceptable. The value of this crosswind is given by

$$V_{CW_{Min}} = \frac{d_{V_t} - B}{t} \qquad (5\text{-}7)$$

Likewise, a larger value of crosswind can be defined that will cause the right vortex to cross the runway and arrive at the opposite hazard boundary in time t. The value of this crosswind is given by

$$V_{CW_{Max}} = \frac{d_{V_t} + B}{t} \qquad (5\text{-}8)$$

Between these two values of crosswind, the vortex will lie within the hazard boundaries at time t. Since the problem is symmetrical, the left vortex wind conditions can be defined similarly.

If t is the separation interval between aircraft, these two values of crosswind define regions of acceptable wind vector for the preceding traffic case as shown in Figure 5-11 for separation times of 30, 60, 120, and 240 seconds. For each time, the wind vector extends in magnitude to the value given by the McGowan vortex lifetime curve presented in Section 2.

When the wind vector lies within a region, a vortex hazard can exist if the vertical separation between the trailing aircraft and the vortex axis is small. This will occur near the ground where vertical settling of the vortices does not occur.

The time increments shown next to each boundary are the

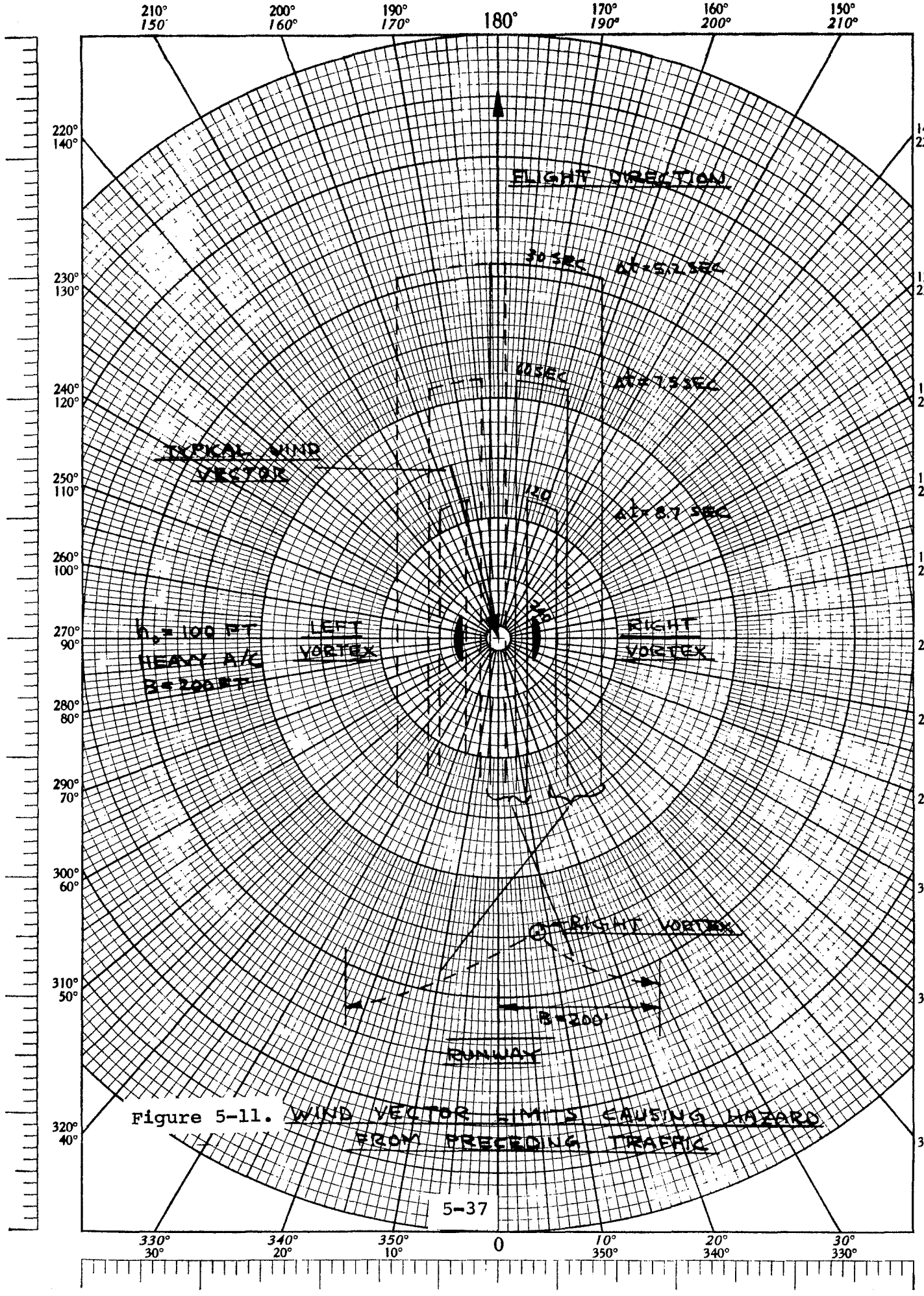

Figure 5-11. WIND VECTOR LIMITS CAUSING HAZARD FROM PRECEDING TRAFFIC

times by which the aircraft vortex encounter is foreshortened due to the maximum downwind component of wind which causes the vortex to drift towards the trailing aircraft.

If these contours are superimposed on the wind rose for Logan Airport and the wind headings corresponding to runway usage are taken into account, the frequency of occurrence can be assessed as a function of separation interval. Figure 5-12 presents the results of this evaluation. Since the frequency data for both runways was similar, they are plotted as a single heavy line corresponding to both runways.

Figure 5-13 presents the vortex monitoring regions for vortices generated by preceding traffic. The region is 400 feet wide centered on the runway centerline and extends 3400 feet off the approach end of the runway and 1400 feet off the departure end of the runway. Beyond these points it is assumed that vortex settling will preclude vortex encounters. However, this only occurs if 1) the trailing aircraft maintains the same or a higher approach or departure path and 2) vortex buoyancy effects are negligible. The former can be achieved with proper pilot training for VFR operations and by using ILS indication of glide slope for landings and some control of climbout path during IFR operations. The latter requires more experimental data for substantiation.

Figure 5-12. FREQUENCY OF VORTEX HAZARD DUE TO PRECEDING TRAFFIC (RUNWAYS 4 & 9)

CONSIDERS LATERAL SEPARATION ONLY - NEGLECTS REDUCTION DUE TO VERTICAL SETTLING OF VORTICES WHEN ABOVE GROUND EFFECT

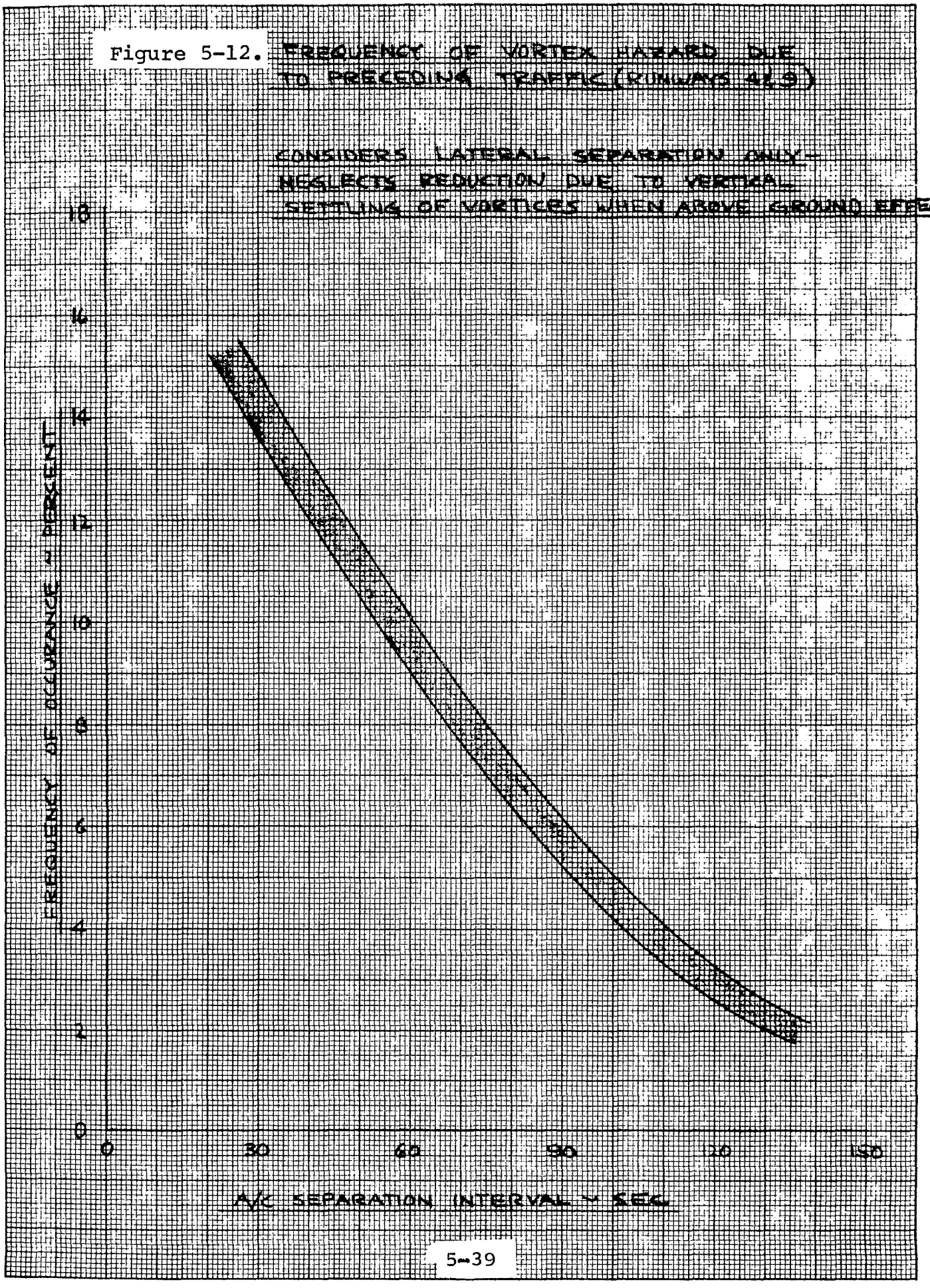

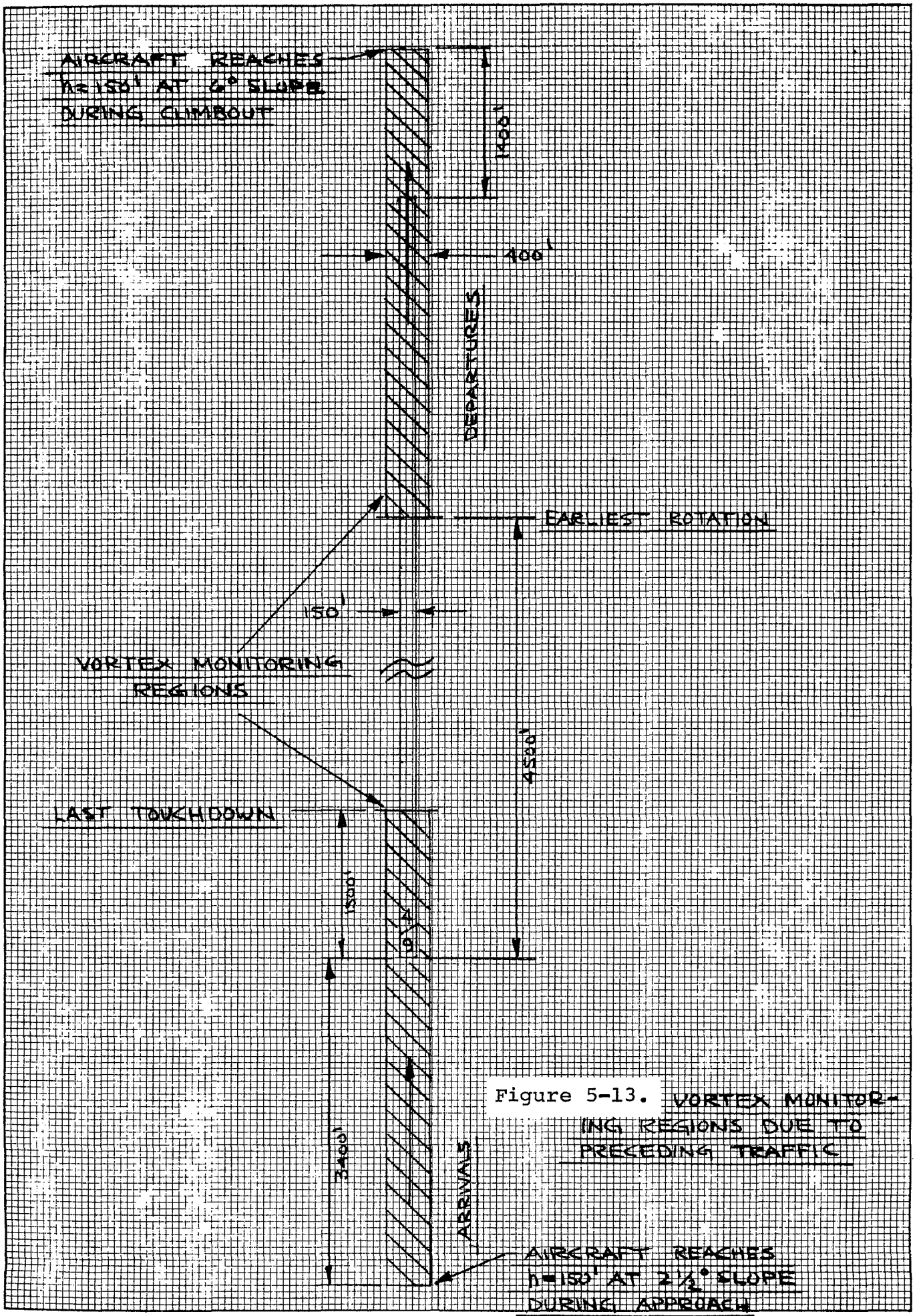

Figure 5-13. VORTEX MONITORING REGIONS DUE TO PRECEDING TRAFFIC

5.4 CONCLUSIONS

The present analysis has defined the search volume requirements for one of the runway combinations used by controllers at Logan Airport in Boston. This combination (4L, 4R, and 9) includes parallel and intersecting runways and these plus the vortex hazards created by preceding traffic were investigated. The analysis has shown that a systematic approach to defining vortex monitoring regions can be used, provided information on runway geometry, operational usage and wind environment is available.

The results obtained depend upon the accuracy of the envelopes used to define the extent of vortex drift as a function of wind vector. These envelopes are generated by a computer program which solves for the motion of an element of each vortex, assuming the vortices are horizontal filaments of infinite length which, in combination with their underground images, induce relative motion. To this self-induced motion, the wind drift is added vectorially. The computer model assumes that the vortex element drifts under these influences until a time is reached which is representative of the maximum lifetime of the vortices. This time is presently determined as a function of wind magnitude.

The drift envelopes generated can be in error because of inaccuracies in the model and because of uncertainties in the maximum age of the vortex. The former might be improved by including three-dimensional vortex effects and wind shear at low altitudes in the model. The latter probably requires further experimental tests of vortex behavior under measured meteorological

conditions.

A preliminary attempt has been made to determine the accuracy with which the basic model predicts vortex drift rates. The standard deviation of the cases examined was 37%, which can be reduced by improvements in the vortex model. If such improvements can be made and an accurate method found to define lifetime as a function of meteorological conditions, vortex hazards can be assessed analytically and predictive techniques for handling the wake turbulence problem may be feasible.

The study has shown that the frequency of occurrence of a vortex hazard is low, even with the conservative lifetime data assumed in this report. More importantly, the hazard frequency is considerably lower than the frequency with which the runway combination is in use. This indicates that even if active sensing is required in certain instances it will only be required for particular wind vector conditions.

The coverage volume can be adequately sensed by most of the active and passive vortex sensing techniques presently being considered for monitoring applications. Pressure sensor arrays could be used between parallel runways where vortices are in ground effect and laser or acoustic sensors could be used where greater height is required.

System resolution and response time considerations have not been examined in detail. Vortex location accuracy of the order of 25 feet should be adequate and perhaps 15 seconds minimum warning to the pilot. In certain instances, the latter allows but 15 seconds for the detection, processing and communication of a vortex hazard to the pilot. This is one reason why predictive

techniques are appealing since they don't require a vortex to be sensed (generated by an aircraft preceding by only 30-60 seconds) to indicate a hazard, but can analytically infer the same information in advance, thus allowing the problem to be solved minutes before at the metering and spacing level.

With improvements in vortex model and knowledge of vortex maximum age, the techniques developed herein could be automated to provide a means for the accurate, rapid assessment of vortex hazards for any airport. At that time a meaningful statistical analysis of the probability of occurrence of vortex hazards at airports can be conducted by including such random effects as the phasing between operations on adjacent runways and the position of the generating and encountering aircraft during approach or departure.

SECTION 6

REFERENCES

(1) Adelfang, S. I., "Measurements of the Intensity and Spectrum of Atmospheric Turbulence at Palmdale Airport", Lockheed, California Company Report No. 23341, December 1969.

(2) Burnham, D. et al, Vortex Sensing Tests at NAFEC, Report No. DOT-TSC-FAA-72-2, January 1972.

(3) Dee, F. W., Nicholas, O. P., "Flight Measurements of Wing-Tip Vortex Motion Near the Ground", RAE Technical Report 68007, January 1968.

(4) Donaldson, Coleman duP., "A Brief Review of the Aircraft Trailing Vortex Problem", NAECON Meeting, Dayton, Ohio, May 17-19, 1971.

(5) Garodz, Leo J., "Investigation of Jet Transport Aircraft Vortex Systems Descending Into and Generated In Ground Effect", FAA Data Report, Project No. 504-303-03X (Special Task Number Two), November 1970.

(6) Garodz, Leo J., "Investigation of the Relatively Long Time History Vortex Characteristics of the Convair CV-880 Airplane in Terminal Area Type Flight Operations", FAA Data Report, Project No. 504-303-03X (Special Task Number Three), November 1970.

(7) Gorstein, M., Hallock, J., McWilliams, I., Goff, R., "System Performance Requirements for Monitoring Trailing Vortices In a Terminal Environment". Presented at NAECON Meeting, Dayton, Ohio, May 1971.

(8) Lynch, H. C., "Logan International Airport Control Tower Bulletin 68-1, Anti-Noise Procedures", July 18, 1968.

(9) McCormick, B. W., "Aircraft Wakes: A Survey of the Problem", FAA Symposium on Turbulence, Washington, D. C., March 22-24, 1971.

(10) McCormick, B. W., Tangler, J. L., and Sherrieb, H. E., "On the Structure of Trailing Vortices", Journal of Aircraft, Vol. 5, No. 3, May-June 1968.

(11) McCormick, B. W., Eisenhuth, J. J., Nelson, R. C., and Garodz, L. J., "Analysis of Experimental Measurements of Trailing Vortex Systems of Large Jet Transport Aircraft", NAECON Meeting, Dayton, Ohio, May 17-19, 1971.

(12) Sprieter, J. R., and Sacks, A. H., "The Rolling Up of the Trailing Vortex Sheet and Its Effect on the Downwash Behind Wings", Journal of Aeronautical Science, Vol. 18, No. 21, 1951.

APPENDIX A

PROGRAM FOR COMPARING THEORETICAL AND EXPERIMENTAL VORTEX DRIFT VELOCITIES

This appendix presents the equations of a program developed to compare measured vortex drift data (from NAFEC) with a theoretical model for computing the 3-dimensional motion of a vortex element.

Input Quantities

The following quantities are input variables:

1) z_o = the aircraft altitude, feet

2) y_o = the lateral distance of the aircraft nose from the measurement tower, feet

3) W = the aircraft weight, lbs.

4) b = the aircraft span, feet

5) V_{AC} = the aircraft speed, knots

6) V_W = the wind speed, MPH

7) β_W = the wind heading measured with respect to the aircraft track, deg.

8) ρ_o = the air density, slugs/ft^3

9) Δt = the computation step size, sec.

10) t_{MAX} = the maximum stopping time, sec.

11) AGE_E = the vortex age when passing tower measured with respect to the time when the wing was abreast of the tower (from measurements at NAFEC), sec.

12) Pass Number = used to identify the NAFEC run

13) Aircraft Type = (B-727, B-747, DC-9, etc.) used to identify aircraft type making run

14) Vortex number; 1 = vortex nearest tower; 2 = vortex away from tower

15) Print Option; 1 = print data every step; 2 = print final results

The flyby geometry is shown in Figure A-1.

From the initial conditions the vortex position at each time step is computed:

Vortex Number 1.	Vortex Number 2.
$x_1 = x_W$	$x_2 = x_W$
$y_1 = y_W + \Delta y$	$y_2 = y_W - \Delta y$
$z_1 = \Delta z$	$z_2 = \Delta z$

where

$$x_W = -\frac{5280}{3600} V_W \text{ Cos } \beta_W \, t$$

$$y_W = -\frac{5280}{3600} V_W \text{ Sin } \beta_W \, t$$

and

$$\Delta y^2 = \frac{2\left[\frac{64\pi^2}{AK^2} + A(t + B)\right]}{\frac{64\pi^2}{K^2}} \left\{ 1 \mp \left[\frac{64\pi^2}{A^2 K^2 (t + B)^2} + 1\right]^{-1/2} \right\}$$

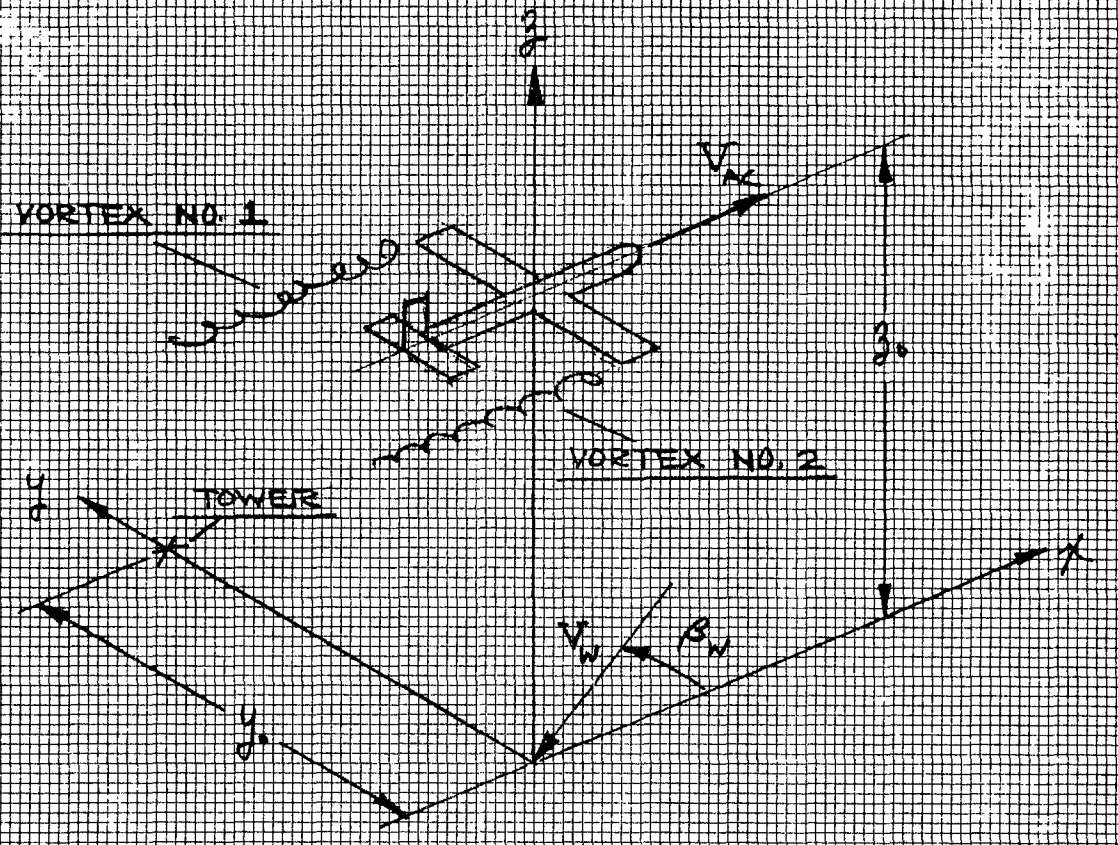

FIG. A-1 FLYBY GEOMETRY

$$\Delta z^2 = \frac{2\left[\frac{64\pi^2}{AK^2} + A(t + B)\right]}{\frac{64\pi^2}{K^2}}\left\{1 \pm \left[\frac{64\pi^2}{A^2 K^2 (t + B)^2} + 1\right]^{-1/2}\right\}$$

the lower sign is used when - $t < B$

the upper sign is used when - $t > B$

$$A = \text{Constant} = \frac{1}{\left(\frac{\pi}{8} b\right)^2} + \frac{1}{z_o^2}$$

$$B = \text{Constant} = \left|\frac{4\pi}{AK}\left\{\frac{A\left(\frac{\pi}{8} b\right)^2 - 2}{\left[A\left(\frac{\pi}{8} b\right)^2 - 1\right]^{1/2}}\right\}\right|$$

$$K = \text{Constant} = \frac{4W}{\rho\pi b V_{AC}\ (6076.1/3600)}$$

At the end of each time step test whether

$$y_{1,2} \geq y_o$$

If no, continue to next time.

If yes, interpolate for conditions (x, t) when

$$y_{1,2} \equiv y_o$$

The time at this point is the true age of the vortex when passing the tower (t_T). Compute the equivalent age of the vortex

(as determined in NAFEC tests) at this point, AGE_T. (AGE_T is the theoretical time from the point where the aircraft wing is abreast of the tower to the point where the vortex passes the tower.)

$$AGE_T = t_T - \frac{x}{V_{AC}\left(\frac{6076.1}{3600}\right)}$$

Compute the percentage error in drift velocity

$$\epsilon(v) = \left[\left(\frac{AGE_T}{AGE_E}\right) - 1\right] \times 100\%$$

The program output includes for Option 1: case, aircraft type, pass no., vortex no., t_T, AGE_T, $\epsilon(v)$ and as a function of time x, y, z of vortex 1 or 2.

Print out Option 2 includes: case, aircraft type, pass no., vortex no., t_T, AGE_T, and $\epsilon(v)$.

APPENDIX B

REPORT OF INVENTIONS

After a diligent review of the work performed under this contract during the reporting period no new innovation, discovery, improvement or invention was made.